



A University of Sussex DPhil thesis

Available online via Sussex Research Online:

<http://eprints.sussex.ac.uk/>

This thesis is protected by copyright which belongs to the author.

This thesis cannot be reproduced or quoted extensively from without first obtaining permission in writing from the Author

The content must not be changed in any way or sold commercially in any format or medium without the formal permission of the Author

When referring to this work, full bibliographic details including the author, title, awarding institution and date of the thesis must be given

Please visit Sussex Research Online for more information and further details



The Old and New Universe in the era of precision cosmology

Marina Cortês

Submitted for the degree of Doctor of Philosophy
University of Sussex
October 2008

Declaration

I hereby declare that this thesis, either in the same or different form, has not been previously submitted to this or any other University for a degree.

Signature:

Marina Cortês

UNIVERSITY OF SUSSEX

MARINA CORTÊS, DOCTOR OF PHILOSOPHY

THE OLD AND NEW UNIVERSE IN THE ERA OF PRECISION COSMOLOGYSUMMARY

These are privileged times to be a cosmologist. Recent years have witnessed unprecedented progress in observational and computational techniques and we now are able to quantify cosmological properties with unprecedented accuracy. My work builds upon this observational accuracy by establishing a connection with viable theoretical models. I focus on two specific eras of the universe's evolution, namely inflation and today's cosmic acceleration. In the context of single field inflationary models I illustrate the relation between the spectra of curvature and gravitational wave perturbations. I conclude that their mutual interdependence extends beyond the usual amplitude consistency relation and can be traced all the way to infinite order of accuracy. This yields an infinite hierarchy of consistency relations between these spectra and their derivatives. On an observational perspective, using WMAP's data, I explore the dependence of CMB constraints on inflation with the cosmological scale at which these are chosen to be presented. I develop a technique that allows for an appropriate choice of this scale and show that this way constraints may be improved by as much as 5 times. In the context of the particle physics motivated quintessence models I have looked at the ability of early universe probes - namely Big Bang Nucleosynthesis - for distinguishing between different dark energy proposals when combined with standard distance modulus or the Hubble rate techniques. I conclude that more yet more accurate measurements are required if observations are to successfully confirm or rule out these models as potential candidates against a cosmological constant. I also analyze possible effects that may mimic or underlie cosmic acceleration effects. I focus on a potential lack of knowledge of the precise values of particular cosmological parameters such as the curvature and matter content of the universe. I find that even a small uncertainty in any of these two quantities leads

to significant bias on the reconstruction of dark energy properties, when typical probes like the distance luminosity and the Hubble rate are considered. I conclude that in order to disentangle between these effects a combination of distance and expansion history measurements is required.

Acknowledgements

I am deeply grateful to Andrew Liddle whom I am privileged to have had as a supervisor. Andrew provides subtle guidance, never forcing his views and with great regard for the students ideas. He was always receptive to my suggestions, and allowed me to pursue different topics even when they shifted between extremes of theory and observation. I am also thankful he allowed me to set off and establish collaborations with other groups, sometimes in fields which were not directly part of our initial research plans. Equally important Andrew provided advice in many aspects of academic life not directly related to physics, which have helped me many times and will continue to guide me in making decisions and find my way in academia. I benefited greatly from his expertise, wit, and extensive knowledge of physics, and feel fortunate to have had the chance to work under his supervision.

Bruce Bassett has given me the opportunity to work with him and his group at the university of Cape Town in South Africa. I am indebted to him and the entire Cosmology and Gravity group for hosting me, and for a productive and joyful atmosphere during my seven months stay. I am ever grateful to Bruce for his teachings, and innovative views and working methods (and for casting upon me the spell of dark energy that is still working!). To Renée, Chris, Yabe, Jacques, Patrice and Mike, I keep the best memories of our work and fun together. Thank you for showing me your beautiful country and making me feel at home from the first day.

At the Astronomy Centre at Sussex many are those who helped me in different stages during my studies. I thank Pia Mukherjee for her patience in teaching me CosmoMC, and for telling there's a solution to every problem; David Parkinson for introducing me to Bruce Bassett and for always being willing to answer my questions on physics; Ed Lloyd-Davies for getting me out of trouble everytime my machine decided to break down; Anthony Smith for helping me in the thesis style and layout; and foremost Gianluca Calcagni, for allowing me persuade him to work on LQC with me, which for him meant a 180° change in research field.

I also had the opportunity to spend some weeks at SISSA in Trieste. I am grateful to Carlo Baccigalupi for hosting me, and for an enjoyable February spent in the fair setting of Miramare; and for showing me about what's behind the beautiful CMB maps (and most of all for the *cannolo sicilianos*).

I have to thank Roy Maartens at the Institute for Cosmology and Gravitation in Portsmouth for always having a space for me and providing me with all the facilities I needed. I am grateful to have met Elisabetta Majerotto, Mehri Toriki, Jussi Vallivita, Tommaso Giannantonio, Federico Arroja and Bjoern Schaefer. Thanks to them weekends at Portsmouth and the meetings we attended together were always great fun. I hope we all keep in touch and see each other often around!

I'll remain ever in debt to my dear friends whom I can not thank enough. Dearest Muriel, Jon, Leyla, and Rehab, you made my stay in Brighton special, lifted my mood now and again, and never let me feel lonely when miles away from home. I hope I may be able to return your friendship and unconditional support. To Bhabani for worrying and asking after me, and giving me incentive to proceed, you are a true friend; Sus, Rob, Francesca, Andrea, my housemate who didn't mind me working in the middle of the night; to Steph and Manuela.

To Antonio a big thanks for companionship and for the great times we shared together, and for never finding any subject too silly to discuss.

Finally a special thank you to Paulo Crawford, my first cosmology teacher and a great pedagogue, who didn't mind deviating from the course programme to answer our questions, and who believed in me, and during my undergraduate studies let me work on inflation on my own, in place of attending a whole semester on planetary physics.

Each one of them have, more or less actively and in their own way, contributed to the completion of my Ph.D. and my being able to write these lines now. I feel honoured to have met and shared the past three years with you. *Obrigada*.

I thank and acknowledge support from the Fundação para a Ciência e Tecnologia (Portugal).

Preface

The work on this thesis was done in collaboration with Andrew R. Liddle, Pia Mukherjee, Bruce A. Bassett, Mike Brownstone, Antonio Cardoso, Marina Cortês, Yabebal Fantaye, Renée Hlozek, Jacques Kotze, Patrice Okouma and Chris Clarkson. It is based on the following articles

1. *"The Consistency Equation Hierarchy in Single Field Inflation Models"*
M. CORTÊS, A. R. LIDDLE
PHYS REV D **73** 083523 (2006) – ASTRO-PH/0603016

2. *"On What Scale Should Inflationary Observables be Constrained?"*
M. CORTÊS, A. R. LIDDLE, PIA MUKHERJEE
PHYS REV D **75** 083520 (2007) – ASTRO-PH/0702170

3. *"Dynamical Dark Energy or Simply Cosmic Curvature?"*
C. CLARKSON, M. CORTÊS, B. A. BASSETT
JCAP **0708** 011 (2007) – ASTRO-PH/0702670

4. *"Is the Dynamics of Scaling Dark Energy Detectable?"*
B. A. BASSETT, M. BROWNSTONE, A. CARDOSO, M. CORTÊS, Y. FANTAYE, R. HLOZEK, J. KOTZE, P. OKOUMA
JCAP **0807** 07 (2008) – ARXIV:0709.0526

5. *"Dark energy degeneracies in the background dynamics"*
R. HLOZEK, M. CORTÊS, C. CLARKSON, B. A. BASSETT
SPECIAL ISSUE ON DARK ENERGY OF *General Relativity and Gravitation*
GRG **40** 285 (2008) – ARXIV:0801.3847

Figures (6.1), (6.2) and (6.3), were taken from Spergel et al. (2007), Wang and Mukherjee (2007) and Knox et al. (2006) respectively. Figures (5.1), (5.2), (5.5) were produced by Renée Hlozek. Figures (5.4) and (5.3) were produced by António Cardoso.

Contents

Contents	ix
1 Introduction	1
1.1 General setup	2
1.1.1 The density parameter	3
1.1.2 Distance Measurements	5
1.1.3 Acceleration	6
2 Cosmic Acceleration – Inflation and Dark Energy	7
2.1 Inflation	7
2.1.1 Inflationary Perturbations	9
2.1.2 Next Order in Slow Roll	13
2.2 Dark Energy	13
2.2.1 Probes of Dark energy	14
2.2.2 Acceleration through scalar fields - Scaling Models	15
2.2.3 Early Dark Energy Constraints	16
2.2.4 Parameterizations of Dark Energy	17
2.3 Bayesian Statistics	18
2.3.1 Marginalization	18
3 The Inflationary Consistency Equation	20
3.1 Introduction	20
3.2 Definitions	21
3.3 The consistency equation hierarchy: lowest-order in slow-roll	22
3.4 The consistency equation hierarchy: next-order in slow-roll	24
3.5 Relation to approximate consistency equations	25
3.5.1 Coincidence of scales	25
3.5.2 Constant running	28
3.6 Conclusions	28
4 The Pivot Scale	30
4.1 Introduction	30
4.2 Methodology	31
4.3 Choice of scale: models with scalar running	33

4.3.1	Tilt and running	33
4.3.2	Tilt and the tensor–scalar ratio	35
4.3.3	Inflationary slow-roll parameters: lowest order	37
4.3.4	Inflationary slow-roll parameters: next order	39
4.4	Choice of scale: models with no scalar running	42
4.5	Including more data	43
4.6	Conclusions	44
4.7	Appendix	45
4.7.1	CosmoMC setup	45
4.7.2	Chain manipulation	46
4.7.3	Area Estimation	46
5	Big Bang Nucleosynthesis constraints on Dark Energy	49
5.1	Introduction	49
5.2	General Results	52
5.3	Polynomial $w(z)$ parametrisation	53
5.4	Double Exponential Potential	54
5.5	Performance of standard parametrisations	56
5.6	Conclusions	58
5.7	Appendix	59
6	Non-parametric Dark Energy Degeneracies	61
6.1	Introduction	61
6.1.1	Degeneracies in Dark Energy Studies	62
6.1.2	Future surveys	66
6.2	Dark Energy from observations	66
6.2.1	Expansions of the background observables	67
6.2.2	Obtaining the Dark Energy equation of state from Observations	68
6.3	Reconstructing $w(z)$	69
6.3.1	Zero curvature assumption	69
6.3.2	Uncertainties in the Matter content Ω_m	72
6.4	Parametric Degeneracies	74
6.5	Conclusions and Outlook	75
6.6	Appendix	75
7	Conclusion	79
	Bibliography	92

List of Figures

1.1	Curvature and the density parameter	4
3.1	Relation between consistency equations	25
3.2	Schematic representation of e-foldings separation	26
4.1	Decorrelation of the scalar running	33
4.2	Running versus spectral tilt at several scales	34
4.3	Scalar tilt versus tensor-scalar ratio at several scales	36
4.4	Variation of parameter plane area with scale	37
4.5	ϵ versus η plane at lowest order	38
4.6	ϵ versus η plane at next order	40
4.7	n_S versus r with no running	41
4.8	Degradation of constraints with inclusion of running	42
4.9	ϵ versus η with dataset compilation	43
4.10	Degradation of constraints with dataset compilation	44
4.11	Computational code for chain analysis	47
4.12	Variation of area with bin number	48
5.1	Ω_{DE} for several models	50
5.2	Observables for polynomial models	51
5.3	Evolution of energy density in scaling models	55
5.4	Equation of state in scaling models	56
5.5	Observables for the double exponential potential	57
6.1	The curvature-dark energy degeneracy	63
6.2	Ω_k likelihood for different equations of state	64
6.3	Error contours for the (w_0, w_a) plane	65
6.4	Reconstructing the dark energy assuming zero curvature	70
6.5	Reconstructing dark energy from volume measurements	72
6.6	Reconstructing dark energy from incorrect matter density	73
6.7	Low redshift variation in $w(z)$ from $H(z)$ and $D(z)$	74
6.8	Degeneracies with the CPL parameterisation	76
6.9	Example figure from sample code	78

Aos meus pais

Chapter 1

Introduction

*It is not because things are difficult that we do not dare;
it is because we do not dare that they are difficult.*

SENECA

Cosmology is the one of the oldest forms of human enquiry. Ever since the onset of civilization, mankind has asked itself questions about the universe's origins, extent and destiny. Despite this it was not till recently that cosmology evolved from a mainly speculative and flaky science and matured into a fullgrown data driven research field, with observational cosmologists playing as important a role as model builders, and competitive theories being put to the test with ever increasing precision.

Research fields like the Cosmic Microwave Background (CMB), Large Scale Structure (LSS), Gravitational Lensing, Supernovae, and Big Bang Nucleosynthesis (BBN), all measure different cosmological parameters and complement each other, contributing into providing us with an extraordinarily detailed picture of the universe.

Inflation has given us an elegant and precise quantitative description of the earliest times. Recently, the Wilkinson Microwave Anisotropy Probe (WMAP) ¹ satellite announced results from its 5yr data analysis with implications that continue to provide strong support for the inflationary paradigm. Among its exciting results is a definite evidence for light neutrinos, now at 99.5% confidence, a new upper bound on the tensor-to-scalar ratio of 0.2%, and the exclusion of a scale invariant spectrum with a confidence level of over 80%. Furthermore the combinations of independent datasets is converging towards a preferred value for n_S , and the WMAP5 data alone is now sufficient to rule out the self-interacting $\lambda\phi^4$ potential. These conclusions were not possible with the previous

¹<http://map.gsfc.nasa.gov/>

wmap3yr dataset and come to provide more support for what may be a viable model for the origin of structure from a phenomenological point of view.

Meanwhile the puzzle of what seems to be the dominant component of the universe continues under intense scrutiny by the community challenging us to either change our theories of the fundamental particles or those governing the laws of gravity. The lack of a compelling hypothesis for the mechanism behind acceleration has shifted much of the focus towards observations. Complementing kinematical with dynamical probes will help to shed light on the different effects of dark energy on cosmological parameters.

A joint subcommittee (Albrecht et al. (2006)) has been formed to advise funding agencies and outline a program for dark energy research, by comparing and quantifying the merit of different observational techniques and proposed surveys.

They found that a combination of different observational techniques is the best method to insure progress by increasing the current figure-of-merit of current ongoing experiments by a factor of ten. Upcoming ground and space based surveys should measure w at the percent level and w' at the ten percent level.

We are strongly confident that the next round of precision measurements will provide significant insight into the nature of physics driving acceleration and that of the high energy theories responsible for inflation.

1.1 General setup

Our cosmology today rests on the assumptions that the universe is on large scales isotropic and homogeneous. This is sometimes called the cosmological principle and is based on extensive observational evidence, most notably from the CMB and distribution of large scale structure. Although these are quite simple assumptions they are rather quite restrictive and the only space-time metric compatible with its requirements is the so-called Robertson-Walker (RW) metric (Liddle and Lyth (2000); Dodelson (2003); Kolb and Turner (1990)),

$$ds^2 = -dt^2 + a^2(t) \left[\frac{dr^2}{1 - kr^2} + r^2(d\theta^2 + \sin^2\theta d\psi^2) \right] \quad (1.1)$$

where r , θ and ψ are 'comoving' polar coordinates, which remain fixed for objects that have no other motion than the general expansion of the universe. The parameter k is undetermined and measures the spatial curvature (see Eq. (1.8) below). The dimensionless parameter $a(t)$ is the scale factor and describes cosmological expansion. We normalize it by taking $a_0 \equiv a(t_0) = 1$, where t_0 is the present cosmic time.

For a universe described by the above metric Einstein's equations lead to two independent equations (throughout we use natural units $c = \hbar = 1$, except where explicitly stated),

$$H^2 = \frac{8\pi G}{3}\rho - \frac{k}{a^2}, \quad (1.2)$$

$$\dot{H} = -\frac{4\pi G}{3}(\rho + p) + \frac{k}{a^2}. \quad (1.3)$$

Eq. (1.2) is the Friedman Equation, where $H \equiv \dot{a}/a$ is the Hubble parameter, and ρ and p represent the energy density and pressure of all energy components and particle species in the universe. Eliminating the term k/a^2 in the above Eq. (1.2) and Eq. (1.3) we obtain the equation governing acceleration,

$$\frac{\ddot{a}}{a} = -\frac{4\pi G}{3}(\rho + 3p) . \quad (1.4)$$

The evolution of the energy densities is given by the continuity equation, obtained by combining Eq. (1.2) and Eq. (1.3),

$$\dot{\rho} + 3\frac{\dot{a}}{a}(\rho + p) = 0 \quad (1.5)$$

The continuity equation is a consequence of the Bianchi identities and expresses the conservation of the energy-momentum tensor.

1.1.1 The density parameter

The Friedman equation, Eq. (1.2), can be recast in a form that illustrates the balance between geometry and energy density components in the evolution of the universe,

$$\Omega(t) - 1 = \frac{k}{(aH)^2} . \quad (1.6)$$

Here $\Omega(t) \equiv \rho(t)/\rho_c(t)$ is the dimensionless density parameter and $\rho_c(t)$ is the density required to give a flat universe ($k = 0$),

$$\rho_c(t) \equiv \frac{3H^2(t)}{8\pi G} . \quad (1.7)$$

We see that the density determines the geometry of the universe and we obtain closed, flat or open universes according to ρ values, (see also Fig. 1.1),

$$\begin{aligned} \Omega &> 1 \text{ or } \rho > \rho_c \Rightarrow k = +1 , \\ \Omega &= 1 \text{ or } \rho = \rho_c \Rightarrow k = 0 , \\ \Omega &< 1 \text{ or } \rho < \rho_c \Rightarrow k = -1 . \end{aligned} \quad (1.8)$$

If we also define a density parameter associated with curvature

$$\Omega_k \equiv -\frac{k}{a^2 H^2} , \quad (1.9)$$

the Friedman equation takes the particularly simple form,

$$\Omega + \Omega_k = 1 , \quad (1.10)$$

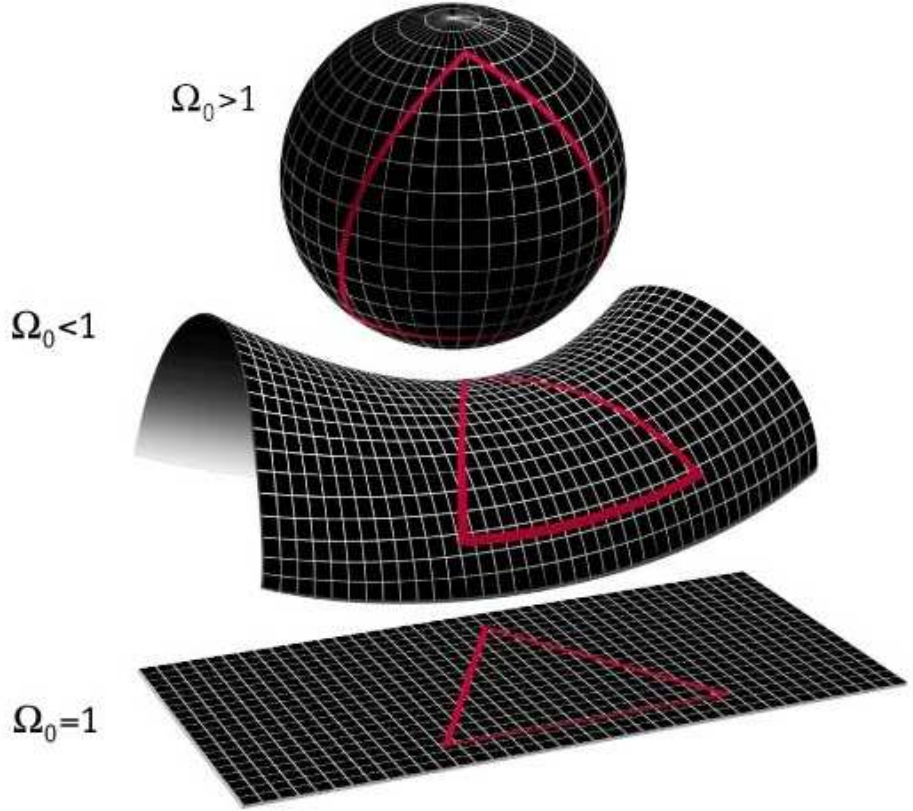


Figure 1.1: The density parameter, Ω determines the spatial curvature of the universe

clearly illustrating the balance between the energy budget and curvature content. If we consider a barotropic perfect fluid — in other words a component which can be completely characterized by its energy density and pressure — and assume a constant Equation of State (EoS), $w = p/\rho$, the energy density has the simple form obtained via Eq. (1.5),

$$\rho \propto a^{-3(1+w)} \quad (1.11)$$

The left hand side of the Friedman equation is to include all energy components in the universe and with the solution Eq. (1.11) we can write,

$$\rho = \sum_i \rho_{i,0} \left(\frac{a}{a_0} \right)^{-3(1+w_i)} = \sum_i \rho_{i,0} (1+z)^{3(1+w_i)} \quad (1.12)$$

where we introduced redshift z as

$$1+z = \frac{a}{a_0}, \quad (1.13)$$

which measures the fractional growth of the scale factor.

For the different fluids we have,

$$\text{radiation} : w_r = 1/3 \rightarrow \rho_r(z) = \rho_{m,0} (1+z)^4, \quad (1.14)$$

$$\text{matter} : w_m = 0 \rightarrow \rho_m(z) = \rho_{r,0} (1+z)^3, \quad (1.15)$$

$$\text{cosmological constant} : w_\Lambda = -1 \rightarrow \rho_\Lambda(z) = \rho_\Lambda. \quad (1.16)$$

Making use of the definition of the density parameter, Ω , the Friedman equation takes yet another useful form,

$$H^2 = H_0^2 \sum_i \Omega_{i,0} (1+z)^{3(1+w_i)}. \quad (1.17)$$

If we drop the assumption of a perfect fluid the EoS can no longer be taken constant and the solution of Eq. (1.11) then takes the generic form,

$$\rho_0 (1+z)^{3(1+w)} \rightarrow \rho_0 \exp \left(3 \int_0^z \frac{1+w(z')}{1+z'} dz' \right). \quad (1.18)$$

1.1.2 Distance Measurements

Distances are a very important tool in cosmology though also extremely difficult to measure. They are traditionally used to map the expansion history, through the distance versus redshift relation, and have recently been of great interest as first indicators of the current accelerated cosmic expansion. In general they are integrals over the expansion history, which involve an integral over the equation of state, so that there exists degeneracy among the several cosmological parameters contributing to the distance. In order to break these degeneracies we require measurements across a range of redshifts, as well as measurements of other complementary non-geometrical quantities. We will return to this subject in chapter 6. There are several ways to define distance of an astrophysical object. They all have the same meaning in a Minkowski universe, but differ if the universe is expanding. The comoving distance, stays constant as the universe expands while physical distances scale with scale factor $a(t)$. An alternative is to consider the luminosity of an object. We define luminosity distance as

$$d_L(z) = \frac{(1+z)}{H_0 \sqrt{-\Omega_k}} \sin \left(\sqrt{-\Omega_k} \int_0^z dz' \frac{H_0}{H(z')} \right), \quad (1.19)$$

where the dependence on the geometry of the universe is clear through Ω_k .

In Astronomy the distance luminosity is determined via the distance modulus, $\mu(z)$, which gives the difference between the apparent and absolute magnitude of an object and is related to the distance luminosity by

$$\mu(z) = m - M = 5 \log_{10} \left(\frac{d_L(z)}{\text{Mpc}} \right) + 25. \quad (1.20)$$

Another useful probe of cosmological parameters and expansion history is the evolution of the *fractional volume as a function of redshift*. It can be measured through num-

ber counts of galaxy clusters (see section 2.2.1) and it relates to the distance luminosity through,

$$V'(z) \equiv \frac{d^2V}{dzd\Omega} = \frac{c^3 D^2(z)}{H_0^2 H(z)}. \quad (1.21)$$

The distance luminosity can be used to identify standard candles, i.e., objects for which we know the intrinsic luminosity. If instead we know the length of an object it is useful to consider the angular diameter distance related to d_L by,

$$d_A = \frac{1}{(1+z)^2} d_L \quad (1.22)$$

1.1.3 Acceleration

Accelerated expansion of the universe occurs because of the existence of states with negative pressure. Eq. (1.4) shows that a positive pressure contributes to deceleration, whereas a negative pressure can cause the expansion to accelerate. Negative pressure acts as a form of repulsive gravity, and acceleration occurs when the balance between energy density and pressure is such that,

$$\rho + 3p < 0. \quad (1.23)$$

For an ideal perfect fluid, with constant equation of state, this means the condition for acceleration becomes,

$$w < -1/3, \quad (1.24)$$

so that in order to explain the current acceleration we need to posit the existence of an exotic fluid dominating the energy budget, with negative EoS. The cosmological constant is the particular case $w = -1$, and for this the continuity equation, Eq. (1.5), yields constant energy density ρ , and constant H . The scale factor then grows exponentially according to,

$$a(t) \propto e^{Ht}. \quad (1.25)$$

States with negative pressure are easily obtained with the physics of a scalar field. For a canonical scalar field ϕ in an FRW background, the energy density and pressure are given by (ignoring spatial derivatives)

$$\begin{aligned} \rho_\phi &= \frac{1}{2} \dot{\phi}^2 + V(\phi), \\ p_\phi &= \frac{1}{2} \dot{\phi}^2 - V(\phi), \end{aligned} \quad (1.26)$$

so that any state which is dominated by the potential energy of a scalar field will give origin to a period of accelerated expansion.

Chapter 2

Cosmic Acceleration – Inflation and Dark Energy

2.1 Inflation

Inflation was proposed in the beginning of the 1980's to solve the long-standing problems of the Hot Big Bang Model, making use of the idea of a period of accelerated expansion in the very early universe. Later it turned out inflation could also solve the problem of generating the density perturbations that gave origin to structure and get rid of the unwanted relics associated with high energy models. Twenty-five years later, and with a wide range of different models having been proposed in the meantime, inflation is in its strongest position ever, with successive measurements and observations of the CMB continuously eliminating its competitors, and placing it as the preferred contender to explain the anisotropies that fill the background sky.

We'll restrict ourselves to single-field slow-roll inflation and briefly describe its dynamics and main properties (for reviews see Liddle and Lyth (2000); Guth and Kaiser (2005); Linde (2008); Langlois (2004)). The basic idea is that at some early time at least some patch of the universe was dominated by the potential energy of a (slowly rolling) scalar field. During inflation this patch expands rapidly transmitting zero-point quantum fluctuations to larger length scales and transferring them into the needed classical inhomogeneities in the mass-energy distribution. The curvature terms becomes negligible with the large amount of expansion, solving the flatness problem. As the field continues to roll down the potential it acquires kinetic energy, that will eventually dominate the potential energy and cause inflation to end. When it reaches the minimum of the potential it begins to oscillate, and decays into a thermal bath of elementary particles.

The equations governing these dynamics are the Klein-Gordon equation, which describes the evolution of a minimally-coupled canonical scalar field, and the corresponding Friedman equation,

$$\ddot{\phi} + 3H\dot{\phi} + V'(\phi) = 0 \quad (2.1)$$

$$H^2 = \frac{8\pi G}{3} \left(\frac{1}{2}\dot{\phi}^2 + V(\phi) \right) \quad (2.2)$$

As we discussed in section 1.1.3 acceleration is attained through domination by the potential energy and one of the ways to achieve this is to ensure the scalar field has small kinetic energy. This is the premiss of the slow-roll approximation which consists in neglecting the kinetic term in Eq. (2.2) and the acceleration term in Eq. (2.1), so that one gets the simplified system,

$$3H\dot{\phi} + V'(\phi) \simeq 0 \quad (2.3)$$

$$H^2 \simeq \frac{8\pi G}{3} V(\phi) \quad (2.4)$$

The velocity of the scalar field is then given by Eq. (2.3)

$$\dot{\phi} \simeq -\frac{V'}{3H} \quad (2.5)$$

so that the slow-roll requirement $\dot{\phi}^2/V \ll 1$ translates to

$$\epsilon_V \equiv \frac{m_{\text{Pl}}^2}{16\pi} \left(\frac{V'}{V} \right)^2 \ll 1 \quad (2.6)$$

where we have introduced the Planck mass,

$$m_{\text{Pl}} \equiv \frac{1}{\sqrt{G}}. \quad (2.7)$$

On the other hand, requiring the field acceleration to be small, using the time derivative of Eq. (2.5) yields,

$$\eta_V \equiv \frac{m_{\text{Pl}}^2}{8\pi} \frac{V''}{V} \ll 1. \quad (2.8)$$

To lowest order in slow-roll these are the requirements for the approximation to hold. ϵ_V and η_V are the first two slow-roll parameters, expressed in terms of the potential and this way the slow roll approximation consists in expressing the dynamics of the scalar field in terms of derivatives of the potential: to first order the requirement is that the potential's slope and curvature be small. However since in principle the potential is a free function, all of its derivatives at each point are independent quantities, so the number of slow-roll parameters we in principle can define is infinite (Lidsey et al. (1997)).

There is an alternative formulation of the slow-roll condition which uses the Hubble parameter H instead of V . There are several advantages to this alternative approach which are discussed in Liddle et al. (1994). Expressing the slow-roll parameters in terms of derivatives of V merely restricts the form of the potential not the dynamics of the solutions and it also, in general, doesn't allow to obtain exact solutions. Placing conditions on the Hubble function instead permits a more clear analytic interpretation. For example with the Hubble Slow Roll parameters the condition for inflation to end is exactly $\epsilon_H = 1$ whereas for the potential slow roll parameters this condition is only approximate. Furthermore, since contrary to the potential H is an observable, the Hubble function is a more natural geometric variable.

This way the potential approach is best suited for studies where one is interested in

a specific form of the potential as the starting point, where H is more appropriate for a general study of inflationary solution properties.

In terms of the Hubble parameters the first few slow roll parameters were given by Liddle et al. (1994),

$$\epsilon \equiv \frac{m_{\text{Pl}}^2}{4\pi} \left(\frac{H'}{H} \right)^2 ; \quad (2.9)$$

$$\eta \equiv \frac{m_{\text{Pl}}^2}{4\pi} \frac{H''}{H} ; \quad (2.10)$$

$$\xi \equiv \frac{m_{\text{Pl}}^2}{4\pi} \left(\frac{H' H'''}{H^2} \right)^{1/2} ; \quad (2.11)$$

$$\sigma \equiv \frac{m_{\text{Pl}}^2}{4\pi} \left(\frac{H'^2 H''''}{H^3} \right)^{1/3} . \quad (2.12)$$

The amount of inflation can be quantified by specifying the fractional growth of the scale factor, i.e., the increase in size of the inflationary patch. This is generally a large number so we take the logarithm of the growth and define the number of e-folds before the end of inflation as (Liddle and Lyth (2000)).

$$N \equiv \ln \frac{a(\text{end})}{a(t)} = \int_t^{t_{\text{end}}} H dt \simeq \frac{8\pi}{m_{\text{Pl}}^2} \int_{\phi_{\text{end}}}^{\phi} \frac{V'}{V} d\phi . \quad (2.13)$$

In order to solve the problems of the horizon and flatness usually around 70 e-folds of inflation are needed.

2.1.1 Inflationary Perturbations

By far the most useful property of the theory of inflation is its ability to generate the inhomogeneities which may explain the observed large scale structure in the universe. These inhomogeneities arise due to the fluctuation of the field about its vacuum state and generate a *gaussian* and *nearly scale invariant* spectrum of primordial fluctuations (for a review of inflationary perturbation theory see Liddle and Lyth (2000) and references therein). In this section we follow the derivation of Lidsey et al. (1997).

Scalar perturbations

The accelerated expansion induces perturbations in the metric. Of these, the scalar perturbations are the ones we are more interested in since they couple to the energy–momentum tensor of matter and radiation, and are ultimately responsible for CMB anisotropies and large scale structure.

These perturbations can be expressed in terms of the curvature perturbation which reads,

$$\mathcal{R} = -\Psi - \frac{H}{\dot{\phi}} \delta\phi \quad (2.14)$$

where $\delta\phi$ represents the fluctuation of the scalar field, and the Hubble rate and $\dot{\phi}$ are obtained with the background Friedmann and acceleration equations, Eq. (1.2) and Eq. (1.4). The evolution of these perturbations is given by the Einstein action, which needs to be taken to second order if we are to derive expressions for the perturbations at first order. In what follows it will prove convenient to introduce the Mukhanov potential

$$u = -z\mathcal{R} \quad (2.15)$$

where

$$z \equiv a \frac{\dot{\phi}}{H} \quad (2.16)$$

After obtaining the momentum conjugate to the Mukhanov variable u and quantizing, we expand the \hat{u} operator in plane waves. We can then derive the field equations for each k mode, u_k , by setting the variation of the second order action to zero to obtain,

$$\frac{du_k^2}{d\tau^2} + \left(k^2 - \frac{1}{z} \frac{d^2 z}{d\tau^2} \right) u_k = 0, \quad (2.17)$$

where τ denotes conformal time.

The solutions to Eq. (2.17) are normalized with the usual Wronskian condition and the boundary conditions for each mode u_k are obtained by requiring the solution to approach a plane wave at small angular scales, and to be constant on large wavelength, super-horizon scales i.e.,

$$u_k(\tau) \rightarrow \frac{1}{\sqrt{2k}} e^{-ik\tau}, \quad k \gg aH, \quad (2.18)$$

and

$$u_k \propto z, \quad k \ll aH. \quad (2.19)$$

In order to revert back to the curvature perturbation, \mathcal{R} , given by Eq. (2.14), we similarly expand \mathcal{R} in plane waves. The power spectrum of the curvature perturbation can then be obtained in terms of the vacuum expectation value,

$$\langle \mathcal{R}_{\mathbf{k}} \mathcal{R}_{\mathbf{l}}^* \rangle = \frac{2\pi^2}{k^3} \mathcal{P}_{\mathcal{R}} \delta^{(3)}(\mathbf{k} - \mathbf{l}) \quad (2.20)$$

The vacuum expectation value on the left hand side can be obtained by combining u given by Eq. (2.15) with the mode expansion of \mathcal{R} , and taking into account the commutation relations for between different modes k, k_* . This yields,

$$\langle \mathcal{R}_{\mathbf{k}} \mathcal{R}_{\mathbf{l}}^* \rangle = \frac{1}{z^2} |u_k^2| \delta^{(3)}(\mathbf{k} - \mathbf{l}). \quad (2.21)$$

So the power spectrum in Eq. (2.20) becomes

$$P_{\mathcal{R}}^{1/2}(k) = \sqrt{\frac{k^3}{2\pi^2}} \left| \frac{u_k}{z} \right|. \quad (2.22)$$

u_k is given by the solution of Eq. (2.17). In order to solve the wave equation we take a solution for the power law inflation, which is exact, and then expand about this solution in terms of slow roll parameters. Such an approach is more useful since it also yields the results for the next-order in slow-roll case, which we consider in the next section. For the lowest-order case this yields,

$$P_{\mathcal{R}}^{1/2}(k) = \frac{1}{m_{\text{Pl}}^2} \frac{H^2}{|H'|} \Big|_{k=aH}, \quad (2.23)$$

where the expression is evaluated at the time the cosmological scales in which we are interest leave the horizon, $k = aH$.

Tensor perturbations

As we pointed out in the previous section, in addition to scalar perturbations, inflation also predicts tensor perturbations in the metric, which yield a spectrum of gravitational waves. These do not couple to density perturbations and so are not responsible for the large scale structure of the universe. However they do induce fluctuations in the CMB and constitute a unique signature of inflation, which we will see in chapter 3.

Tensor perturbations do not couple to any other part of the perturbation components so their technical analysis is considerably simpler than for the scalar perturbation case. We begin similarly by quantizing and fourier decomposing the gravitational waves, and writing down the power spectrum in terms of the expectation value of the tensor modes, ν_k , as

$$\langle \hat{\nu}_{\mathbf{k},\lambda} \hat{\nu}_{1,\lambda}^* \rangle = \frac{m_{\text{Pl}}^2 a^2 2\pi^2}{32\pi k^3} \mathcal{P}_{\text{T}} \delta^{(3)}(\mathbf{k} - \mathbf{l}) \quad (2.24)$$

where λ denotes the two independent polarizations states $\lambda = +, \times$.

Setting the variation of the Einstein action to zero yields a wave equation of a similar form to the one for the scalar case Eq. (2.17),

$$\frac{d\nu_k^2}{d\tau^2} + \left(k^2 - \frac{1}{a} \frac{d^2 a}{d\tau^2} \right) \nu_k = 0, \quad (2.25)$$

However the situation is now simplified since it is the scale factor $a(\tau)$ rather than the variable $z(\tau)$ in Eq. (2.16) which appears here. Again solving for the exact power law case and expanding in terms of slow-roll variables we obtain, for the lowest order case,

$$P_{\text{T}}^{1/2}(k) = \frac{4}{\sqrt{\pi}} \frac{H}{m_{\text{Pl}}} \Big|_{k=aH}, \quad (2.26)$$

where once more we are interested in the perturbation at the time the cosmological scales leave the horizon, $k = aH$.

It will prove convenient to work with rescaled versions of the spectra. Following the

notation of Lidsey et al. (1997),

$$A_S(k) \equiv \frac{2}{5} P_{\mathcal{R}}(k)^{1/2} \cong \frac{4}{5m_{\text{Pl}}^2} \left. \frac{H^2}{|H'|} \right|_{k=aH}; \quad (2.27)$$

$$A_T(k) \equiv \frac{1}{10} P_T(k)^{1/2} \cong \frac{2}{5\sqrt{\pi}} \left. \frac{H}{m_{\text{Pl}}} \right|_{k=aH}, \quad (2.28)$$

where prime is derivative with respect to field value ϕ .

During inflation the Hubble parameter is slowly varying and therefore the spectra acquire a dependence on the scale at which the Hubble radius crosses the horizon. For this reason it is useful to consider a parametrization in terms of cosmological scale k , as a power law with variable spectral indices,

$$A_S^2(k) \propto k^{n_S(k)-1}, \quad (2.29)$$

$$A_T^2(k) \propto k^{n_T(k)}. \quad (2.30)$$

The constant of proportionality also depends on the scale at which they are evaluated and in order to avoid this we take for the spectral indices a more suitable definition,

$$n_S(k) - 1 \equiv \frac{d \ln A_S^2}{d \ln k} \quad (2.31)$$

$$n_T(k) \equiv \frac{d \ln A_T^2}{d \ln k} \quad (2.32)$$

In the slow-roll approximation we can deduce useful relations between the spectral indices and the slow-roll parameters,

$$n_S - 1 = 2\eta - 4\epsilon, \quad (2.33)$$

$$n_T = -2\epsilon. \quad (2.34)$$

We have the relative amplitude of the two spectra as,

$$\frac{A_T^2}{A_S^2} = \epsilon, \quad (2.35)$$

so that by Eq. (2.34),

$$2 \frac{A_T^2}{A_S^2} = -n_T. \quad (2.36)$$

Eq. (2.36) means there exists a simple relation between the tilt of the tensor spectrum and the amplitude of tensor perturbations relative to that of scalar ones. This is called the *consistency equation of slow roll inflationary models*. It was recognized as such by Kosowsky and Turner (1995); Lidsey et al. (1997) and expresses quite a distinctive signature particular to metric perturbations in inflation generated primordial fluctuations. It is hard to develop another mechanism yielding the primordial fluctuations and originating the same spectra.

Eq. (2.36) is in a useful form since it relates purely observable quantities. This means

that were we able to measure primordial gravitational waves we would be able to test directly the slow roll inflationary paradigm.

2.1.2 Next Order in Slow Roll

If we wish to go beyond the slow roll approximation we can derive expressions that estimate the next order corrections using essentially no assumptions other than linear perturbation theory. This was done for the first time by Stewart and Lyth (1993). They obtained the expressions in the square brackets in Eqs. (2.37) and (2.38) which correct the expressions in Eqs. (2.27) and (2.28),

$$A_S(k) \cong \frac{4}{5m_{\text{Pl}}^2} [1 - (2C + 1)\epsilon + C\eta] \frac{H^2}{|H'|} \Big|_{k=aH} ; \quad (2.37)$$

$$A_T(k) \cong \frac{2}{5\sqrt{\pi}} [1 - (C + 1)\epsilon] \frac{H}{m_{\text{Pl}}} \Big|_{k=aH} . \quad (2.38)$$

and $C \simeq -0.73$ is the Euler–Mascheroni constant. Essentially these are derived by comparing the approximate relation $3H\dot{\phi} = -V'(\phi)$ with the exact expression $\ddot{\phi} + 3H\dot{\phi} = -V'(\phi)$. The error is

$$\frac{\ddot{\phi}}{H\dot{\phi}} \simeq \epsilon - \eta \quad (2.39)$$

so that the spectra will pick corrections of order ϵ and η as we can see in Eq. (2.37) and (2.38).

2.2 Dark Energy

In 1998 two independent teams (Perlmutter et al. (1997); Riess et al. (1998)) gave evidence in support of an accelerated expansion of the Universe today. 10 years on, the puzzle of cosmological acceleration — dubbed dark energy — remains one of the most intriguing enigmas in modern day science. Much activity has come from both the theoretical and observational sectors of the physics community in an attempt to pin down its origin.

Among the multitude of proposals to solve the problem of dark energy there have been those that are particle based and those gravity based. The latter consists of altering the left–hand side of the Friedman equation, the geometry content, by introducing higher curvature corrections to the Einstein–Hilbert action; and the former attempts to obtain acceleration by altering the right–hand side, the energy content, by postulating some sort of exotic form of matter with energy density that makes for most of the total Ω today.

A third approach consists of altering the Robertson–Walker metric itself and so in dropping the assumption of homogeneity. These are the perturbative inhomogeneous models which attempt to get acceleration as a metric backreaction effect; and the exact inhomogeneous models that allow for a free distribution of matter to create the illusion of acceleration we observe today.

2.2.1 Probes of Dark energy

Dark Energy affects the evolution of the Universe primarily through the distance luminosity relation, the expansion history, and the growth of structure. It is by measuring these quantities that we expect to infer information about the amount of Dark Energy today as well as its recent evolution.

The Dark Energy Task Force (DETF — Albrecht et al. (2006)) is a consortium set up by a NASA, NSF, and DOE to study and devise a comprehensive program for understanding the origin of Dark Energy. One of its goals is to identify the methods and experimental probes that will optimize immediate, near, and longer term programs to understand the cosmic acceleration phenomenon.

The DETF assessed different experimental methods for probing Dark Energy and advised for focus on the following,

Type 1a Supernovae — Supernovae are one of the main reasons why we now consider dark energy as the main constituent of the universe. They are white dwarf stars that accrete matter until they reach the Chandrasekhar limit and explode. For this reason they are believed to be good standard candles in which case they can be used to infer the distance-redshift luminosity relation. Their redshift can be inferred from their spectral lines or those of the galaxy host.

Baryon Acoustic Oscillations — BAO are pressure waves in the early universe baryon-radiation fluid, traveling at a speed of $c_s = c/\sqrt{3}$. At the moment of proton-electron recombination these waves cease to propagate and the perturbation is frozen in the matter distribution. The distance traveled up till then is called the sound horizon, r_s . The physics of these oscillations is well understood, allowing us to determine this distance to a high degree of accuracy that can thus serve as a standard ruler for distance measurements. Identifying the BAO as a transverse angle gives the combination $d_A(z)/r_s$, where $d_A(z)$ is the angular diameter distance Eq. (1.22), while its determination along the line of sight is sensitive to the Hubble rate through $H(z) * r_s$.

Clusters of galaxies — Clusters of galaxies are tracers of the regions with highest initial density fluctuations that have undergone gravitational collapse. Their abundance can be measured and is sensitive to dark energy through the comoving volume – that is affected by the expansion history – and through the mass function – that is dependent on the growth of the density perturbation.

Weak Lensing— The deflection of light by gravitationally collapsed objects can be used to trace dark energy. The deflection angle depends on the mass of the collapsed object – hence can yield measurements of the growth history – and on the distances between the source lens and the observer, and so can give measurements of the comoving distance.

Furthermore the DETF also provides guidance on evaluating the scientific merits of

long-term proposed experiments, both ground and space based. The evaluation is based on the *figure-of-merit* of the experiment's forecasts. This is defined to be the reciprocal of the area of the error ellipse in the (w_0, w_a) plane that encloses the 95% confidence level contour. (w_0, w_a) are the parameters of the Chevallier–Polarski–Linder parametrization for the equation of state, discussed in section 2.2.4.

2.2.2 Acceleration through scalar fields - Scaling Models

Quintessence is one of the simplest mechanisms for cosmic acceleration. It makes use of the physics of a scalar field, which most certainly has its origins in the theory of early universe inflation. Scalar fields arise naturally in extensions of the standard model, and as we discussed in Section 1.1.3, demanding some requirements on their dynamics induces acceleration making them good candidates for dark energy. Furthermore dynamical scalar fields – quintessence – have a varying energy density and so can help explain the smallness of the dark energy density today.

So far many scalar field models have been proposed as an alternative to a cosmological constant. Here we examine a particular property of a class of scalar fields that enables the mimicking of the evolution of the background dominant energy component. This means the energy density of the scalar field satisfies

$$\frac{\rho_\phi}{\rho_m} = \text{const.}, \quad (2.40)$$

where ρ_ϕ is the energy density of the scalar field and ρ_m is the energy density of the background. These are the *scaling solutions* and have been extensively studied in many dark energy scenarios, (Ratra and Peebles (1988); Wetterich (1988); Copeland et al. (1998b); Ferreira and Joyce (1998); Copeland et al. (2006)). There are many potentials that give origin to the scaling behaviour, and here we focus on the exponential potential, presenting the general framework for studying these models.

Scaling fields dynamics

Consider a canonical scalar field ϕ , minimally coupled to gravity, with the following exponential potential

$$V(\phi) = M^4 e^{-\lambda\kappa\phi}, \quad (2.41)$$

where M is a constant with dimensions of mass, λ is a dimensionless constant, and $\kappa^2 = 8\pi G = 8\pi m_{\text{pl}}^{-2}$.

If the field is evolving in a spatially flat FRW universe in which there is a background fluid with equation of state $w_b = p_m/\rho_m$, then the evolution equation for this scalar field has two attractor solutions, which depend on the values of λ and w_b (Copeland et al. (1998b); Ferreira and Joyce (1998)):

- if $\lambda^2 > 3(1 + w_b)$ then the scalar field will enter a scaling regime and will follow the evolution of the background fluid with $w_\phi = p_\phi/\rho_\phi = w_b$ and $\Omega_\phi = 3(1 + w_b)/\lambda^2$;

- if $\lambda^2 < 3(1 + w_b)$ then the field will be the dominant component of the universe, with $w_\phi = -1 + \lambda^2/3$ and $\Omega_\phi = 1$.

Exiting the scaling regime

In order to give rise to late time accelerated expansion the field must at some point exit the scaling regime and become the dominant component. This is realized if the slope of the potential becomes shallow at late times, when compared with the slope of the scaling solution. In Chapter 5 we will study one of the ways to achieve this by considering a double exponential potential (Barreiro et al. (2000); Sen and Sethi (2002); Neupane (2004a,b)).

2.2.3 Early Dark Energy Constraints

One of the aspects that arises when considering dynamical behaviour for dark energy is the possibility of a considerable contribution of dark energy at early times as well. The mechanism which provides us the best constraints on early dark energy is Big Bang Nucleosynthesis (BBN) - the synthesis of the lightest elements by the weak interactions taking place during the initial few minutes (Pagel (1997); Schramm and Turner (1998)). The introduction of an extra fluid during this era will alter the abundance rate of the lightest elements being generated by the weak interactions at that time.

At the temperature of about 1MeV the universe will have cooled enough so that protons and neutrons are non relativistic and in thermal equilibrium. When the temperature drops sufficiently the weak interactions keeping proton to neutron conversion reactions in equilibrium freeze and their abundance ratio becomes fixed. The expression controlling this balance is

$$\frac{N_n}{N_p} = \frac{m_n}{m_p} \exp \left[-\frac{m_n - m_p}{k_B T} \right]. \quad (2.42)$$

The temperature at which the weak interactions cease to take place depends on the number of particle species. If we wish to consider the presence of a dark energy component at early times we need to introduce a new degree of freedom. This affects the freeze-out temperature and hence the expansion rate at that time. Since the dependence is exponential, a small change in the temperature will have a large effect on the proton–neutron ratio today, making the BBN bound a good test for early universe dark energy.

Ferreira and Joyce (1998) found a relation between the effective number of degrees of freedom introduced with the addition of an extra component and the value of the energy density of that extra component at nucleosynthesis,

$$\Omega_{\text{DE}}(1\text{MeV}) < \frac{7\Delta N_{\text{eff}}/4}{10.75 + 7\Delta N_{\text{eff}}/4}. \quad (2.43)$$

ΔN_{eff} is the maximum number of relativistic degrees of freedom additional to those in the standard model, 10.75 is the number of degrees of freedom in the standard model, and $\Omega_{\text{DE}}(1\text{MeV})$ is the corresponding maximum contribution to the energy density of a scalar field at that time.

The value to consider for ΔN_{eff} is not unanimous and subject to discussion in the literature (Schramm and Turner (1998); Kernan and Sarkar (1996); Birkel and Sarkar (1997); Copi et al. (1995)). It depends on the data, through observational method and statistical treatment. The range $\Delta N_{\text{eff}} \simeq 0.9 - 1.5$ translates into

$$\Omega_{\text{DE}}(1\text{MeV}) \simeq 0.13 - 0.2 \quad (2.44)$$

However Bean et al. (2001) were able to obtain a tighter bound by considering the abundance of deuterium instead,

$$\Omega_{\text{DE}}(1\text{MeV}) < 0.045. \quad (2.45)$$

This is the value we'll consider later on in chapter 5 for deriving considerations about early dark energy contribution in relation to its evolution today.

2.2.4 Parameterizations of Dark Energy

In section 2.2.2 we considered a reconstruction of dark energy properties based on the properties of a scalar field for which we know the potential. We may instead parametrise the dark energy $w(z)$ by assuming some functional form based on a number of chosen parameters. Such an approach, based on the reconstruction of the equation of state, is also the route most followed by current and planned surveys (Albrecht et al. (2006); Riess et al. (2007); Wood-Vasey et al. (2007))

Among the vast number of EoS parametrizations proposed so far (see for example Bassett et al. (2004); Johri (2004); Johri and Rath (2007); Linder (2008a)), likely the most commonly used is the Chevallier–Polarski–Linder (CPL) parametrization (Chevallier and Polarski (2001); Linder (2003)),

$$w_{\text{CPL}} = w_0 + w_a \frac{z}{1+z}. \quad (2.46)$$

Its parameters are the value of the equation of state today, w_0 , and its time variation $w_a = dw/d \ln a$. Unlike a parametrization linear in z , that becomes unsuitable at $z > 1$, the expansion variable $x = z/(z+1) < 1$ makes it a more suitable expansion. Furthermore it has bounded behaviour at high redshift, $w(\infty) = w_0 + w_1$, and linear behaviour at low redshift.

The CPL parametrization also has a simple physical interpretation, its time derivative is related to the slow roll parameter V'/V (in the case that dark energy originates in the potential of a scalar field) and hence determines when the expansion enters the accelerated phase. It's also argued to describe accurately a wide variety of dark energy physics and exhibit good sensitivity to observational data (Linder (2008b)). For this reason it's widely used as the basis for the figure-of-merit of most current and upcoming experiments.

2.3 Bayesian Statistics

Statistics plays a crucial role in cosmological data analysis nowadays. In order to process and extract the maximum leverage of the unprecedentedly large volume of data at our disposal we must ensure we employ and develop optimal and adequate statistical methods. Cosmology must resort to a particular concept of probability. A frequentist analysis is not possible given that we can't study different realizations of the same experiment to examine different possible outcomes.

In this situation one resorts to the concept of probability as the degree-of-belief in a result, an idea that is the basis for Bayesian Estastics, for reviews see for example Mackay (2003); Parkinson (2008) and references therein. Bayes' theorem is one of the most commonly used results in cosmological parameter estimation and relates the conditional and marginal probabilities of two possible realizations of a particular event,

$$P(\theta|D) = \frac{P(D|\theta)P(\theta)}{P(D)}. \quad (2.47)$$

Eq. (2.47) is Bayes' theorem and states that the probability of a set of parameters being the correct within the data is given by the probability that that data could have originated in those set of parameters, multiplied by the probability of the prior which represents the probability of the parameters before any data is taken.

The left-hand side is the posterior probability and depends on the prior $P(\theta)$ (our a priori knowledge of the setup conditions), and on the data dependent term on the right-hand side, the likelihood, $P(D|\theta)$. The denominator, $P(D)$, is a normalization factor so its value is not important if we only wish to examine the relative probabilities of the various parameter sets.

Bayes' result allows us not only to infer our present degree of knowledge of the cosmological parameters but it also allows us to make predictions about observations we will make in the future (Parkinson (2008)).

2.3.1 Marginalization

Quite often when analysing constraints on a set of cosmological parameters, θ , one is not interested on the full set of parameters but on a subset thereof. Then the remaining are merely nuisance parameters that nevertheless contribute to the full posterior distribution. Marginalizing over one or a group of parameters consists in obtaining the probability of the parameter we are interested in, independently of the probability of the remaining set of parameters. In this sense it is a summation, or integral, over the probability of the remaining set of parameters,

$$P(A|D) = \int_0^\infty P(A, B|D)dB, \quad (2.48)$$

where A is the parameter we are interested in, and B represents the remaining set of parameters over which we are marginalizing.

This is also the case when we wish to present constraints and need to project the full

parameter volume onto a 1D or 2D surface. The subject of marginalizing over a group of parameters for presenting purposes will be discussed in chapter 4, where we analyse the loss of information on the distribution of the remaining parameters when doing so.

Chapter 3

The Inflationary Consistency Equation

3.1 Introduction

The inflationary proposal for the Early Universe is arguably the most promising theory capable of explaining the problems of the Hot Big Bang Model and the observed anisotropies present in the microwave sky. Among its key features are the prediction of an approximate scale invariant spectrum of density perturbations and the presence of a small amount of gravity waves. So far inflationary models and in particular single-field models are in good shape after release of the WMAP 3yr and 5yr analysis. The new data are consistent with a near to scale invariant red spectrum and put better constraints on the amount of the tensor fluctuations present in the CMB sky. However, in order to be a fully successful theory it needs a unique feature which would, if observed, strongly favour the inflationary paradigm against other proposals. Such a signature is provided by the consistency relation.

All single-field models predict a connection between the amplitude of density perturbations and that of gravity waves. That such a connection exists can readily be understood by noting that in these models both scalar and tensor perturbations have origin in the same function — the potential of the self interacting scalar field — and so can be related by eliminating this quantity in their defining equations.

In this chapter, we point out that this consistency relation is the first of an infinite hierarchy of consistency relations, connecting ever higher derivatives of the spectra. This hierarchy exists even at lowest-order in the slow-roll approximation. That such a hierarchy exists was first noted in the review of Lidsey et al. (1997), but we give here for the first time explicit expressions for these relations, both at lowest-order and next-order in slow-roll. Our analysis is restricted to the simplest class of inflation models, namely single-field slow-roll inflation with general relativity assumed valid.

To some extent this exercise is an academic one, as there seems little prospect of testing any of these relations beyond the first, and even it is likely to prove challenging (Song and Knox (2003)). Nevertheless, these relations offer a complete account of the connec-

tions between the two spectra, and so any other claimed consistency relation, exact or approximate, must follow from them if they are indeed consistency relations. In particular we examine the relationship between our formalism and the approximate consistency relation introduced by Chung et al. (2003) and further explored by Chung and Romano (2006). We demonstrate that it is indeed equivalent to the second consistency equation in the hierarchy, as already given by Lidsey et al. (1997).

3.2 Definitions

The perturbation spectra can be expressed in terms of the inflationary potential or the Hubble parameter. The two are connected by the approximate relation $3H^2 m_{\text{Pl}}^2 / 8\pi = V$ and represent slightly different approximation schemes (Liddle et al. (1994)). The Hubble rate provides a better geometrical interpretation and is a direct solution to the Friedmann equation, whereas an expansion based on the potential may have less analytical information given that the potential is an input to the Friedmann equation and so presupposes some approximation for obtaining a solution. For this reason here we choose to consider the Hubble-Slow-Roll expansion.

Following the notation of Lidsey et al. (1997), the spectra of scalar and tensor modes to next order in the slow-roll approximation are given by Eq. (2.37) and Eq. (2.38). The terms in square brackets are the Stewart–Lyth slow-roll correction to the spectrum (Stewart and Lyth (1993)); setting the square brackets to one gives the slow-roll result. We will use the symbol ‘ \cong ’ to indicate expressions as being equal within the slow-roll approximation to the order indicated by the included terms. In chapter 2 we introduced the first few slow-roll parameters in terms of the Hubble parameter as (Liddle et al. (1994)),

$$\epsilon \equiv \frac{m_{\text{Pl}}^2}{4\pi} \left(\frac{H'}{H} \right)^2 ; \quad (3.1)$$

$$\eta \equiv \frac{m_{\text{Pl}}^2}{4\pi} \frac{H''}{H} ; \quad (3.2)$$

$$\xi \equiv \frac{m_{\text{Pl}}^2}{4\pi} \left(\frac{H' H'''}{H^2} \right)^{1/2} ; \quad (3.3)$$

$$\sigma \equiv \frac{m_{\text{Pl}}^2}{4\pi} \left(\frac{H'^2 H''''}{H^3} \right)^{1/3} . \quad (3.4)$$

The wavenumber k can be related to the scalar field value via the exact relation

$$\frac{d \ln k}{d\phi} = \frac{4\pi}{m_{\text{Pl}}^2} \frac{H}{H'} (\epsilon - 1), \quad (3.5)$$

where without loss of generality we have assumed ϕ to increase during inflation.

The spectral indices given by Eq. (2.31) and Eq. (2.32) and their derivatives can be

written in terms of the slow-roll parameters by expressions such as

$$\begin{aligned}
n_S - 1 &\cong -4\epsilon + 2\eta + [-(8C + 8)\epsilon^2 + (6 + 10C)\epsilon\eta - 2C\xi^2] ; \\
n_T &\cong -2\epsilon + [-(6 + 4C)\epsilon^2 + (4 + 4C)\epsilon\eta] ; \\
\frac{dn_S}{d\ln k} &\cong -8\epsilon^2 + 10\epsilon\eta - 2\xi^2 + [-(40 + 32C)\epsilon^3 + (60 + 62C)\epsilon^2\eta \\
&\quad - (12 + 20C)\epsilon\eta^2 - (8 + 14C)\epsilon\xi^2 + 2C\eta\xi^2 + 2C\sigma^3] \\
\frac{dn_T}{d\ln k} &\cong -4\epsilon^2 + 4\epsilon\eta + [-(28 + 16C)\epsilon^3 + (40 + 28C)\epsilon^2\eta - (8 + 8C)\epsilon\eta^2 - (4 + 4C)\epsilon\xi^2] .
\end{aligned} \tag{3.6}$$

In each case the term enclosed in square brackets is higher order in the slow-roll expansion, and is omitted when discussing lowest-order results.

3.3 The consistency equation hierarchy: lowest-order in slow-roll

In this section we restrict ourselves to the slow-roll case, setting the square brackets in Eqs. (2.37) and (2.38) equal to one. Some simple algebra immediately leads to the standard consistency equation Eq. 2.36,

$$2\frac{A_T^2}{A_S^2} \cong -n_T \tag{3.7}$$

Note that n_T is always negative by definition. This relation was implicit in the results of Lyth and Liddle (1992), which was the first to write down the full slow-roll expressions, and was made explicit and named the consistency equation in Copeland et al. (1993).

Although this is the standard form of the relation (sometimes with a different coefficient if the spectra are defined with a different normalization), it somewhat conceals the physical underpinning of the consistency equation. It can be cast in the form of a differential equation for the tensors or equivalently an integral equation for the tensors, which becomes more explicit if we write all the scalar terms on one side and all the tensor ones on the other, to obtain

$$A_S^2 \cong -2\frac{A_T^2}{n_T}. \tag{3.8}$$

It is clear from this expression that specifying the tensors completely defines the physical situation, and the corresponding scalar spectrum can be uniquely obtained from the consistency relation. If instead the scalars are specified, however, this is a differential equation for the tensors whose solution yields a one-parameter set of physical models giving that scalar spectrum and each obeying the consistency equation.

In order to investigate further the underlying dependences of the spectra and their derivatives beyond this relation, we note that the above equation is usually assumed to hold at one particular scale, often combined with the somewhat inconsistent assumption that the spectra are power-laws with different spectral indices ($n_S - 1 \neq n_T$). However

further consistency relations can be obtained, as first shown in Lidsey et al. (1997), by realizing that the consistency equation is supposed to hold on all scales. For instance, one can proceed by Taylor expanding both sides of Eq. (3.8) in $\ln k$ about some characteristic scale k_0 ,¹ giving

$$A_S^2 + \frac{dA_S^2}{d \ln k} \ln \frac{k}{k_0} + \frac{1}{2} \frac{d^2 A_S^2}{d \ln k^2} \ln^2 \frac{k}{k_0} + \dots \cong \quad (3.9)$$

$$-2 \frac{A_T^2}{n_T} + \frac{d[-2 \frac{A_T^2}{n_T}]}{d \ln k} \ln \frac{k}{k_0} + \frac{1}{2} \frac{d^2[-2 \frac{A_T^2}{n_T}]}{d \ln k^2} \ln^2 \frac{k}{k_0} + \dots$$

where the expansion coefficients are all evaluated at k_0 .

By equating the coefficients on both sides we arrive at an infinite hierarchy of consistency relations given generally by

$$\frac{d^{(i)} A_S^2}{d \ln k^{(i)}} \cong \frac{d^{(i)}[-2 \frac{A_T^2}{n_T}]}{d \ln k^{(i)}}, \quad i = 0, 1, \dots, \quad (3.10)$$

with both sides evaluated at some arbitrary scale k_0 . This form of presenting the dependence between scalar and tensor spectra completes the description of its inter-relational properties, as predicted by single-field models, and can be used to test the inflationary scenario to any order of accuracy the observations may one day present us with.

The first derivative, of Eq. (3.10), $i = 1$, gives the lowest-order version of the second consistency equation

$$\frac{dn_T}{d \ln k} \cong 2 \frac{A_T^2}{A_S^2} \left[2 \frac{A_T^2}{A_S^2} + (n_S - 1) \right]. \quad (3.11)$$

$$\cong n_T [n_T - (n_S - 1)]. \quad (3.12)$$

This equation first appeared in Kosowsky and Turner (1995) without being explicitly recognized as a consistency equation, that role being pointed out in Lidsey et al. (1997). Eq. (3.10) is the first time an explicit form for the full infinite hierarchy has been written down.

Should we wish to focus on observationally more attainable quantities we can rewrite Eq. (3.10) in an interesting alternate form using only the spectral indices

$$\frac{d^{(i-1)}(n_S - 1)}{d \ln k^{(i-1)}} \cong \frac{d^{(i-1)} n_T}{d \ln k^{(i-1)}} - \frac{d^{(i)} \ln(-n_T)}{d \ln k^{(i)}}, \quad i = 1, 2, \dots. \quad (3.13)$$

This does not encode the normal (first) consistency relation, but does capture all the others in quite an elegant form.

¹In carrying out these manipulations, note that the order-by-order slow-roll expansion is preserved both by taking derivatives and logarithms.

3.4 The consistency equation hierarchy: next-order in slow-roll

To lowest order in slow roll this set of relations completes the relation between density and gravitational waves. However, as observations of the CMB begin to constrain higher-order derivatives of the density spectrum of perturbations, if we wish to constrain the inflationary scenario in general it becomes necessary these consistency relations be derived to an order of approximation that matches that of observations.

The above hierarchy of equations can readily be generalized to next-order in slow roll by retaining the full form of Eqs. (2.37) and (2.38).

The next order of the first consistency equation was first given in Ref. Copeland et al. (1994), and quoted in Ref. Lidsey et al. (1997) as

$$n_T \cong -2 \frac{A_T^2}{A_S^2} \left[1 - \frac{A_T^2}{A_S^2} - (n_S - 1) \right]. \quad (3.14)$$

To analyze the physical relation underlying this expression we once again wish to separate the scalar from the tensor quantities. We write

$$-\frac{A_T^2}{A_S^2} \frac{2}{n_T} \cong 1 - \frac{1}{2} n_T + (n_S - 1) \quad (3.15)$$

and use small-parameter manipulations to obtain

$$A_S^2 [1 + (n_S - 1)] \cong -\frac{2A_T^2}{n_T} \left[1 + \frac{1}{2} n_T \right], \quad (3.16)$$

where the scalars all stand to the left and the tensors to the right.

To next order the relation no longer presents itself as a simple differential equation relating both types of perturbations. The tensors no longer uniquely specify the scalars, though the requirement of a subdominant next-order term (for the expansion to make sense) will give a practically-unique scalar spectrum for a given tensor one.

The hierarchy of consistency equations to next-order, with scalars and tensors separated, is obtained by differentiating Eq. (3.16) repeatedly with respect to $\ln k$. For instance, we can take Eq. (3.12) to next order by differentiating Eq. (3.14) once to get

$$\frac{dn_T}{d \ln k} \cong n_T [n_T - (n_S - 1)] + n_T \left[\frac{n_T}{2} (n_T - (n_S - 1)) - \frac{dn_S}{d \ln k} \right].$$

The first term on the right-hand side is of course the first-order version of the second consistency equation.

As way of a summary illustration of the described relations we can take the first few equations and examine the quantity and nature of the observables they each relate, shown in Fig (3.1). According to which direction we proceed in — going to next order in slow roll or moving on to the next consistency equation in the hierarchy — different quantities arise. When we move to the following consistency equation a tensor quantity is introduced, but the number of related observables remains the same. If we instead include next order corrections, we are connecting more quantities, (four quantities related

First Consistency Equation Lowest Order ■

$$n_T \cong -2 \frac{A_T^2}{A_S^2}$$

First Consistency Equation Next Order ■

$$n_T \cong -2 \frac{A_T^2}{A_S^2} \left[1 - \frac{A_T^2}{A_S^2} + (1 - n_S) \right]$$

Second Consistency Equation Lowest Order ■

$$\frac{dn_T}{d \ln k} \cong n_T [n_T - (n_S - 1)]$$

Second Consistency Equation Next Order ■

$$\frac{dn_T}{d \ln k} \cong n_T [n_T - (n_S - 1)] + n_T \left[\frac{n_T}{2} (n_T - (n_S - 1)) - \frac{dn_S}{d \ln k} \right]$$

$$\vdots$$

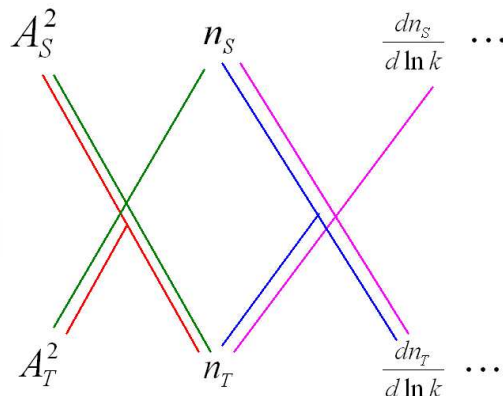


Figure 3.1: First few consistency equations and observables they relate.

by next order expressions versus three for lowest order) but the new quantity is in turn a scalar quantity which is more readily accessible from data. For this reason a prescription for which consistency equation to consider does not immediately follow from the quantities observations provide us with. The underlying reason for this is the different nature of the two spectra. While the tensor spectrum is fundamentally setting the energy scale for inflation and so appears at an earlier stage in the dependences, observationally the scalar quantities are much easier to measure and contrast with the hierarchy present in the equations.

3.5 Relation to approximate consistency equations

Since Eq. (3.10) and its higher-order equivalents give a complete account of relations between the scalar and tensor spectra, any other consistency relations claimed in the literature, approximate or otherwise, must follow from them. One such is a relation proposed by Chung et al. (2003) and explored in detail by Chung and Romano (2006), concerning a near coincidence of scales in models with strong running. Another appears in Lidsey and Tavakol (2003) under the assumption of constant running. We examine each in turn.

3.5.1 Coincidence of scales

The authors of Chung et al. (2003); Chung and Romano (2006) claim to have found an approximate consistency condition in models with large running. They note that in such models there is a near coincidence of scales between the scale at which the Harrison–Zeldovich spectrum is obtained $n_S - 1 = 0$ and the scale at which the tensor-to-scalar

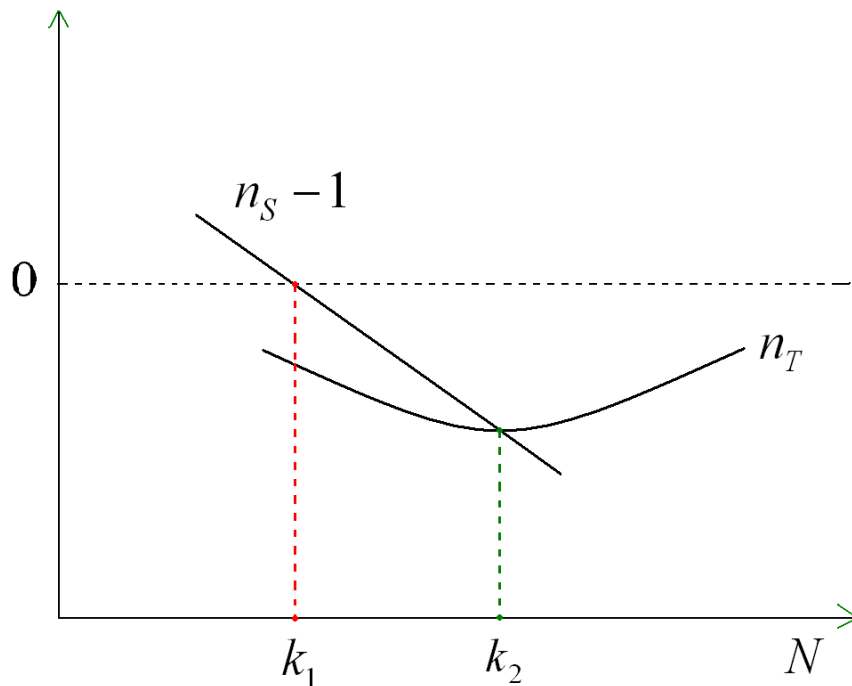


Figure 3.2: Arbitrary curves for the scalar and tensor spectral indices and the number of e-folds separating any two scales

ratio reaches a minimum, i.e. a flat bump in the potential.

The first of those scales is denoted k_1 , and the second k_2 . By definition²

$$\left. \frac{d \ln(A_T^2/A_S^2)}{d \ln k} \right|_{k_2} = 0 \implies n_S(k_2) - 1 = n_T(k_2). \quad (3.17)$$

Since the two conditions equate n_S to different values, the relation is clearly not exact. The difference between the two scales can be defined as $\Delta N = \ln k_2/k_1$. If we assume that the runnings are constant, but make no assumption that the spectra arise from inflation, we can derive a general expression for the distance between these scales simply by taking two arbitrary curves for the k -dependence of both spectral indices and examining the number of e-folds separating them, as in Fig (3.2),

$$\Delta N = \frac{(n_S - 1) - n_T}{dn_T/d \ln k - dn_S/d \ln k} + \frac{n_S - 1}{dn_S/d \ln k} \quad (3.18)$$

where the observables are evaluated at an arbitrary scale k_0 . If we further specialize that the expansion scale is chosen to be one of the scales k_1 or k_2 (bearing in mind that before the fit to the data we wouldn't know where those scales are, and that they may not lie

²In parts of their paper, Chung and Romano define scale k_2 as being where ϵ reaches its extremum. Beyond the slow-roll approximation this is not quite equivalent to our definition, which we believe is more appropriate since ϵ is not a direct observable.

where the data is), this expression simplifies to

$$k_1 : \quad \Delta N = -\frac{n_T}{dn_T/d \ln k - dn_S/d \ln k}; \quad (3.19)$$

$$k_2 : \quad \Delta N = \frac{n_S - 1}{dn_S/d \ln k}. \quad (3.20)$$

Two things to note about these equations are as follows. Firstly, slow-roll inflation predicts that the two scales are far apart, not close, since the denominator is one order higher in slow-roll than the numerator and hence $\Delta N \sim \mathcal{O}(1/\epsilon)$ in the absence of cancellations. If they are close, partial cancellations will have allowed the running to be large while the scalar spectral index remains close to unity (this can happen plausibly, for instance, in running-mass inflation models, Stewart (1997)). Secondly, the above relations are *not* consistency relations, as no inflationary input has been added and they are true of arbitrary spectra, not just those tied together as inflation predicts. In particular, if n_S is already measured at k_2 , then measuring ΔN and measuring $dn_S/d \ln k$ at k_2 are the same thing.

The above equations can be converted into consistency equations by substitution of the inflationary spectra, thus enforcing the relation between tensor and scalars. For instance, doing this in Eq. (3.19) to lowest order yields

$$\Delta N \cong \frac{\epsilon}{\xi^2 - 4\epsilon^2}, \quad (3.21)$$

where the slow-roll parameters are evaluated at k_1 . This is precisely Eq. (151) of Chung et al. (2003) rewritten in our notation. Carrying out the same procedure to second-order in Eq. (3.20) yields Eq. (21) of Chung and Romano (2006) (note that their definition of the constant C is different to ours).

That these relations are equivalent to the consistency equations, specifically the second one given by Eq. (3.12) or Eq. (3.17), is rather subtle. Now, Eq. (3.21) is not actually a useful form, since ϵ and ξ are not directly observable. Sufficient observables to determine them are n_T and $dn_S/d \ln k$, bearing in mind that by definition $n_S = 1$ at the scale k_1 where their relation applies (and hence $2\epsilon \cong \eta$ to the required order). This allows us to rewrite as

$$\Delta N \cong -\frac{n_T}{n_T^2 - dn_S/d \ln k}. \quad (3.22)$$

Their test therefore proposes to measure the three quantities in this expression and verify that this relation holds.

However we know that the general expression for ΔN is Eq. (3.19). Comparing with Eq. (3.22), we see that their test actually seeks to confirm that

$$\frac{dn_T}{d \ln k} \cong n_T^2. \quad (3.23)$$

This is nothing other than the second consistency equation, Eq. (3.12), evaluated at k_1 so that $n_S - 1$ vanishes. Transforming to any other scale would then give the full version of the (lowest-order) second consistency equation.

In conclusion, while it appears that their method does not measure $dn_T/d \ln k$, in fact the measurement of ΔN along with the other observables does so implicitly, and their test is precisely equivalent to the second consistency equation, the lowest-order version of which was already given in Lidsey et al. (1997).

3.5.2 Constant running

A different relation, advertised as independent of the inflationary potential, was given by Lidsey and Tavakol (2003). They noted that if it were assumed that the scalar running is constant, then the (lowest-order) equation for it, Eq. (3.7) with the square bracket set to zero, can be written in terms of the scalar spectral index, the tensor-to-scalar ratio, and an undetermined constant \tilde{c} , eliminating the dependence on the potential. Their Eq. (18) reads

$$\frac{A_S^2}{A_T^2} \exp \left[-\frac{(n_S - 1)^2}{2dn_S/d \ln k} \right] - \left(\frac{2\pi}{dn_S/d \ln k} \right)^{1/2} \operatorname{erf} \left[\frac{n_S - 1}{\sqrt{2dn_S/d \ln k}} \right] = \tilde{c}.$$

As they acknowledge, in the usual interpretation where the observables are given at a fixed (though arbitrary) expansion scale, this is not a consistency equation as determining \tilde{c} is equivalent to determining $dn_S/d \ln k$. It is further evident that it is not a consistency equation since it does not mention the tensor spectral index or its derivatives, whereas all members of our consistency equation hierarchy, an exhaustive list of relations between observables, do feature those.

They suggest that the equation can be given content by evaluating it at two different scales, the first used to fix \tilde{c} and the second to test the relation. However this appears primarily to be a test of the assumption of constant running, with the implications for inflationary dynamics depending on the details of how that assumption might fail — typical inflation models do predict some deviation from constant running. In any event, their relation does not follow from the consistency equation hierarchy we have described.

3.6 Conclusions

Single-field inflation predicts not just one consistency relation, but an infinite hierarchy, each of which can be considered at different orders in the slow-roll expansion (Lidsey et al. (1997)). We have for the first time written down explicit expressions for all these relations, and shown how they relate to other consistency equations found in the literature. Observed violation of these consistency relations would exclude single-field slow-roll inflation under Einstein gravity, pointing instead perhaps to multi-field phenomena, non-Einsteinian gravity, or a non-inflationary origin of perturbations.

It is difficult to be optimistic about attempts to test any other than the lowest-order version of the first consistency equation, the famous $A_T^2/A_S^2 = -n_T/2$ relation, which itself is quite challenging. Song and Knox (2003) have made a comprehensive study of the ability of cosmic microwave background experiments to test this consistency relation.

They also discuss taking that relation to next order; doing so introduces an extra observable n_S , which should be accurately measurable, but current observational constraints already place us in a parameter regime where the next-order correction should be too small to observe due to the expected observational uncertainty on n_T . Going instead to the lowest-order version of the second consistency relation, Eq. (3.11), introduces the distinctly challenging observable $dn_T/d \ln k$. This observable is also required to meaningfully test the coincidence of scales described in Chung et al. (2003); Chung and Romano (2006), which we have shown is equivalent to our results and indeed those given in Lidsey et al. (1997).

Chapter 4

The Pivot Scale

4.1 Introduction

In this chapter we examine the choice of cosmic scale at which results from CMB data analysis are presented. We continue the work from last chapter by illustrating an example of an implementation of the hierarchy of consistency equations that insures for consistency in the method we develop. The high accuracy CMB sky maps the WMAP team provided us with represent two distinct challenges for cosmology: observationally, we wish to constrain the amplitude and scale dependence of the power spectrum, and from the viewpoint of theory we aim at understanding the origin of perturbations, such as those that may have been generated by an inflationary potential.

When presenting observational constraints on these perturbation spectra we need to specify the cosmological scale k at which the observable parameters are being determined. Provided the full posterior distribution over all parameters is given, this choice is an arbitrary one. However, if the information is to be compressed via marginalization, the choice of this scale matters, and should be chosen in order to optimize the presentation of constraints.

In the WMAP three-year cosmological parameters paper (Spergel et al. (2007)) the scale 0.002 Mpc^{-1} is used, which is close to the observable horizon, while Kurki-Suonio et al. (2005) and Finelli et al. (2006) found that the choice of 0.01 Mpc^{-1} worked better in constraining inflationary observables as it is closer to the statistical center of the data. The scale 0.05 Mpc^{-1} is also commonly used, being the default scale of the CosmoMC package (Lewis and Bridle (2002)). The pivot scale was also discussed in Liddle et al. (2006), who sought the scale where the perturbation amplitude was best determined (decorrelated with other power spectrum parameters), and in Peiris and Easter (2006b) who sought the scale at which the perturbation spectrum reconstructed using the flow formalism was best constrained.

In this chapter we make a systematic exploration of the choice of scale in the context of inflation models. This choice is particularly important in cases where models with significant spectral index running are allowed.

4.2 Methodology

For definiteness we concentrate on single-field inflationary models, though many of the issues we discuss are more general. These models predict spectra of scalar and tensor perturbations which are related by the hierarchy of consistency equations we discussed in the previous chapter. The first of these is, at lowest-order, the well-known relation $r = -8n_T$ where r is the tensor-to-scalar ratio and n_T the tensor spectral index. These parameters can in turn be related to the inflationary slow-roll parameters describing the shape of the potential.

Our main aim in this chapter is to examine the optimal choice of scale at which to present observational constraints on inflation. In order to fit the spectra from data, they must first be parametrized, which is usually done by specifying their amplitude and some number of derivatives (i.e. the spectral index, running, etc) at a particular scale. So far, this scale has been chosen by hand.

The choice of scale, being arbitrary, ought not to affect the conclusions one draws. There is nothing physical about the pivot scale and in a slow roll context it merely represents a different point about which the slow roll expansion is performed. However this is only the case if one specifies the full multi-dimensional posterior parameter distributions, and provided the model definition is internally self-consistent. The first of these is often not the case. For presentation purposes, usually the full parameter volume is compressed via marginalization, as one commonly wishes to condense information onto a one or two dimensional parameter plane. In such case this choice of scale matters, since while projecting onto a given surface we lose information on the correlations with other parameters (given that one 2D plane contains more information than two 1D likelihood distributions), and this information is otherwise necessary to translate between scales. The second condition of model self-consistency holds in most circumstances, but often *not* in the way inflationary spectra are implemented, as we explain here.

The problem of model definition in inflationary models is the enforcement of the consistency equations between scalars and tensors. Typically both spectra are allowed to be power-laws but with different indices; if the usual consistency equation is enforced at one scale, it will then no longer hold at any other. Put another way, if the scalars are a perfect power-law, then the tensor spectrum implied by the consistency relations is not (unless the spectral indices are the same). Yet another way, the set of models generated by imposing the consistency equation at one scale is a different set of models from that obtained using another scale. This problem is further exacerbated if authors go on to include scalar spectral index running, while perhaps still leaving the tensors as a power-law. Before discussing the choice of scale, we should therefore first fix this problem (while admitting that the difference may be too small to be very important).

This is achieved by implementing the full inflationary consistency equation hierarchy as we gave in chapter 3. As well as the first consistency equation, this enforces that each *derivative* of the consistency equation also holds at a given scale. When using a Taylor expansion to shift from one scale to another, this hierarchy then ensures that the consistency equations will still hold at the new scale (up to some level set by the truncation of

the hierarchy).

We note that these complications are needed only if one fits the phenomenological parameters (amplitude, spectral index, running, etc) from the data and then translates to inflationary observables. If instead one fits the slow-roll parameters directly (e.g. Grivell and Liddle (2000); Leach et al. (2002); Martin and Ringeval (2006); Finelli et al. (2006)) or via flow equations (Hoffman and Turner (2001); Kinney (2002); Peiris and Easther (2006a); Kinney et al. (2006); Peiris and Easther (2006b)), then the consistency equation hierarchy is automatically enforced.

We consider a parametrization of the scalar and tensor perturbations as follows, Taylor expanding the spectral indices in Eq. (2.29) and Eq. (2.30),

$$A_S^2(k) \propto (k/k_*)^{(n_S-1)+(dn_S/d \ln k) \ln k/k_*} \quad (4.1)$$

$$A_T^2(k) \propto (k/k_*)^{n_T+(dn_T/d \ln k) \ln k/k_*}, \quad (4.2)$$

the constants of proportionality being the amplitude of the perturbations at scale k_* . The tensor-to-scalar ratio is defined by $r(k) \equiv 16A_T^2(k)/A_S^2(k)$, and the tensor spectral index is determined via the first consistency equation.

In order that the first consistency equation be enforced at all scales (to linear order in $\Delta \ln k$), we need to implement the second consistency equation to fix the tensor running, which is not a genuine new degree of freedom. This second equation is given by Eq. 3.12 and we enforce this when carrying out our data-fitting.

One could further enforce higher consistency equations, so that for instance the second consistency equation also is preserved under change of scales. However current data quality is a long way from the point where doing so would make any practical difference, since the tensors are potentially observable only over a limited range of scales.

We use the Monte Carlo Markov Chain (MCMC) technique to explore the parameter space, using the CosmoMC package (Lewis and Bridle (2002)). We consider a Λ CDM model in a flat universe and take $k_* = 0.05 \text{ Mpc}^{-1}$ as the scale where all power spectrum parameters are defined when fitting to data. We vary up to eight parameters

$$\Omega_b h^2, \Omega_{\text{dm}} h^2, \theta, \tau, n_S(k_*), r(k_*), \ln[10^{10} A_S(k_*)], \left. \frac{dn_S}{d \ln k} \right|_{k_*}$$

where $\Omega_b h^2$ and $\Omega_{\text{dm}} h^2$ are the physical baryon and dark matter densities, θ is the ratio of the sound horizon to the angular-diameter distance, τ is the optical depth, and the remaining parameters specify the power spectra. We apply a set of uniform priors:

$$\begin{aligned} 0.005 < \Omega_b h^2 < 0.1 & & 0.01 < \Omega_{\text{dm}} h^2 < 0.99 \\ 0.5 < \theta < 10 & & 0.01 < \tau < 0.8 \\ 0.5 < n_S < 1.5 & & 2.7 < \log(10^{10} A_S) < 4 \\ 0 < r < 2 & & -0.2 < dn_S/d \ln k < 0.2 \end{aligned}$$

Until Section 4.5, our constraints are from WMAP3 data alone.

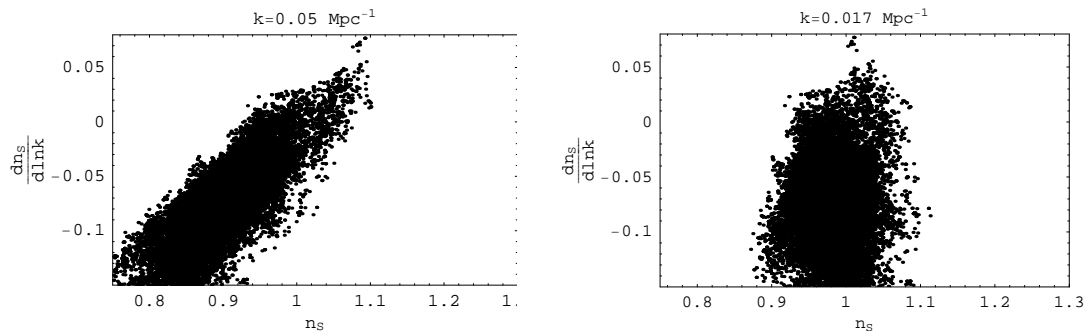


Figure 4.1: The $dn_S/d \ln k$ and n_S plane shown both at the scale where the chains are run, $k = 0.05 \text{ Mpc}^{-1}$, and the decorrelation scale, $k = 0.017 \text{ Mpc}^{-1}$, at which the uncertainty on this 2D distribution is minimum.

4.3 Choice of scale: models with scalar running

We first consider models which allow running of the scalar spectral index, which we will see is the case where the choice of scale is most important. For comparison, models without running are studied in the next section.

4.3.1 Tilt and running

The simplest combination of observables to consider is the tilt and running of the scalars. Observational implications of this were first discussed in Copeland et al. (1998a), which forecasted CMB constraints from the Planck satellite on running spectral index models. The paper pointed out that there would be a scale at which the uncertainties on tilt and running would become uncorrelated, and that (at least in a gaussian approximation) on that scale the uncertainty in n_S would recover its value for the case of no running, thus by bracketing out the level of uncertainty n_S when including running in the analysis.¹ This could be spoiled by degeneracies with other parameters, but at Planck accuracy appears not to be (Copeland et al. (1998a)).

Anyway, we wish to find the scale at which the tilt and running decorrelate for actual current data. To do this we take the distribution of these two variables at the CosmoMC default scale, $k_* = 0.05 \text{ Mpc}^{-1}$ as in the left panel of Fig. (4.1).

We then fit the chain elements with a linear relation, $n_S = A + B dn_S/d \ln k$, and by inserting into the expression

$$n_S(k) = n_S(k_*) + \frac{dn_S}{d \ln k} \ln \frac{k}{k_*}, \quad (4.3)$$

we arrive at a condition for the difference in scale which decorrelates n_S and $dn_S/d \ln k$: $B = -\ln k/k_*$. This scale turns out to be $k = 0.017 \text{ Mpc}^{-1}$. Then we use Eq. (4.3) to convert the distribution at scale k_* to the one at scale $k = 0.017 \text{ Mpc}^{-1}$ to obtain the decorrelated n_S and $dn_S/d \ln k$ shown in the right panel of Fig. (4.1). More generally, we can explore the constraints at other scales via the same formalism. The constraints at a

¹This observation was actually credited to Daniel Eisenstein, who was not an author of that paper.

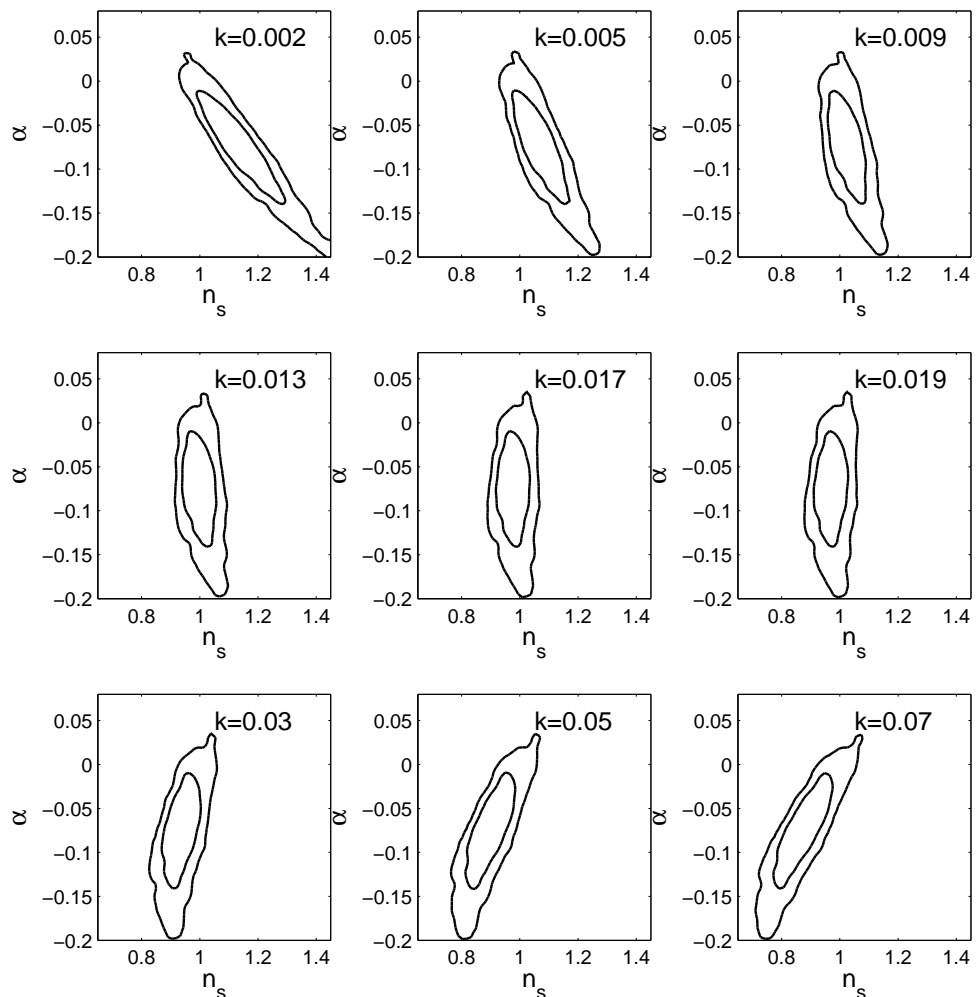


Figure 4.2: Constraints in the n_s - α plane (where $\alpha = dn_s/d \ln k$) at several scales. $k = 0.017 \text{ Mpc}^{-1}$ is the decorrelation scale for these parameters.

set of different scales, including the WMAP scale and the decorrelation scale, are shown in Fig.(4.2).

In this particular case (but not those that follow), the transformation between parameters induced by the scale change is linear and has unit Jacobian – meaning the 2D contour areas are preserved and only the shape of the contours is altered. This can be easily seen if we consider the area contours as built up of a stack of thin rectangles. Then the transformation only slides the rectangles across, the higher ones sliding more, and clearly the area remains unaltered. However it is evident from Fig. (4.2) that the marginalized uncertainty on n_s at the decorrelation scale is significantly smaller. The WMAP choice, 0.002 Mpc^{-1} , gives a significantly-angled constraint area and is clearly to be avoided if useful marginalized constraints on n_s are to be quoted. Unfortunately, the main WMAP3 results for models with running are presented at this scale.

For our choice of parameters and dataset (WMAP3 alone), from separate fits where running is not included we find the marginalized constraint on n_s is $n_s = 0.993_{-0.030, -0.053}^{+0.029, +0.067}$ (at 68% and 95% confidence). With running, the marginalized constraint at the decorrelation scale is $n_s = 0.981_{-0.034, -0.063}^{+0.034, +0.067}$. As anticipated, therefore, when including running

the shift in the best-fit n_S at the optimized scale is negligible within the uncertainty. This is somewhat trivial as it could have been chosen to match exactly by specific choice of scale — choosing $k = 0.015 \text{ Mpc}^{-1}$ achieves this. Much more importantly, we see that the *uncertainty* on n_S at the decorrelation scale is hardly increased when running is included, whereas it is greatly increased at e.g. 0.002 Mpc^{-1} . The 1D marginalized constraints on all parameters have minimum uncertainty at the decorrelation scale.

For the scalar running we obtained the marginalized constraints,

$$dn_S/d \ln k = -0.075_{-0.043, -0.093}^{+0.041, +0.082},$$

very similar to those quoted by WMAP3 for models with running and tensors (Spergel et al. (2007)).

4.3.2 Tilt and the tensor–scalar ratio

We now turn to other combinations of observables, relevant to constraining inflation.

To obtain r at other scales we perform an expansion, to the order considered, of the scalar and tensor amplitudes.

$$r(k) = 16 \frac{A_T^2(k)}{A_S^2(k)} = 16 \frac{A_T^2 + \frac{dA_T^2}{d \ln k} \ln \frac{k}{k_*} + \frac{1}{2} \frac{d^2 A_T^2}{d \ln k^2} \ln^2 \frac{k}{k_*}}{A_S^2 + \frac{dA_S^2}{d \ln k} \ln \frac{k}{k_*} + \frac{1}{2} \frac{d^2 A_S^2}{d \ln k^2} \ln^2 \frac{k}{k_*}} \quad (4.4)$$

where all observables without an argument ‘(k)’ are evaluated at $k_* = 0.05 \text{ Mpc}^{-1}$. Applying the definitions of the spectral indices and making use of the lowest-order version of the second consistency equation, Eq. (3.12) to set $dn_T/d \ln k$ we arrive at an expression for relating r between different scales,

$$\frac{r(k)}{r(k_*)} = \frac{1 + n_T \ln \frac{k}{k_*} + \frac{1}{2} \left[n_T^2 + \frac{dn_T}{d \ln k} \right] \ln^2 \frac{k}{k_*}}{1 + (n_S - 1) \ln \frac{k}{k_*} + \frac{1}{2} \left[(n_S - 1)^2 + \frac{dn_S}{d \ln k} \right] \ln^2 \frac{k}{k_*}}. \quad (4.5)$$

Having expressions for n_S and r at different scales, we can now choose several scales and get the distribution of the two variables at each, shown in Fig. (4.3).

In this case the transformation alters the contour areas as well as distorting them, since the transformation here is no longer a simple linear shift. The middle panel of Fig. (4.4) shows the areas enclosed by the 95% confidence contour in the n_S – r plane at different scales.² The top panel shows the same for n_S and running discussed in the previous subsection. In the n_S – r plane the minimum area was near $k = 0.017 \text{ Mpc}^{-1}$ as expected (the precise value found was slightly smaller). As inflation model builders typically just look at these marginalized plots to decide if their model is viable, it is clearly important to present the constraints at a good scale. Compression into one- or two-dimensional

²These values were obtained by taking the number of points in a 50×50 grid that lie within that contour. The number of grid points across each axis corresponds also to the number of bins used to sample the distribution. We found that accurate area estimation needed at least 50 bins, though such an aggressive binning level leads to less smooth contours than are usually seen.

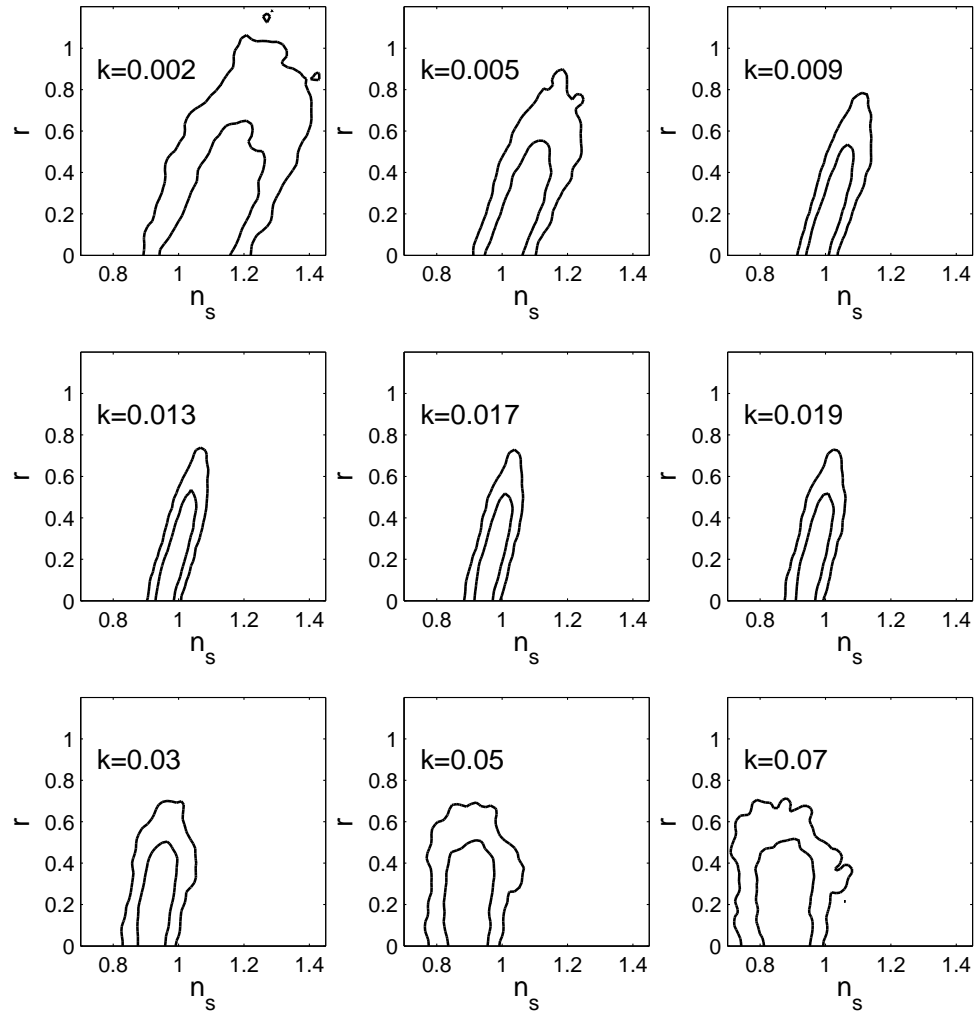


Figure 4.3: Constraints on n_s versus r at several scales.

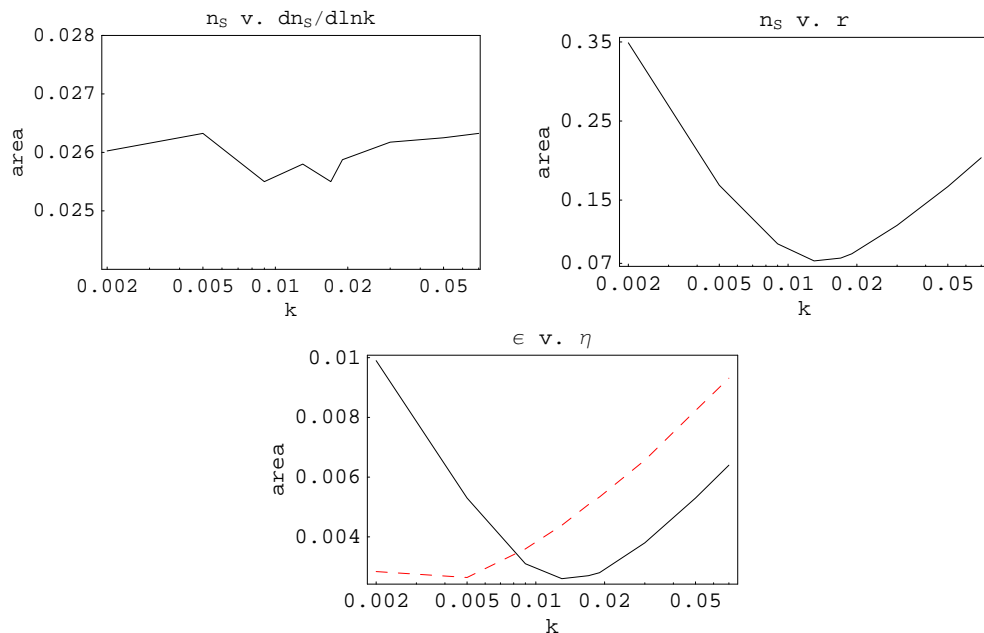


Figure 4.4: Variation of parameter plane area with scale. For the ϵ - η case both lowest (black, full) and next order (red, dashed) are shown. For n_s versus running the area should be independent of scale, and the variations indicate the noise level in the area estimation.

surfaces should happen where the data is strongest, i.e. at scales at which the parameters decorrelate. 0.002 Mpc^{-1} is clearly not a good scale for this purpose, as has previously been stressed also in Peiris and Easter (2006b).

4.3.3 Inflationary slow-roll parameters: lowest order

We now examine how the constraints on the first two slow-roll parameters ϵ and η are affected by scale change. We take the usual definitions in terms of the potential given by Eq. (2.6) and Eq. (2.8). The pivot scale k_* corresponds to some particular scalar field value ϕ_* (defined as the field value when $k_* = aH$ during inflation), in the vicinity of which the scalar field potential is being reconstructed. Shifting the pivot scale means expanding about a different point on the potential.

We first concentrate on the constraints given at lowest order, taking the expressions for the potential at this order given by Lidsey et al. (1997):

$$\begin{aligned}
 V(\phi) &\simeq \frac{75m_{\text{Pl}}^4}{32} A_{\text{T}}^2(k), \\
 V'(\phi) &\simeq -\frac{75\sqrt{\pi}}{8} m_{\text{Pl}}^3 \frac{A_{\text{T}}^3(k)}{A_{\text{S}}(k)}, \\
 V''(\phi) &\simeq \frac{25\pi}{4} m_{\text{Pl}}^2 A_{\text{T}}^2(k) \left[9 \frac{A_{\text{T}}^2(k)}{A_{\text{S}}^2(k)} - \frac{3}{2} [1 - n_{\text{S}}(k)] \right],
 \end{aligned} \tag{4.6}$$

(where without loss of generality we take ϕ to increase in time). From these the first two

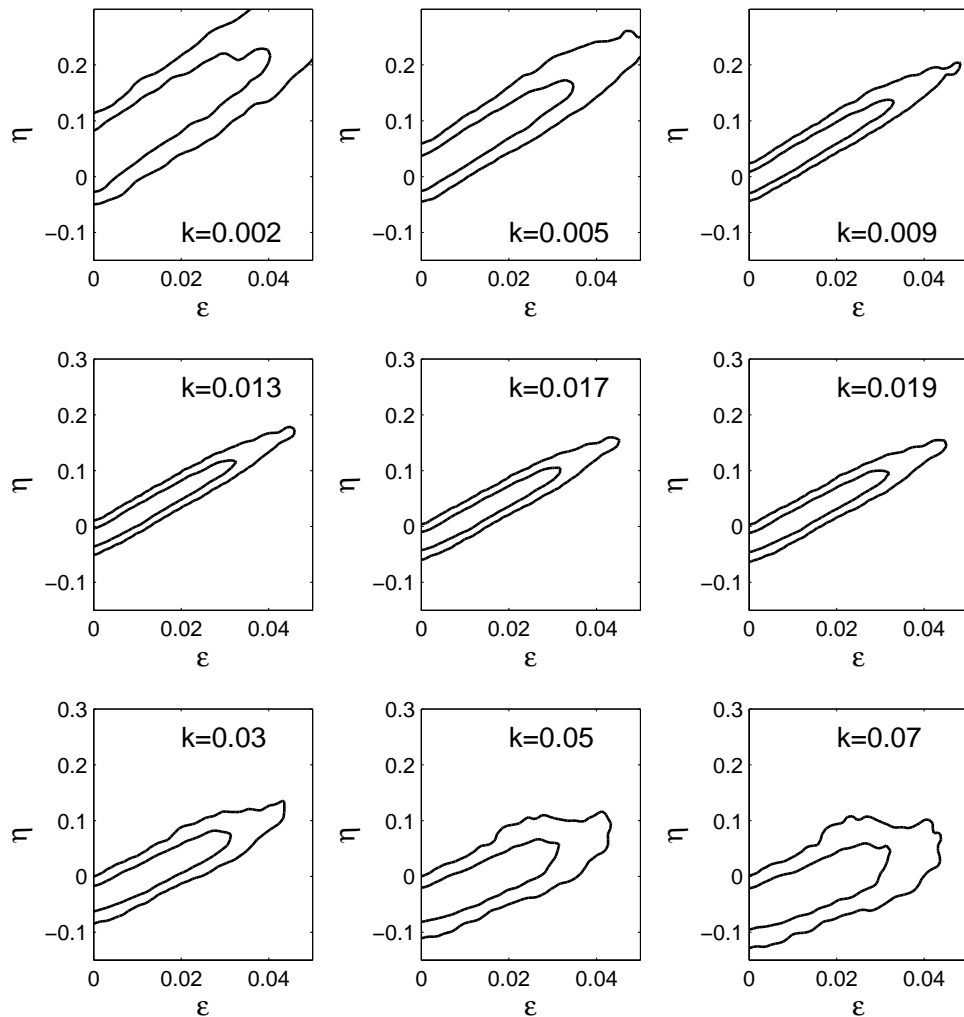


Figure 4.5: Constraints on ϵ versus η , at lowest order, evaluated at several scales.

slow-roll parameters are expressed in terms of the observables, to lowest order, by

$$\epsilon \simeq \frac{r}{16} \quad ; \quad \eta \simeq \frac{3}{16}r - \frac{1}{2}(1 - n_s). \quad (4.7)$$

Shifting the scale of the observables shifts the location on the potential, and at lowest-order the constraints on ϵ and η then become independent of the running at that scale (which could be used to determine a third slow-roll parameter $\xi \equiv m_{\text{pl}}^2/8\pi\sqrt{V'V'''}/V^2$).

The results are presented in Fig (4.5), and again show strong variation of the allowed parameter area with choice of scale, as indicated in Fig. (4.4)³.

³The noise referred to on the lower panel of Fig. (4.4) reflects the dependence of the area estimation on the shape of the contours. When the contours are aligned with the grid the area is slightly smaller, than when they are diagonally aligned since the tipping over of the contours causes for more grid points to be partially filled and the estimated area artificially increases.

4.3.4 Inflationary slow-roll parameters: next order

Now we can take the expressions for the potential to next order (Stewart and Lyth (1993)), also given by Lidsey et al. (1997):

$$\begin{aligned}
V(\phi) &\simeq \frac{75m_{\text{Pl}}^4}{32} A_{\text{T}}^2 \left[1 + \left(\frac{5}{3} + 2C \right) \frac{A_{\text{T}}^2}{A_{\text{S}}^2} \right], \\
V'(\phi) &\simeq -\frac{75\sqrt{\pi}}{8} m_{\text{Pl}}^3 \frac{A_{\text{T}}^3}{A_{\text{S}}} \left[1 - 0.85 \frac{A_{\text{T}}^2}{A_{\text{S}}^2} + 0.53(1 - n_{\text{S}}) \right], \\
V''(\phi) &\simeq \frac{25\pi}{4} m_{\text{Pl}}^2 A_{\text{T}}^2 \left\{ 9 \frac{A_{\text{T}}^2}{A_{\text{S}}^2} - \frac{3}{2}(1 - n_{\text{S}}) \right. \\
&\quad + \left[(36C + 2) \frac{A_{\text{T}}^4}{A_{\text{S}}^4} - \frac{1}{4}(1 - n_{\text{S}})^2 - \right. \\
&\quad \left. \left. (12C - 6) \frac{A_{\text{T}}^2}{A_{\text{S}}^2} (1 - n_{\text{S}}) - \frac{1}{2}(3C - 1) \frac{dn_{\text{S}}}{d \ln k} \right] \right\}, \tag{4.8}
\end{aligned}$$

where $C = -2 + \ln 2 + \gamma \simeq -0.73$, γ is the Euler–Mascheroni constant, and again the ϕ value corresponds to horizon crossing of the scale at which the constraints are being imposed.

With these next-order expressions for the potential, ϵ and η are

$$\epsilon = \frac{r}{16} \frac{1 - 0.85 r/16 + 0.53(1 - n_{\text{S}})}{1 + 0.21 r/16} \tag{4.9}$$

$$\begin{aligned}
\eta &= \frac{1}{3} \frac{1}{1 + 0.21 r/16} \left\{ \frac{9}{16} r - \frac{3}{2}(1 - n_{\text{S}}) \right. \\
&\quad + (36C + 2) \left(\frac{r}{16} \right)^2 - \frac{1}{4}(1 - n_{\text{S}})^2 \\
&\quad \left. - (12C - 6) \frac{r}{16} (1 - n_{\text{S}}) - \frac{1}{2}(3C - 1) \frac{dn_{\text{S}}}{d \ln k} \right\}. \tag{4.10}
\end{aligned}$$

The second parameter now depends on the running. The running term has a coefficient of about one half, and given how weakly running is constrained this term has a significant impact on the constraints.

The constraints at each scale are presented in Fig (4.6). The picture here is rather different, with the area changing much more slowly as k is decreased, and the minimum area being at a much smaller k . This is because for typical models the next-order correction from the running happens to be comparable to the change in the lowest-order expression for η coming from the changing n_{S} , also induced by the running, as the scale changes. These terms approximately cancel going to smaller k , i.e. the constraints change less when simultaneously reducing k and introducing next-order corrections than they would if only one of these were done. This is just a coincidence (and not much of a coincidence at that, since partial cancellation would have to happen as k was changed in one or other direction) of no great significance, and will go away when in future running is better constrained.

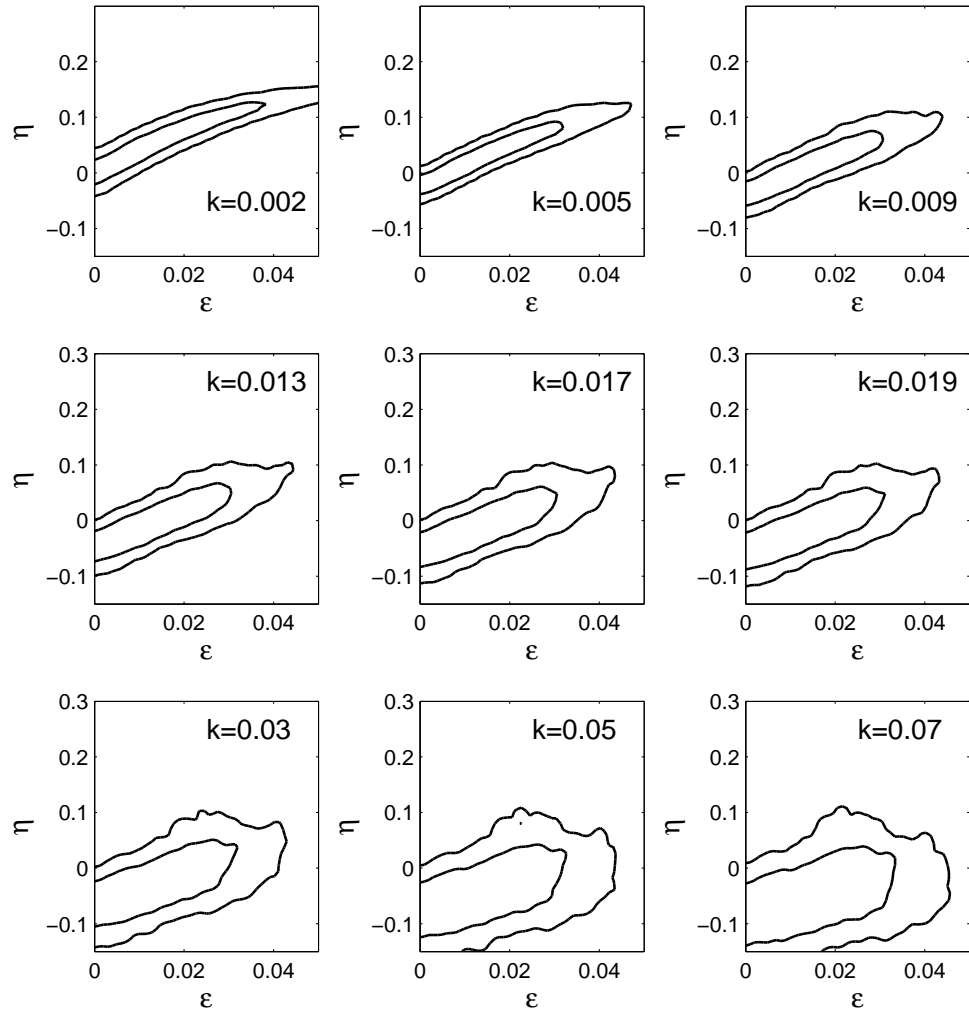


Figure 4.6: Constraints on ϵ versus η , to next order, at several scales.

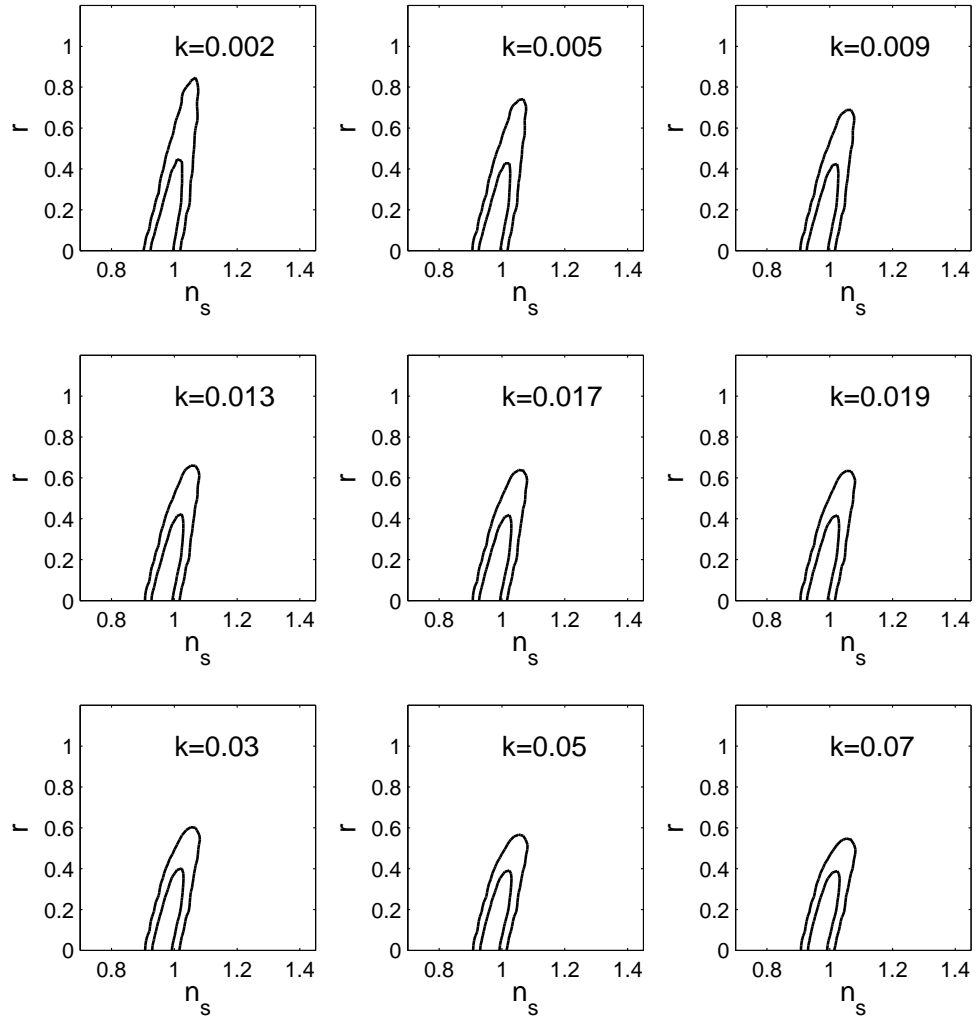


Figure 4.7: Constraints on n_s and r when no scalar running is present.

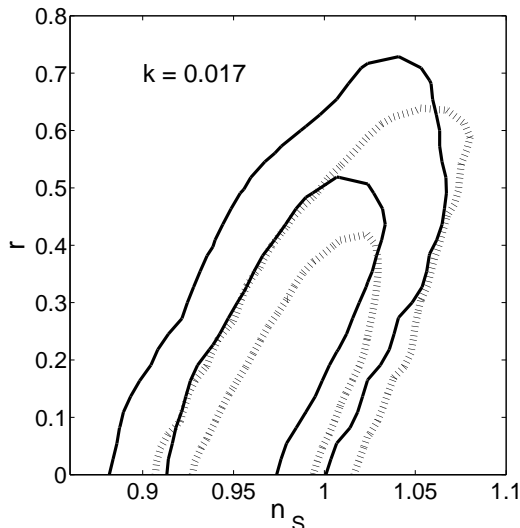


Figure 4.8: Comparison of constraints in the n_s - r plane at the optimal scale with no running (dotted contours) and when running is included (full contours). The area enclosed by the 95% contour increases by around 20% when running is included.

4.4 Choice of scale: models with no scalar running

For comparison, we now take a look at models where no running of the scalar index is allowed.⁴ In this case the variation in the constraints with scale is much less, as for instance is seen in Fig. (4.7) showing the n_s - r plane. Indeed in this case we find that minimization of the area is not only unnecessary, but can actually be misleading, because parameters such as r can appear to be well constrained even on large angular scales where there is no meaningful data. The reason for this is that the restrictive class of models under consideration force the spectra to behave in a particular way as they are extrapolated away from the region where the bulk of the data lie, i.e. such constraints contain significant prior information as well as data information. This is also true to some extent for constraints on r in the running case studied earlier.

Nevertheless, it is now interesting to compare the running and no-running constraints. In the WMAP3 analysis the impression, from comparison of the top-left panels of Figs. (12) and (14) of Spergel et al. (2007), is of a huge deterioration in the constraints in the n_s - r plane once running is included. The same is seen in Fig. (1) of Kinney et al. (2006). However we now see that this is an artifact of the choice of scale where the constraints are portrayed. At the optimal scale there is some deterioration, due to parameter degeneracy, but the area increase within the 95% contour is only by about 20% as seen in Fig. (4.8), not by a factor of five as at $k = 0.002 \text{ Mpc}^{-1}$. Consequently, inclusion of running leads only to a moderate deterioration in constraints on ϵ and η .

⁴We still keep the tensor running in the analysis, however. It is not an additional degree of freedom, its inclusion ensuring the validity of the first consistency equation at all scales.

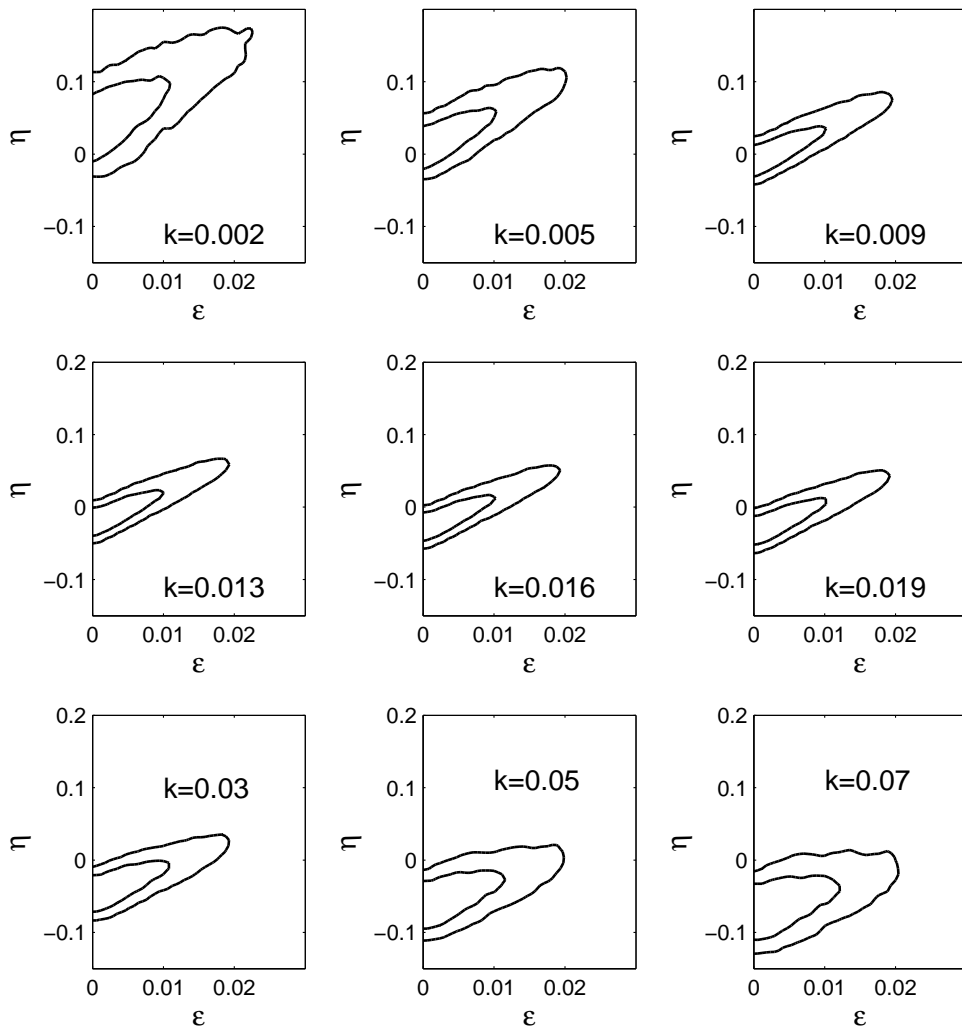


Figure 4.9: As Fig. 4.5, but now with the full dataset compilation. Note the modified axis ranges.

4.5 Including more data

We explore the robustness of our results by carrying out the same analysis for a broader compilation of data, now including shorter-scale CMB experiments and galaxy correlation data from ACBAR (Kuo et al. (2004)), CBI (Pearson et al. (2003)), VSA (Dickinson et al. (2004)), Boomerang (Jones et al. (2006)), SDSS (Tegmark et al. (2004)), and 2dFGRS (Percival et al. (2001)).

Everything goes through as before. We find that the decorrelation scale of n_s and running is 0.016 Mpc^{-1} , which is not significantly different from WMAP3 alone. Though in general one would expect the decorrelation scale to change with dataset, in this case the WMAP3 data are powerful enough that a shift is not seen.

The constraints, particularly on r and hence ϵ , do tighten significantly with the extra data, as is clear also in previous analyses including Spergel et al. (2007). As an illustration of the results we obtained in this case, we show the array of constraints on the lowest-order ϵ and η at different scales, Fig. (4.9), and the overlay of contours in the n_s - r plane

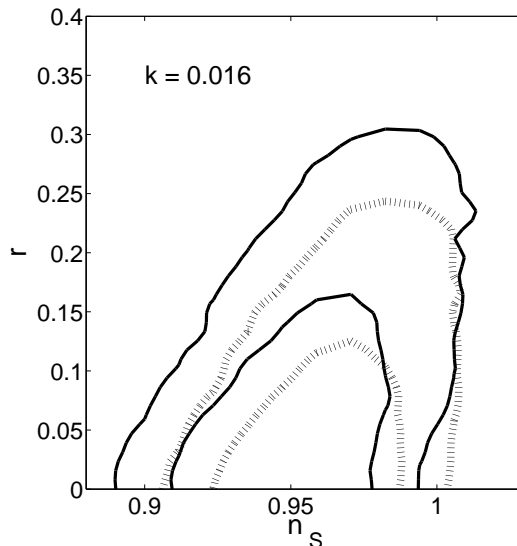


Figure 4.10: As Fig. (4.8), but now with the full dataset compilation. Note the modified axis ranges. The area enclosed by the 95% contour increases by around 30% when running is included.

at the optimal scale, with and without running, in Fig. (4.10).

4.6 Conclusions

We have investigated the issue of choice of scale in presenting marginalized parameter constraints. While we have focussed on WMAP constraints applied to inflationary models, the same considerations apply much more widely. For example, in constraining density perturbations using galaxy clusters, commonly the parameter σ_8 , being the normalization of density perturbations smoothed on the scale $8h^{-1} \text{Mpc}^{-1}$, is quoted. However typically the normalization is best determined at a somewhat larger scale than $8h^{-1} \text{Mpc}$, and marginalizing over parameters such as Ω_0 to quote constraints on σ_8 can unnecessarily increase the statistical uncertainty on the normalization.

In the inflationary context, choosing an optimal scale is important primarily in models where large running is allowed. We found that an appropriate scale is the one which decorrelates estimates of n_s and running, which for WMAP3 is 0.017Mpc^{-1} . This criterion can be used to define such a scale for any dataset compilation, and we found that the scale shifts hardly at all when other available data are added to WMAP3. The optimal scale may also have some modest dependence on the choice of model parameters varied in a fit, for instance if non-negligible neutrino masses were included. One might even wonder whether it might be best to choose different scales for different observables, as the scalars and tensors are best constrained on quite different length scales, but we have not attempted this here.

We have shown that the marginalized constraints on n_s and r , or on ϵ and η , depend significantly on the choice of scale in the presence of running. By choosing the optimal scale, we find that constraints on those parameters are only mildly degraded by the in-

clusion of running as a parameter, in contrast to the impression given if constraints are quoted at a non-optimal scale such as 0.002 Mpc^{-1} .

4.7 Appendix

4.7.1 CosmoMC setup

CosmoMc is a Monte Carlo Markov Chain machine used to probe the posterior parameter-space distribution, introduced by Lewis and Bridle (2002). It generates an MCMC file of independent samples of the posterior distribution and attributes a likelihood to each set of parameter values, given the data. It scales only linearly with the number of parameters being varied, so that introducing new variables has very little computational impact.

- **MCMC runs:** the chains were run with the default values set by the `PARAMS.INI` file provided with the package. We applied a 10% BURN IN of initial steps and maximum 100000 chain steps. We implemented the second consistency equation as additional constraint on the tensor power spectrum.
- **Prior setup:** we vary up to eight parameters,

$$\Omega_b h^2, \Omega_{\text{dm}} h^2, \theta, \tau, n_S(k_*), r(k_*), \ln[10^{10} A_S(k_*)], \left. \frac{dn_S}{d \ln k} \right|_{k_*},$$

applying uniform priors and giving values of start, min, max, start width, and standard deviation estimate as follows,

parameter	start	min	max	start width	st. dev. estim.
$\Omega_b h^2$	0.0223	0.005	0.1	0.001	0.001
$\Omega_{\text{dm}} h^2$	0.105	0.01	0.99	0.01	0.01
θ	1.04	0.5	10	0.002	0.002
τ	0.09	0.01	0.8	0.03	0.03
n_S	0.95	0.5	1.5	0.03	0.01
$dn_S/d \ln k$	0	-0.2	0.2	0.01	0.01
$\log[10^{10} A_s]$	3	2.7	4	0.01	0.01

- **Chain convergence:** Monitoring chain convergence is essential before deciding when to terminate a MCMC run. The `GETDIST` program supplied together with CosmoMC for chain analysis outputs convergence diagnosis files. However a good stopping rule to use while the runs are ongoing is the number of independent samples in each file. Provided the step sizes are well matched to the corresponding parameter standard deviations this number is a good indicator that a chain is converged. To obtain an estimate of the number of independent samples we look at the acceptance rate of the proposed points (fraction of proposals that are being accepted along the chain). If this number is too large ($\sim 70\%$) the points won't be independent. We considered 20% to be a good target to ensure independent samples and chain convergence.

4.7.2 Chain manipulation

After output of the chain files by `cosmomc`, these were read into `MATHEMATICA`⁵, where a code was built for chain manipulation, auxiliary plot production and shift of cosmological scale k . Each chain element is manipulated individually. The chain is plotted and fitted with a linear relation using a least squares fit. Each element is then shifted in scale according to the expressions in the text, and finally a new chain of the shifted elements is produced and subsequently fed into `GETDIST` for area computation, statistical analysis and confidence contours production. We provide in Fig. (4.11) a `MATHEMATICA` sample code of the steps above.

4.7.3 Area Estimation

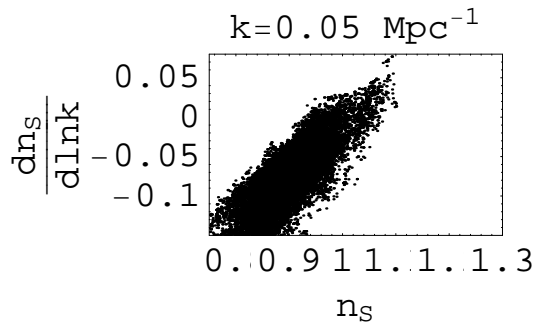
The area is calculated by a modified version of the `MATLAB`⁶ code provided by `GETDIST`. We fit each plot area with a grid and count the number of grid points totally or partially filled by the contour. Our aim is to get an accurate area estimate, but increasing the number of bins in order to achieve this makes for highly irregular ellipse contours. There's a tension between the smoothness of contours and the accuracy of the areas calculated from the grid. In Fig. (4.12) we show the contours obtained with 20, 50 and 100 bins. While the area accuracy increases from (a) to (c) the smoothness of contours is clearly deteriorated. The optimal compromise between the two is 50 bins.

⁵©Wolfram Research, Inc., Mathematica, Version 5.2, Champaign, IL (2005)

⁶©1994-2008 The MathWorks, Inc

```
chain_orig = Import["CE2_Run_thin.txt", "Table"];
```

```
ListPlot[chain_orig[[All, {10, 12}]], PlotRange → {{0.75, 1.3}, {-0.15, .08}},
  AxesOrigin → {.75, -0.15}, PlotLabel → "k=0.05 Mpc-1",
  TextStyle → {FontSize → 14}, Frame → True, FrameLabel → {ns, dns/dlnk};
```



```
FindFit[chain_orig[[All, {12, 10}]], d x + e, {d, e}, x]
```

```
{d → 1.06566, e → 0.980521}
```

```
(*decorrelation scale*)
```

```
Δlnk = -1.066; k_* = 0.05 Exp[Δlnk];
```

```
0.017225
```

```
(*ns scale shift*)
```

```
chain_decorr = chain_orig;
```

```
chain_decorr[[All, 10]] = chain_orig[[All, 10]] + Δlnk chain_orig[[All, 12]];
```

```
(*Plot ns and dns/dlnk at the decorrelation scale k=0.017 Mpc-1*)
```

```
ListPlot[chain_decorr[[All, {10, 12}]], PlotLabel → "k=0.017 Mpc-1",
  PlotRange → {{.75, 1.3}, {-.15, .08}}, Frame → True, FrameLabel → {ns, dns/dlnk},
  AxesOrigin → {.75, -.15}, TextStyle → {FontSize → 14}];
```

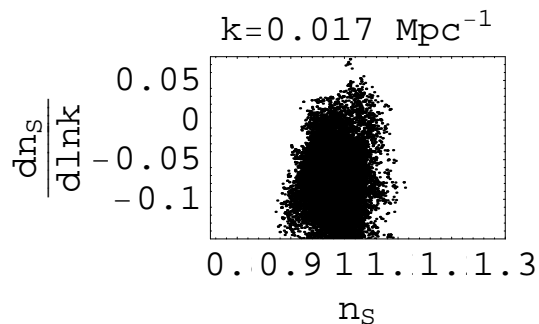


Figure 4.11: Sample code of MATHEMATICA used to read in, plot and find decorrelation scale for the variables n_s and $dn_s/d \ln k$

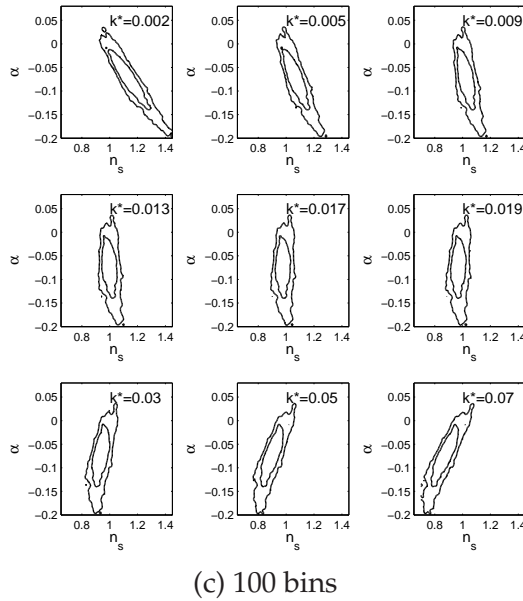
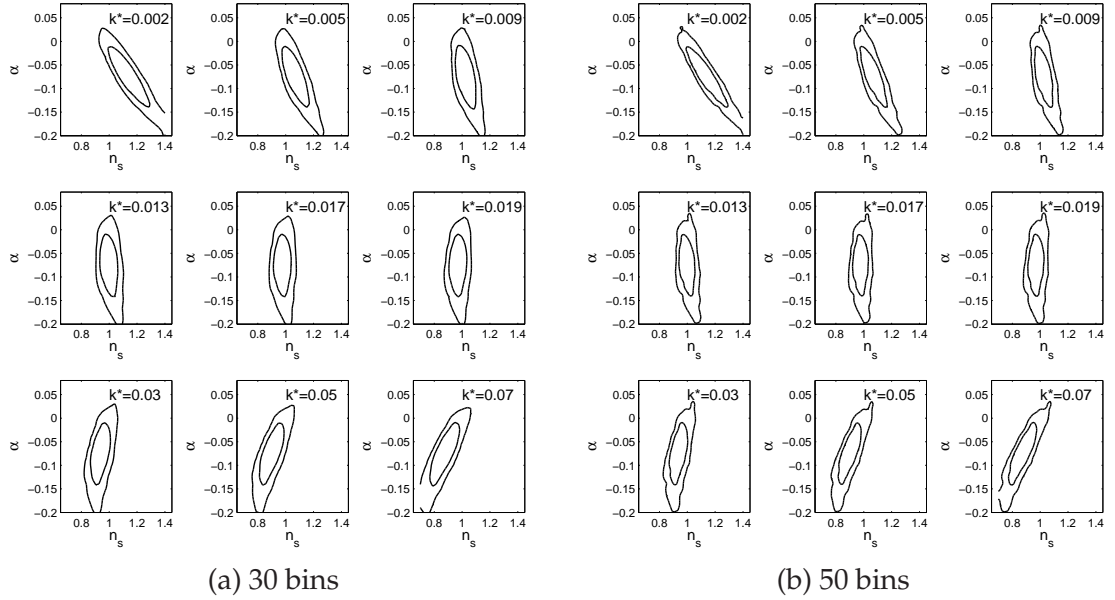


Figure 4.12: The accuracy of the estimated area competes with the smoothness of the contours obtained. In (a) 30 bins provides smooth contours but not accurate enough area values whereas with 100 bins (c) the opposite occurs. An optimal solution is (b) with 50 bins.

Chapter 5

Big Bang Nucleosynthesis constraints on Dark Energy

5.1 Introduction

Scalar fields are arguably the best-motivated alternatives to a cosmological constant, being consistent with current constraints and simultaneously theoretically well-founded. The more exotic alternatives are either claimed to have theoretical pathologies or likely to be indistinguishable from the vanilla Λ CDM model which, given all current data, remains flavour of the month (Spergel et al. (2007); Astier et al. (2006); Tegmark et al. (2006); Wood-Vasey et al. (2007)). Models in the former category include K-essence (Armendariz-Picon et al. (2000); Bonvin et al. (2006)) and the DGP model (Dvali et al. (2000); Deffayet et al. (2006); Charmousis et al. (2006)) while those in the latter class include $f(R)$ modifications of gravity (Song et al. (2007); Faulkner et al. (2007)), and unified dark energy (Sandvik et al. (2004)).

Of the scalar fields however, arguably the best-motivated and most compelling are the tracking/scaling quintessence models (Ratra and Peebles (1988); Wetterich (1988); Copeland et al. (1998b); Ferreira and Joyce (1998); Copeland et al. (2006)), which we discussed in section 2.2.2, where the dark energy equation of state, $w \equiv p/\rho$, tracks the dominant energy density component of the cosmos ($w = \frac{1}{3}, 0$), until a redshift $z = z_t$ at which it undergoes a transition to $w < 0$ which triggers the onset of acceleration.

As we discussed in section 2.2.3, Big Bang Nucleosynthesis provides strong constraints on the energy density of dark energy during the radiation dominated era at a temperature of $T \sim 1\text{MeV}$, implying that $\Omega_{\text{DE}}(T \sim 1\text{MeV}) < \epsilon = 0.045$ at 2σ (Bean et al. (2001)). The Cosmic Microwave Background provides similar or better constraints, $\Omega_{\text{DE}}(T \sim 1\text{eV}) < 0.04$ (Doran et al. (2005); Doran and Robbers (2006)) at decoupling. Constraints on $w(z)$ from BBN taken together with recent data require that $z_t > 5$ (Corasaniti et al. (2004)).

In the case of tracking dark energy models these constraints at early times are preserved by the subsequent evolution of the cosmos, implying that the limit $\Omega_{\text{DE}} < \epsilon = 0.045$ holds for all redshifts greater than z_t , the redshift at which the equation of state

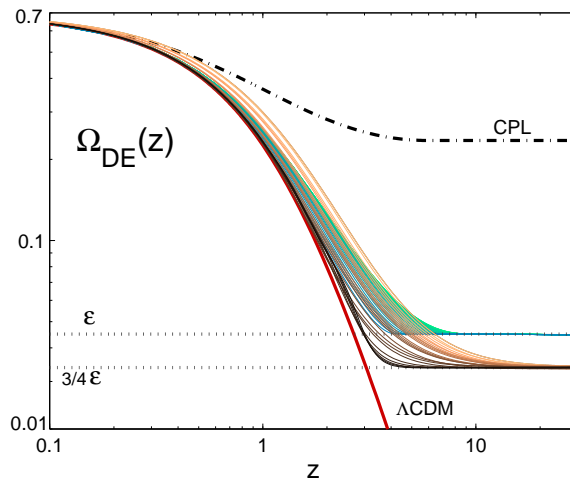


Figure 5.1: **Evolution of $\Omega_{\text{DE}}(z)$** for the models we consider, showing their approach to the BBN limits of $\epsilon = \Omega_{\text{DE}}(z = z_{\text{BBN}}) = 0.045$ and $\frac{3}{4}\epsilon$ (double exponential potential). For comparison we also show the curves for Λ and the CPL $w(z)$ with the lowest asymptotic value of Ω_{DE} assuming $w \geq -1$, showing its inability to match the BBN constraint. Figures 5.2 and 5.5 shows the corresponding observational quantities.

stops tracking and becomes negative. In this chapter, we find new implications for the magnitude of allowed deviations from Λ .

To motivate our results consider a toy, step-function model for $w(z)$,

$$w(z) = \begin{cases} \text{const.} & \text{for } z < z_t \\ 0 & \text{for } z \geq z_t \end{cases} \quad (5.1)$$

Requiring $\Omega_{\text{DE}}(z_t) < \epsilon = 0.045$ with $w \geq -1$ and $\Omega_{\text{DE}} = 0.7$ today implies that $z_t > 2.6$. This is an unexpectedly large number given that most cosmic probes in the next decade will be limited to $z < 2$. To achieve $z_t = 1$ instead, one requires a very phantom equation of state, $w = -1.88$, a value disfavoured by current observations (Spergel et al. (2007); Astier et al. (2006); Tegmark et al. (2006); Wood-Vasey et al. (2007)). Figures (5.2) and (5.5) show that the early dark energy constraints force the derivative of $w(z)$ to be very small: $|w'(0)| < 0.2$ for all our models, significantly smaller than will be detectable in the next decade (Albrecht et al. (2006)). If $w(0) < -0.9$ the deviation of the Hubble rate from Λ is less than 3% and the deviation of the distance modulus is less than 0.04 mag. In addition, we find the surprising result that the standard Chevallier–Polarski–Linder parametrisation (Chevallier and Polarski (2001); Linder (2003)) cannot be used to describe tracking minimally coupled scalar fields (which automatically have $w \geq -1$) and simultaneously match the nucleosynthesis bound. We assume a flat universe throughout with $\Omega_m = 0.3$ today and all results are valid for redshifts less than matter-radiation equality.

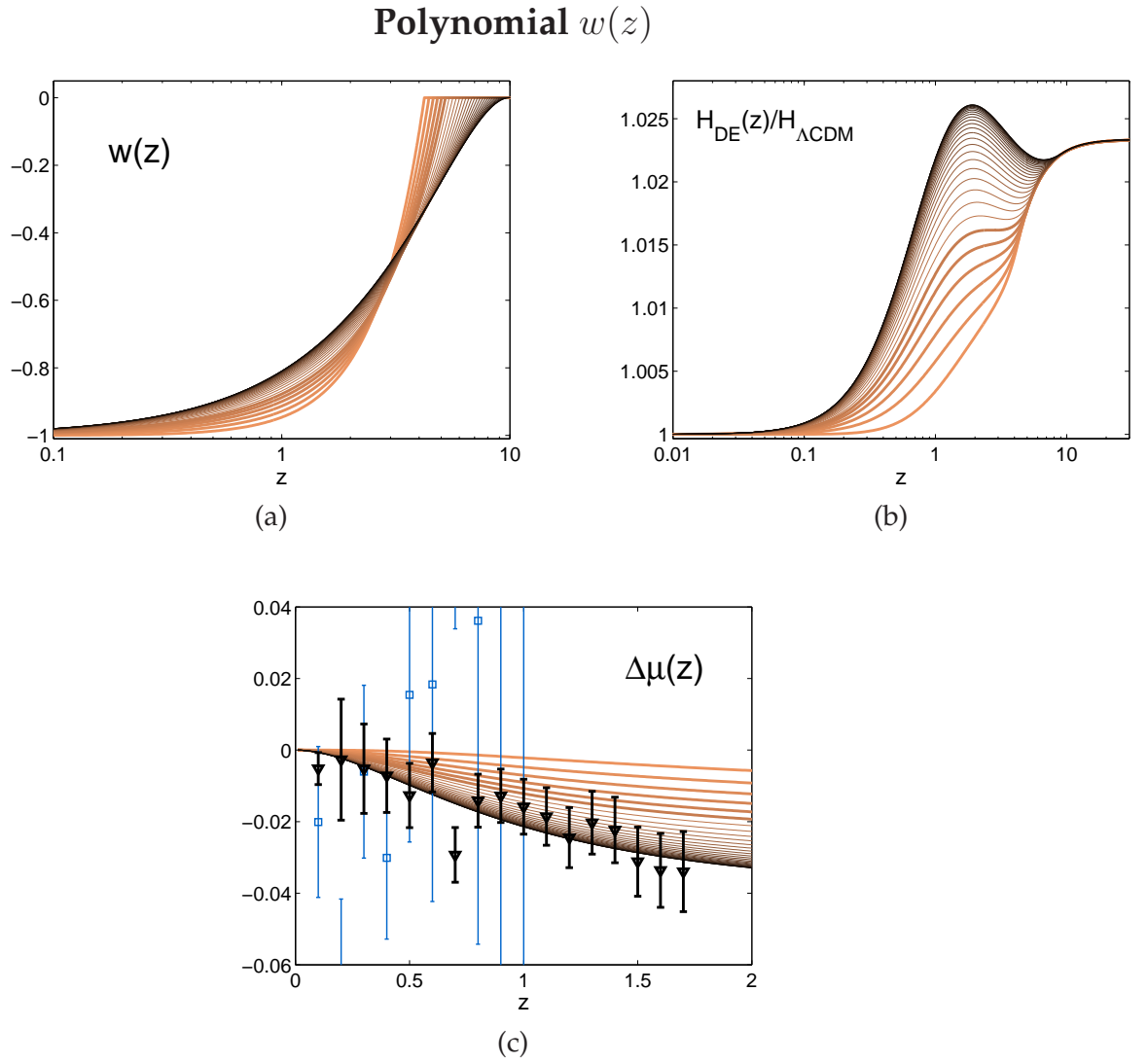


Figure 5.2: **BBN compatible tracking dark energy models:** allowed observables for the polynomial $w(z)$ showing the small deviations from the Λ predictions. In (a) the equation of state, in (b) The Hubble ratio, in (c) the distance modulus. All models have $|dw/dz(0)| < 0.2$. and imply a deviation in distance modulus of less than 0.05 mag. The error bars in the right panel correspond to the Stage-III (large boxed errors) and Stage-IV (small triangular errors) supernova surveys respectively and are produced for the bottom curve in each case.

5.2 General Results

We wish to derive model-independent constraints on cosmological observables, the Hubble rate, $H(z)$, and distance modulus, $\mu(z)$, for tracking models. The BBN constraint implies that $\Omega_{\text{DE}}(z \geq z_t) < \epsilon = 0.045$ since $\Omega_{\text{DE}}(z \geq z_t)$ is constant in perfectly tracking models. Making use of Eq. (1.17) we define

$$\Omega_{\text{DE}}(z) \equiv \frac{\rho_{\text{DE}}(z)}{\rho_{\text{cr}}(z)} \equiv \frac{\rho_{\text{DE},0} \exp \left[3 \int_0^z \frac{1+w(z')}{1+z'} dz' \right]}{\rho_{\text{cr}}(z)}, \quad (5.2)$$

and from the tracking requirement that $w(z \geq z_t) = 0$, we have

$$f(z \geq z_t) = \frac{\epsilon(1+z)^3}{r(1-\epsilon)} = \frac{0.047}{r}(1+z)^3, \quad (5.3)$$

where $r = \Omega_{\text{DE}}/\Omega_m$ is evaluated today (see Fig. (5.1)).

Using this result implies the following general but stringent constraint:

$$\begin{aligned} \frac{H_{\text{DE}}}{H_{\Lambda}}(z \geq z_t) &= \sqrt{\frac{(1+z_t)^3}{(1-\epsilon)((1+z_t)^3 + r)}} \\ &\leq \sqrt{\frac{1}{1-\epsilon}} = 1.023. \end{aligned} \quad (5.4)$$

where the last equality arises from imposing $\epsilon = 0.045$ and the upper bound from setting $r = 0$ or $z_t \rightarrow \infty$. This limit can clearly be seen in the middle panel of Fig. (5.2). This robust result implies that detecting deviations from Λ at high redshift will be difficult using Hubble rate measurements alone since they are bound to be less than 2.3%. This does not, however, strongly constrain the behaviour of the ratio $H_{\text{DE}}/H_{\Lambda}$ for $z < z_t$. We will show in two classes of models that its maximum value is less than 5% and occurs around $z \simeq 1$. The latter result is good news for Baryon Acoustic Oscillation (BAO) surveys such as WiggleZ (Glazebrook et al. (2007)), BOSS and WFMOS (Bassett et al. (2005)) which will probe this range of redshifts.

One can also place robust bounds on the deviation of the distance modulus, $\mu(z)$, from the Λ prediction. The quantity $\Delta\mu \equiv \mu_{\text{DE}}(z) - \mu_{\Lambda}(z)$ is given by

$$\Delta\mu = 5 \log_{10} \left(\frac{d_{L,\text{DE}}(z)}{d_{L,\Lambda}(z)} \right), \quad (5.5)$$

where we used Eq (1.20). If we assume that there exists a number α such that for all z

$$\frac{H(z)}{H_{\Lambda}(z)} \leq 1 + \alpha^2, \quad (5.6)$$

then

$$\frac{d_{L,\text{DE}}(z)}{d_{L,\Lambda}(z)} \geq (1 + \alpha^2)^{-1}, \quad (5.7)$$

and hence $\Delta\mu(z)$ obeys the inequality

$$0 \geq \Delta\mu(z) \geq -5 \log_{10}(1 + \alpha^2). \quad (5.8)$$

A bound of $\alpha^2 = 0.025$ gives $|\Delta\mu(z)| \leq 0.034$ mag - see Fig. (5.2). This is a conservative upper bound since we have shown that for $z \geq z_t$, $\alpha^2 \leq \epsilon/2$. For the oscillating double exponential $w(z)$ models considered later (for which $-30 \leq \mu < 0$) one has $\alpha^2 < 0.015$, yielding the constraint $|\Delta\mu(z)| \leq 0.032$ mag. These general results do not constrain $H(z)$ for $0 < z < z_t$, which instead requires a specific model for $w(z)$. For this purpose we now consider two classes of models describing a wide range of scalar field dynamics.

5.3 Polynomial $w(z)$ parametrisation

First we consider a quadratic parametrisation of the dark energy equation of state, $w(z)$ (Weller and Albrecht (2002)):

$$w(z) = \begin{cases} w_0 + w_1 z + w_2 z^2 & \text{for } z < z_t \\ 0 & \text{for } z \geq z_t \end{cases} \quad (5.9)$$

We apply the constraint $w(z) \geq -1$ since we want to describe minimally coupled scalar fields with canonical kinetic terms.

The linear case with $w_2 = 0$ requires $z_t \simeq 6.2$ to match BBN (for $\epsilon = 0.045$) if $w_0 = -1$ and if we allow w_0 to be free the BBN constraint implies the correlation

$$w_1 \simeq -0.4w_0 - 0.2 \quad (5.10)$$

for the interesting region $-1 < w_0 < -0.8$. The other case we consider is $w_0 = -1, w_2 \neq 0$. Continuity at $z = z_t$ then implies,

$$w_2 = \left(\frac{1}{z_t^2} - \frac{w_1}{z_t} \right). \quad (5.11)$$

The BBN constraint provides w_1 in terms of z_t . The resulting family of curves and observables are shown in Fig. (5.2). We note that for $z \leq 1$ the BBN constraint is so strong that all models have $w(z) < -0.8$ and the largest deviation of $H(z)$ from the Λ comparison model is about 2.7% with the largest deviation in the distance modulus only about 0.03 magnitudes (occurring at $z = 2$). This shows that if $w \simeq -1$ today we cannot expect significant deviations from Λ at any redshift and only Stage-IV experiments (Albrecht et al. (2006)) are likely to detect dark energy dynamics with any real significance.

However while current data favour $w(0) \simeq -1$ they are consistent with larger values. To study how this zero-point affects our results we now consider simulations of a scalar field with a popular family of scalar field potentials, $V(\phi)$, which also allows us to examine the impact of oscillations in $w(z)$.

5.4 Double Exponential Potential

A single exponential potential is well known to give early tracking (Copeland et al. (1998b); Ferreira and Joyce (1998)) but cannot also lead to late-time acceleration. One well-studied way to combine the two effects is via the double exponential potential. Barreiro et al. (2000) have considered a model where the scalar field has a potential which is a sum of two exponential terms,

$$V(\phi) = M_1^4 e^{-\lambda\kappa\phi} + M_2^4 e^{-\mu\kappa\phi}, \quad (5.12)$$

where $\kappa^2 = 8\pi m_{\text{pl}}^{-2}$. This potential, with a correct choice of the parameters λ and μ (we assume that λ is positive), allows for a scenario where the universe goes through a radiation and matter dominated epochs, during which the field scales with the background fluid, and recently evolves into the scalar field dominated regime. Such a potential is theoretically well motivated, because it is expected to arise as a result of compactifications in superstring models. We assume the field to be scaling during radiation domination and then satisfying the BBN constraint implies (Ferreira and Joyce (1998); Copeland et al. (2006)),

$$\lambda \geq \frac{2}{\sqrt{\epsilon}} \geq 9.43 \quad (5.13)$$

We choose $\lambda = 9.43$ to maximise deviations from Λ . Unlike a perfectly scaling model of the form we assumed in the previous section, Ω_ϕ actually decreases in the transition to matter domination and we have

$$\Omega_\phi < \frac{3}{4}\epsilon = 0.034 \quad (5.14)$$

during matter domination, leading to even more stringent results - see Fig. (5.1). The extra $3/4$ factor is specific to the double exponential potential and is responsible for the reduction of the asymptotic values of $H_{\text{DE}}(z)/H_{\Lambda\text{CDM}}$, seen in the middle panel of Fig. (5.5), relative to the predictions of Eq.(5.4).

If the constraint in Eq. (5.13) is satisfied we will have scaling during radiation and matter dominated eras, and we need $\mu^2 < 2$ if we want the field to leave the scaling regime at late times and give rise to an accelerated expansion. We must choose M_2 such that the energy density of the field today is equal to the value measured by observations, $\rho_0 \sim 10^{-47} \text{GeV}^4$ (which implies $M_2 \sim 10^{31} m_{\text{pl}}$ for $\mu \sim 1$). We take $M_1 = 10^{-14} m_{\text{pl}}$ and use Planck units where $\kappa = 1$. It was shown that the scaling regime occurs for a wide range of initial conditions (Barreiro et al. (2000)). We have written a code to solve numerically the evolution equations for a scalar field with the potential in Eq. (5.12) and for radiation and matter fluids¹,

¹We provide an example of the code used to integrate the equations in the Appendix

$$\begin{aligned}
\ddot{\phi} + 3H\dot{\phi} + V_{,\phi} &= 0, \\
\dot{\rho}_m + 3H\rho_m &= 0, \\
\dot{\rho}_r + 4H\rho_r &= 0, \\
H^2 &= \frac{\kappa^2}{3} \left[\frac{1}{2}\dot{\phi}^2 + V(\phi) + \rho_m + \rho_r \right].
\end{aligned} \tag{5.15}$$

We can see from Figure (5.3) that the field enters a scaling regime during the radiation dominated era with equation of state $w_\phi = w_r = 1/3$, then starts to scale with matter when the universe enters in the matter dominated regime with $w_\phi = w_r = 0$ and will finally dominate the energy density of the universe at late times (see Fig. (5.4)). The shape of the curve for w_ϕ during the transition from zero to the final value today depends on the value of the parameter μ (Barreiro et al. (2000)). We can consider three cases:

- $\mu > 0$ simply modifies the slope of the potential which becomes shallow at late times and the equation of state for ϕ has a final value $w_\phi > 1$;
- if $\mu = 0$ the potential will become constant at late times and we will have a final $w_\phi = 1$;
- if $\mu < 0$ the potential has a global minimum and the field will oscillate about the minimum until it stops and we get $w_\phi = 1$.

The more negative the value of μ the larger (and more negative) the slope of the curve of w_ϕ after the matter dominated era, and the later (smaller redshift) the field leaves the scaling regime, see Figures (5.4) and (5.5).

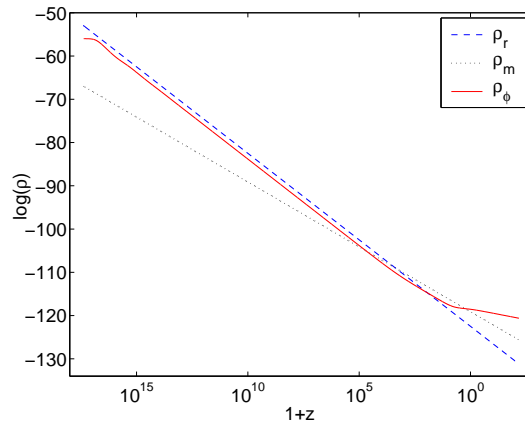


Figure 5.3: Energy densities of the different components present in the universe as a function of redshift, for $\lambda = 9.43$, $M_1 = 10^{-14}$, $\mu = 1$ and $M_2 = 10^{-27.9}$ (we set $\kappa = 1$). We have chosen M_2 such that $\Omega_\phi \sim 0.7$ and $\Omega_m \sim 0.3$ today.

The resulting $w(z)$ curves for a range of values of μ , are shown together with the predicted observables ($H(z)$, $\Delta\mu(z)$) in Fig. (5.5). For negative μ (we study $-30 \leq \mu < 0$)

and for $z \lesssim 0.2$ the equation of state satisfies $w_\phi \leq -0.98$. As a result all the negative μ models show tiny deviations from Λ : less than 1.5% for $H(z)$ and less than 0.015 mag for $\Delta\mu$ (see Fig. (5.5)). This will make detection extremely difficult even with the Stage-IV dark energy experiments such as EUCLID², JDEM³, LSST⁴ and SKA⁵ (Albrecht et al. (2006)).

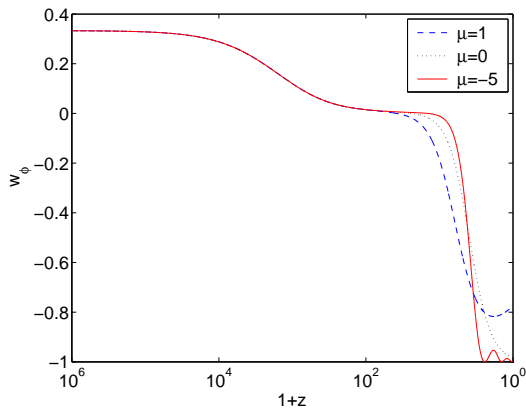


Figure 5.4: Equation of state of the scalar field as a function of redshift, for $\lambda = 9.43$, $M_1 = 10^{-14}$ and different values of μ ($\kappa = 1$). For each case we choose M_2 such that $\Omega_\phi \sim 0.7$ and $\Omega_m \sim 0.3$ today.

In contrast, positive values of μ ($0 \leq \mu \leq 1$) can yield values of w_ϕ significantly different from -1 today, e.g. for $\mu \sim 1$ one finds $w_\phi(0) \sim -0.8$ which is consistent (at about the 2σ level) with current observations (Spergel et al. (2007); Astier et al. (2006); Tegmark et al. (2006); Wood-Vasey et al. (2007); Corasaniti et al. (2004)), and which we therefore take as the upper bound for μ .

Fig. (5.5) shows that the maximum allowed deviation for $H(z)$ from $H_\Lambda(z)$ in this case is about 5%, peaking at $z \sim 1$ with a maximum value of $\Delta\mu \sim 0.09$ mag. Such a model will be detectable with Stage-III supernova surveys (at the 99.97% confidence level) and with the upcoming BAO experiments, since the maximum deviation in $H(z)$ coincides with the redshift ranges in which they will operate, i.e. $z \sim 0.7$ to 1.1. However, for values more consistent with the current best-fits, $w_\phi(0) < -0.9$ one finds much smaller deviations of 2.7% and 0.045 mag respectively for $H(z)$ and $\Delta\mu$ which again will require Stage-IV experiments for conclusive detection as can be seen in the right-hand panels of Fig. (5.5).

5.5 Performance of standard parametrisations

The most widely used parametrisation for dark energy, is the Chevalier-Polarski-Linder parametrisation given by Eq. (2.46) which is also the basis for the DETF figure-of-merit

²<http://sci.esa.int>

³<http://jdem.gsfc.nasa.gov>

⁴<http://www.lsst.org>

⁵<http://www.skatelescope.org>

Double Exponential

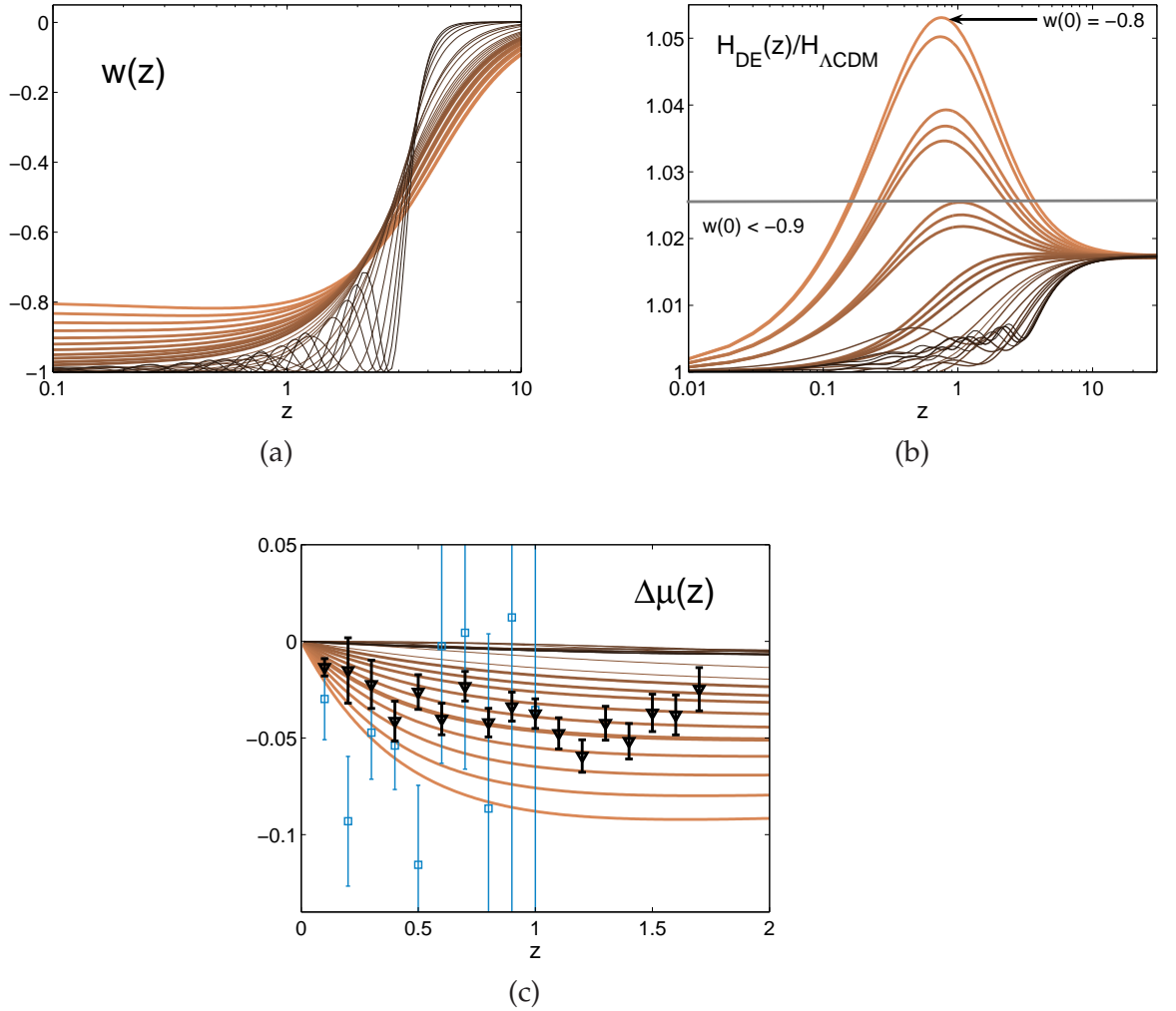


Figure 5.5: **BBN compatible tracking dark energy models:** allowed observables for the double exponential potential with $-30 \leq \mu \leq 1$ showing the small deviations from the Λ predictions. In **(a)** the equation of state, in **(b)** The Hubble ratio, in **(c)** the distance modulus. All models have $|dw/dz(0)| < 0.2$. For $w(0) < -0.9$ $H_{\text{DE}}(z)$ deviates from $H_{\Lambda}(z)$ by at most 2.7% (marked by the horizontal line in the middle panel) and implies a deviation in distance modulus of less than 0.05 mag. Error bars for the distance modulus are calculated as as in Fig (5.2) except for the Stage-IV (SNAP-like) errors which correspond to the $w(0) = -0.9$ model (thicker line asymptoting to ~ 0.04 mag). Note that the ratio $H(z)/H_{\Lambda}$ for the double exponential potential does not converge to 1.023 since the matter-dominated value of $\Omega_{\text{DE}}(z)$ is constrained to be $3/4$ of the radiation-dominated value. Hence the Hubble rate is forced to $\sim 1 + (3/8)\epsilon \sim 1.017$.

(Albrecht et al. (2006)). Surprisingly, we found that this parametrisation fails to meet the BBN constraint if we assume as before, scaling until transition to dark energy domination and $\Omega_{\text{DE}} \sim 0.7$ today.

To examine this we take $w(z) \geq -1$ and $w(z \geq z_t) = 0$ and try to find the value of z_t that gives $\Omega_{\text{DE}}(z = 0) \sim 0.7$ and $\Omega_{\text{DE}}(z_t) = 0.05$ just like in previous sections. The result is presented in Fig. (5.1) and shows the lowest attainable value of Ω_{DE} with $w_0 = -1$. There is no value of z for which the BBN limit on Ω_{DE} is achieved. The CPL parametrization is not flexible enough to bring Ω_{DE} from its observed value today to $\Omega_{\text{DE}}(z_t) \sim 0.05$ required by a scaling field meeting the BBN constraints.

In retrospect this is understandable since to reach the tracking value $w = 0$ for some z_t requires $w_a > -w_0$. In this case $w(z)$ doesn't spend enough time at sufficiently negative values to force $\Omega_{\text{DE}}(z)$ down to the BBN value. The least phantom value of w_0 that is able to satisfy the BBN constraint is $w_0 = -1.3$. In contrast the logarithmic expansion $w(z) = w_0 + w_1 \ln(1 + z)$ is able to match the BBN constraint with $w(z) \geq -1$, but only for $z_t > 12.4$.

5.6 Conclusions

Tracking scalar field models are arguably the best-motivated alternatives to the cosmological constant. We show that the constraints on the energy density of the scalar field at the time of Big Bang Nucleosynthesis and decoupling strongly limit the allowed dynamics of such models today and allow the derivation of model-independent constraints on the Hubble rate which cannot deviate by more than 2.3% from Λ CDM (for $z \geq z_t$), with similar limits on the distance modulus μ . If w today is close to the maximum value allowed by current data then next-generation surveys such as WiggleZ and BOSS could detect dark energy dynamics. However, if this is not the case, detection of dynamics will likely have to wait a decade for the Stage-IV DETF experiments. Of course, these strong conclusions are only true for tracking models and if one allows exotic phantom behaviour ($w < -1$) the conclusion is much more rosy. In particular, it would be interesting to construct approximately tracking models in which Ω_{DE} increases with time, since these would be allowed a wider range of dynamics today.

Finally we have shown that the standard CPL parametrisation, $w(z) = w_0 + w_a z / (1 + z)$, fails clearly to match the BBN constraint when describing tracking scalar fields which satisfy $w \geq -1$. This is particularly important given that the CPL parametrisation is the basis of the DETF figure-of-merit which is now the *de facto* standard for the optimisation of future cosmological surveys, e.g. (Parkinson et al. (2007); Virey and Ealet (2007); Yamamoto et al. (2007)). A concern therefore is that optimisations may be systematically biased *away* from tracking dark energy models. More work in this area is clearly needed to assess the implications of early dark energy constraints for cosmological survey design, but it is clear that the current non-detection of dark energy dynamics should neither come as a surprise, nor should it discourage us from the hunt.

5.7 Appendix

The numerical computations necessary for this work were performed using MATLAB. The system of differential equations for the coupled fluids was numerically integrated and in this appendix we provide and describe the functioning of the code built.

We used the MATLAB function `ODE45` which employs variable size Runge–Kutta integration methods. The system of differential equations is defined in a function file that returns the solutions stored in a vector. A separate file then invokes this function and simulates the solution over the specified range and initial conditions.

In `BBN_set` we define a function `dydt` which describes the system of coupled differential equations Eqs. (5.15) and stores the solutions in a vector y composed of

$$y = \{\phi(t), \dot{\phi}(t), \rho_r(t), \rho_m(t)\}.$$

This function is called in `BBN_rho` where the simulation is performed. where we specify the accuracy, range of integration, initial conditions and determine the plots to be drawn.

The accuracy is specified by the functions `AbsTol` and `RelTol`. `RelTol` is the relative tolerance and controls the number of correct digits in every component of the solution. `AbsTol` is a threshold below which the value of the solution is unimportant. We choose

$$\text{AbsTol} = \text{RelTol} = 10^{-20} \quad (5.16)$$

which translates into an accuracy of $10^{-18}\%$. As integration variable we used $\log a$ and considered the range $[a^{-40}, a^0]$. The initial conditions are

$$\{\phi_0 = 0, \dot{\phi}_0 = 0, \rho_{r,0} = 10^{-53}, \rho_{m,0} = 10^{-67}\} \quad (5.17)$$

The energy scale is set by requiring the Dark Energy density today to match observations which translates in $M_2 \sim 10^{31}$. Here we reproduce the two files of code `BBN_set` and `BBN_rho` and Fig (5.3) shows an example of the plot produced by the code.

`BBN_set`

```
function dydt = f(t,y)
```

```
MP1=1.;
```

```
M1=10.^(-14.)*MP1;
```

```
M2=10.^(-29.69)*MP1;
```

```
lambda=9.43;
```

```
mu=0.;
```

```
V=M1.^4.*exp(-lambda.*y(1)./MP1)+M2.^4.*exp(-mu.*y(1)./MP1);
```

```
Vphi=-lambda.*M1.^4./MP1.*exp(-lambda.*y(1)./MP1)-mu.*
```

```

M2.^4./MP1.*exp(-mu.*y(1)./MP1);

H=sqrt(1./(3.*MP1.^2.).*(1./2.*y(2).^2.+V+y(3)+y(4)));

dydt = [y(2)./H;-3.*y(2)-Vphi./H;-4.*y(3);-3.*y(4)];

```

BBN_rho

```

options = odeset('RelTol',1e-20,'AbsTol',1e-20);

[t,y] = ode45(@BBN_set,[-40. 0.],[0.; 0.; 10.^(-53.);
 10.^(-67.)],options);

MP1=1.;
M1=10.^(-14.).*MP1;
M2=10.^(-29.69).*MP1;
lambda=9.43;
mu=0.;

V=M1.^4.*exp(-lambda.*y(:,1)./MP1)+M2.^4.*exp(-mu.*y(:,1)./MP1);
Vphi=-lambda.*M1.^4./MP1.*exp(-lambda.*y(:,1)./MP1)-mu.*
M2.^4./MP1.*exp(-mu.*y(:,1)./MP1);

H=sqrt(1./(3.*MP1.^2.).*(1./2.*y(:,2).^2.+V+y(:,3)+y(:,4)));
edphi=1./2.*y(:,2).^2.+V;
pphi=1./2.*y(:,2).^2.-V;
Omegam=y(:,4)/(3.*H.^2);
Omegaphi=edphi/(3.*H.^2);

plot(t./log(10.),log10(y(:,3)),'--',t./log(10.),log10(y(:,4)),'-.',
t./log(10.),log10(edphi),'-')
xlabel('log(a)')
ylabel('log(\rho)')
legend('\rho_r','\rho_m','\rho_\phi')

```

Chapter 6

Non-parametric Dark Energy Degeneracies

6.1 Introduction

In the last chapter we discussed a particular class of dark energy models, scaling quintessence fields which propose dark energy as an extra fluid component, and presented constraints from Big Bang Nucleosynthesis within the frame of work of these models.

In this chapter we aim at deriving constraints which are model independent and parametrisation free. This approach is more fruitful since it allows us to draw conclusions about dark energy behaviour which are valid for all studies. This is here the more important given the unexpected results we obtain which have implications for all dark energy analyses.

The current drive in the search for the origin of acceleration is focused on trying to establish its dynamical behaviour as a function of redshift, $w(z)$. The simplest explanation remains a Λ CDM universe with $w = -1$ for all redshift but evidence for dynamics would provide a window into new physics and therefore, uncovering the dynamics of dark energy as described by the ratio of its pressure to density, $w(z) = p_{DE}/\rho_{DE}$, has become the focus of multiple proposed experiments using a wide variety of methods. Several of these planned surveys aim at redshifts above unity - as high-redshift measurements are useful to constrain dark energy parameters and test for deviation from the concordance Λ CDM model (see e.g. Albrecht et al. (2006)). Unfortunately the search for dynamical behaviour in w is a many-fold problem. The nature of dark energy is elusive: cosmic observations depend not only on dark energy but also on other cosmic parameters such as the cosmic curvature, Ω_k , and the total matter content, Ω_m , leading to degeneracies between these and $w(z)$ parameters, an issue which has recently been under intense scrutiny by the community (Kunz (2007); Clarkson et al. (2007); Linder (2005); Huang et al. (2007)). Kunz (2007) argues that observations are only sensitive to the full energy-momentum tensor and thus cannot see beyond a combination of the “dark component” – dark matter *plus* dark energy. Also, the degeneracy between the geometry of the universe and the equation of state of dark energy has been discussed in light of the well-known result that a

cosmological constant in the presence of spatial curvature can mimic a dynamical dark energy (Clarkson et al. (2007)).

In this chapter we review current constraints on cosmic curvature and discuss the reconstruction of $w(z)$ that would follow from an incorrectly assumed value for Ω_k from observations of Hubble rate, distance luminosity and rate of change of cosmic volume with redshift, dV/dz .

Further we analyse reconstruction of $w(z)$ from the wrong value of the matter content, Ω_m . We assume perfect data for all observations, which allows us to probe fundamental, “in-principle” degeneracies that are not due to finite errors and incomplete redshift-coverage. This implies that given a specific bias in a cosmological parameter, the degeneracies will be true no matter what progress is made in improving future cosmic surveys. Furthermore, the key point in our reconstruction of $w(z)$ is that it is performed in a fully non-parametric manner, and so does not rely on the validity of any particular parameterisation of $w(z)$. To illustrate the power of this non-parametric approach, we compare our method with a standard equation of state parameterisation (Chevallier and Polarski (2001); Linder (2003)), which cannot fully resolve the above degeneracies.

6.1.1 Degeneracies in Dark Energy Studies

The success of the inflationary scenario for the early Universe and its standard prediction of flatness to high precision ($\Omega_k < 10^{-10}$) is perhaps the main reason why curvature has traditionally been left out in analyses of dark energy. However, possible scenarios in which inflation is consistent with non-zero spatial curvature have recently been investigated in Freivogel et al. (2006). It is also interesting to note that the backreaction of cosmological fluctuations may cause effective non-zero curvature that may yield practical limits on our ability to measure $w(z)$ accurately at $z > 1$ (see e.g. Buchert and Carfora (2003); Li and Schwarz (2007); Rasanen (2006); Coley and Pelavas (2007)). Since measurements of the CMB have so far proved consistent with flatness (e.g. Spergel et al. (2007)) statistical quantities that measure the necessity of introducing extra parameters — such as Bayesian Evidence or information criteria (Bassett et al. (2004); Kunz et al. (2006); Trotta (2007)) — do not favour the inclusion of curvature as a parameter in current analyses (Liddle (2007)). However, Bayesian evidence or information criteria do not take into account the power of the biases that may be introduced by falsely neglecting a parameter. We will show below that the biases introduced in neglecting curvature are very significant at $z > 1$.

In general constraints on curvature are very fragile to assumptions about the dark energy since they are primarily derived from distance measurements (d_L or d_A) which are completely degenerate with curvature (Weinberg (1970)). One way to illustrate the degeneracy between curvature and dynamics is as follows. Let us assume that we know all cosmic parameters perfectly other than the curvature Ω_k and the dark energy equation of state, $w(z)$. At any redshift, z_* , a perfect measurement of $d_L(z_*)$ (or $d_A(z_*)$) allows us to measure a single quantity. If we know $w(z_*)$ then that quantity can be Ω_k . However, if $w(z)$ is truly a free function, then its value at z_* is completely free and we are left trying

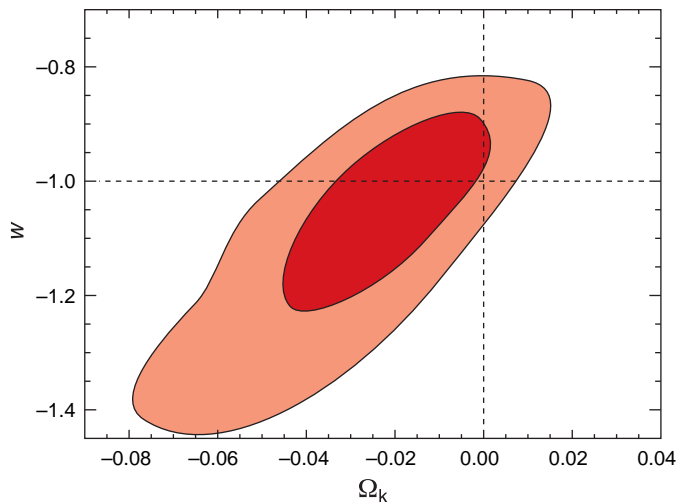


Figure 6.1: **The curvature-dark energy degeneracy** Contours showing the 2D marginalized contours for w and Ω_k based on combined data from WMAP3, 2dFGRS, SDSS and supernova surveys. While the slope of the degeneracy differs for this combination of data, the sign of the degeneracy is consistent with the w_0 term in Eqs. (6.18),(6.19). Taken from Spergel et al. (2007).

to find two numbers from a single observation, which is impossible.

Only when we start to correlate the values of $w(z)$ at different redshifts can we begin to use distance measurements alone to constrain the curvature. The standard way to do this is to assume that $w(z)$ can be compressed onto a finite-dimensional subspace described by n parameters, e.g.

$$w(z) = \sum_j^n w_j z^j \quad (6.1)$$

In this case perfect distance measurements at $n + 1$ different redshifts will allow a complete solution of the problem and will yield the w_j and Ω_k . The most extreme version of this is to assume Λ CDM, $w(z) = -1$. Within this context it is of course possible to derive very stringent constraints on the curvature. For example, combining the WMAP 3 year data and the SDSS DR5 Luminous Red Galaxy (LRG) sample leads to $\Omega_k = -0.003 \pm 0.010$ assuming $w = -1$ (Tegmark et al. (2006)). The addition of extra data is crucial since the WMAP data alone provides only the constraint $\Omega_k = -0.3040 + 0.4067\Omega_\Lambda$ (Spergel et al. (2007)).

It is a highly non-trivial statement that flat Λ CDM models provide such a good fit to all the data, but we must be aware that such constraints on the curvature are artificially strong in the sense that adding more dark energy parameters will lead to an almost perfect degeneracy with the curvature. This is visible in Fig. 17 of the WMAP3 paper, Spergel et al. (2007) (here Fig. 6.1), which shows the correlation between a constant w and Ω_k .

Hence we can currently say very little about the true value of the Ω_k and the belief that the spatial curvature is small is essentially based on Occam's Razor. Although one could fit distance measurements with any value of Ω_k , the required $w(z)$ functions would be disfavoured by Bayesian model selection which penalize models with extra parame-

ters that do not significantly improve the fit. We show in detail later the required $w(z)$ functions to do precisely this.

At present a well-defined programme for measuring the spatial curvature of the cosmos does not exist. To illustrate this, consider fixing the dark energy to be described by only n parameters. One would hope that given this restriction the resulting constraints on Ω_k would be independent of the precise choice of the n parameters, i.e. independent of the parameterisation. However a little thought makes it clear that this cannot be true. A parameterisation of $w(z)$ which does not allow mimicry of curvature will provide good, decorrelated constraints on the curvature (which does not mean the corresponding best-fit will be a good fit to the data) while a model which allows perfect mimicry of the dynamics of the curvature (i.e. $(1+z)^2$) will show highly correlated constraints.

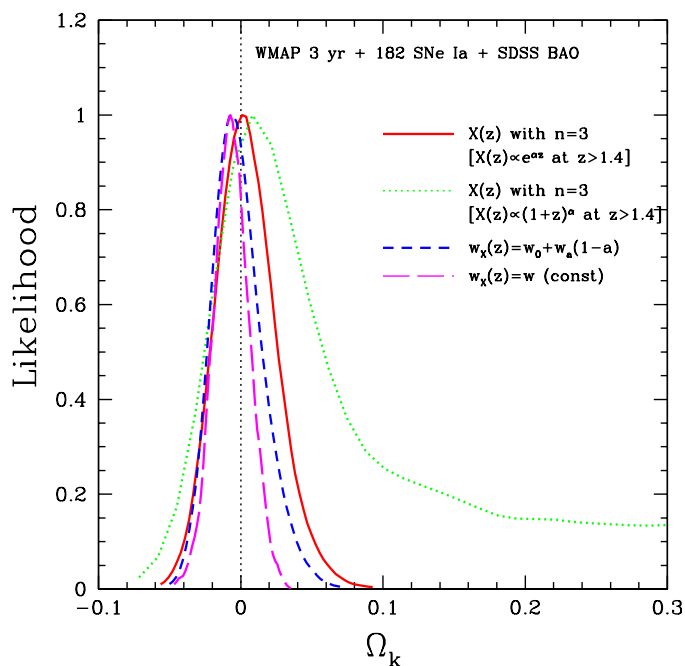


Figure 6.2: **The curvature-dark energy degeneracy** likelihood for Ω_k for different parameterisations of dark energy. Assuming a constant model for w , allows Ω_k to be tightly constrained at 2σ to be near 0. However introducing dynamics reduces these constraints significantly. Here $X(z) = \rho_X(z)/\rho_X(0)$ is the dark energy density, which Wang and Mukherjee (2007) assume is a free function below some cut-off redshift z_{cut} . The value of X at redshifts $z_i = z_{cut}(i/n), i = 1, 2, \dots, n$ are treated as n independent model parameters that are estimated from the data. A specific functional form for X is assumed above the cut-off redshift. The likelihoods are given for two such forms of $X(z)$; namely a power law, $X \propto (1+z)^\alpha$ for $z > z_{cut}$, and an exponential function $X \propto e^{\alpha z}$. In these figures there are $n = 3$ independent redshifts below a cut-off redshift of $z_{cut} = 1.4$. Taken from Wang and Mukherjee (2007).

This dilemma is visible in various recent studies attempting to constrain cosmic curvature in the presence of multiple dark energy $w(z)$ parameters Gong et al. (2008); Mersini-

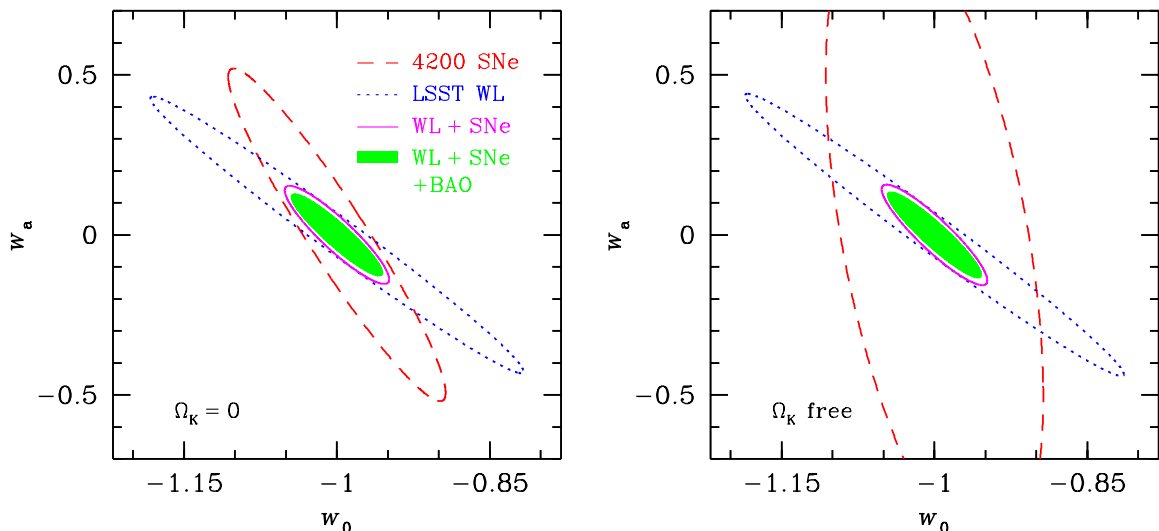


Figure 6.3: **Left** - 1σ error contours assuming flatness for the dark energy parameters w_0 and w_a for the CPL parameterisations. **Right** - as on the left but with curvature left free and marginalised over. Note how pure distance measurements suffer strongly even with the very limited $w(z)$ parameterisation but that when all the surveys are combined the final error ellipse is essentially unaffected. This is to be expected from Equation (6.5) which shows how Ω_k can be determined from simultaneous Hubble rate and distance measurements. Figure from Knox et al. (2006).

Houghton et al. (2008); Wright (2007); Ichikawa et al. (2006); Zhao et al. (2007); Ichikawa and Takahashi (2007); Wang and Mukherjee (2007); Huang et al. (2007). For some popular parameterisations constraints on Ω_k are of order $|\Omega_k| < 0.05$ at 2σ . For other parameterisations the constraints evaporate and even $\Omega_k \sim 0.2$ cannot be ruled out (see Fig. 6.2, which is taken from Wang and Mukherjee (2007)).

Alternative cosmic measurements sensitive to curvature include the Integrated Sachs Wolfe (ISW) effect, which is sensitive to the growth of the metric fluctuations Φ , which is in turn sensitive to both dark energy and curvature. Recent work to investigate the ISW effect as a function of redshift uses the combination of CMB data with information on large scale structure (Giannantonio et al. (2006); Ho et al. (2008)). Combining WMAP with such suitable tracers of large scale structure shows that Φ has been decreasing with cosmic time (Aguirre et al. (2001)), which rules out a large positive curvature which would have predicted the opposite trend.

Another measurement sensitive to the growth function is differential number counts dN/dz , e.g. of clusters. This is a potentially sensitive test which, given a constant comoving number of objects, reduces to a test of the rate of change of cosmic volume with redshift, dV/dz . We discuss in detail below how perfect measurements of dV/dz allow reconstruction of $w(z)$, and we discuss the resulting errors on dark energy when systematic biases in cosmic parameters are present.

Measurements of the power spectrum from CMB data and from measurement of Baryon Acoustic Oscillations (BAO) provide estimates of the matter content of the universe. While constraints on Ω_m are sharpened by combining data from many observa-

tions, the best-fit value is often derived on the assumption of flatness (Tegmark et al. (2006); Percival et al. (2007)). Unlike the case for cosmic curvature the degeneracy between observables and the matter content is perfect and we show that incorrectly assuming a particular value for Ω_m can also mimic deviations from Λ CDM.

6.1.2 Future surveys

We will show in equation (6.5) that simultaneous measurements of the Hubble rate $H(z)$, distance $D \propto d_A, d_L$ and $D'(z)$ allow for a perfect measurement of Ω_k . BAO allow for the simultaneous measurement of both distance and Hubble rate at the central redshift (Seo and Eisenstein (2003); Blake and Glazebrook (2003)). For a flat universe $D'(z) \propto 1/H(z)$, but in a curved universe this is not true: the curved geodesics mean that $D'(z)$ contains extra information encoded in Ω_k .

Measuring $D'(z)$ is in principle possible with future BAO, weak lensing and supernova surveys. In particular, cross-correlation tomography of deep lensing surveys appears to be a very powerful probe of curvature when combined with BAO surveys (Bernstein (2006)), assuming that self-calibration is possible. In principle it should be possible to measure the cosmic curvature to an accuracy of about $\sigma(\Omega_k) \simeq 0.01$ for an all-sky weak lensing and BAO survey out to $z = 10$. In principle such a survey would be able to measure distances to about $10^{-4} f_{sky}^{-1/2}$ in redshift bins of width $\Delta z = 0.1$ out to $z = 2.5$ (Bernstein (2006)). This relies critically on the combination of weak lensing and BAO data since constraints from either observations alone are significantly degraded. This can also be seen in Fig. (6.3) which shows the error ellipses for the parameters in the CPL parameterisation, Eq. (2.46), assuming flatness (left) and leaving Ω_k free (right). Note that although individual error ellipses are significantly degraded, the combined data sets have an almost unchanged error ellipse.

6.2 Dark Energy from observations

There are three key observables of the background geometry which play an important role in determining $w(z)$, namely measurements of distances, of the expansion history (i.e. the Hubble parameter) and of the change in the fractional volume of the Universe (e.g. from number-counts).

The principal method to date is to relate measurements of the distances of objects to the cosmology of the Universe. This is done via either standard ‘rulers’ of known length - giving the angular diameter distance $d_A(z)$ — or via standard ‘candles’ of known brightness which results in the luminosity distance $d_L(z)$, Eq. (1.19). These are related via the reciprocity relation Eq. (1.22). It will prove useful to define

$$D(z) = \frac{1}{\sqrt{-\Omega_k}} \sin \left(\sqrt{-\Omega_k} \int_0^z dz' \frac{H_0}{H(z')} \right). \quad (6.2)$$

Here, Ω_k is the usual curvature parameter given by Eq. (1.9), and $H(z)$ is given by the

Friedmann equation, Eq. (1.17), where we now include curvature as well as matter and dark energy,

$$H(z)^2 = H_0^2 [\Omega_m(1+z)^3 + \Omega_k(1+z)^2 + \Omega_{DE}f(z)] \quad (6.3)$$

where from Eq. (5.2)

$$f(z) = \exp \left[3 \int_0^z \frac{1+w(z')}{1+z'} dz' \right] \quad (6.4)$$

and $\Omega_{DE} = 1 - \Omega_m - \Omega_k$. Thus, given a cosmological model, we may calculate any distance measure we choose.

The Hubble parameter is in itself an observable which will play an important role in future dark energy experiments. Knowledge of $H(z)$ allows us to directly probe the dynamical behavior of the universe, and it will be directly determined from BAO surveys which simultaneously provide the angular diameter distance, d_A at the same redshift by exploiting the radial and angular views of the acoustic oscillation scale (Seo and Eisenstein (2003); Blake and Glazebrook (2003)), a fact that will provide key new data in coming years (Tegmark et al. (2006); Bassett et al. (2005); Glazebrook et al. (2007)).

The third key background test we will discuss here is the observation of fractional volume change as a function of redshift, given by Eq. (1.21), which can in principle be determined via number-counts or the BAO.

Given any two of the above observables we may deduce the third. Perfect observations of these observables should allow us, in principle, to be able to reconstruct two free *functions* when in fact we only need to reconstruct one, namely $w(z)$, as well as two cosmological parameters, Ω_m and Ω_k . (Note that if we know $H(z)$ perfectly, we know $H_0 = H(0)$, and so this is no longer a free parameter in the same sense.) How do we find these?

We may determine the curvature directly, and independently of the other parameters or dark energy model, via the relation (Clarkson et al. (2007)),

$$\Omega_k = \frac{[H(z)D'(z)]^2 - H_0^2}{[H_0D(z)]^2}, \quad (6.5)$$

which may be derived directly from Eq. (6.2). Such independent measurements of the curvature of the universe can in turn be used to test the Copernican Principle in a model-independent way (Clarkson et al. (2008)).

6.2.1 Expansions of the background observables

To illustrate the dependency of the background observables we consider here we expand them in terms of the cosmological parameters ϵ_m , Ω_k and the parameter $x = z/(1+z)$. Here $\epsilon_m := \Omega_{m*} - \Omega_m$, where Ω_{m*} is the true value of the matter energy density and Ω_m is the assumed value, as seen in Eq. (6.17).

The expansions for $H(x)$, $d_L(x)$, $V'(x)$ yield

$$x = \frac{z}{1+z} \quad (6.6)$$

$$H(x) = H_0 \left[1 + \frac{1}{2} \{ 3(1 + w_0(1 - \Omega_{m*}))x - (1 + 3w_0)\Omega_k x - 3w_0\epsilon_m \} \right] \quad (6.7)$$

$$d_L(x) = \frac{cx}{H_0} \left[1 + \{ (5 + 3w_0(\Omega_{m*} - 1)) + (1 + 3w_0)\Omega_k + 3w_0\epsilon_m \} x \right] \quad (6.8)$$

$$V'(x) = \frac{c^3 x^2}{H_0^3} \left[1 + \{ (-1 + 3w_0(\Omega_{m*} - 1)) + (1 + 3w_0)\Omega_k + 3w_0\epsilon_m \} x \right] \quad (6.9)$$

It can be seen from Eqs.(6.7, 6.8, 6.9) that the leading term corresponds to that of the standard flat Λ CDM model. From these equations we can directly compute the error on the particular observable as a function of redshift based on the difference between the ‘true’ cosmology and the ‘assumed’ cosmological model.

6.2.2 Obtaining the Dark Energy equation of state from Observations

Assuming we have ‘perfect’ and uncorrelated data from observations we would like to reconstruct $w(z)$ without assuming a specific parameterisation. Depending on the particular observable of interest, there are different ways to reconstruct w .

Dark energy from Hubble

It is straightforward to find $w(z)$ from the Hubble rate Eq. (6.3), and is given by Huterer and Turner (2001); Linder (2005):

$$w(z) = -\frac{1}{3} \frac{\Omega_k H_0^2 (1+z)^2 + 2(1+z)HH' - 3H^2}{H_0^2 (1+z)^2 [\Omega_m (1+z) + \Omega_k] - H^2}. \quad (6.10)$$

This tells us $w(z)$ *provided* we already know Ω_m and Ω_k . However, this reveals a degeneracy between Ω_m and $w(z)$ which cannot be overcome by background tests alone (Kunz (2007)). In essence, geometric background tests can measure the combination $\Omega_m + \Omega_{DE}f(z)/(1+z)^3$, but not the two separately. Another way to view this is by differentiating Eq. (6.10), and eliminating Ω_m to give a differential equation for $w(z)$ in terms of H, H' and H'' ; the constant arising in the general solution to this differential equation is Ω_m .

Similarly, we can reconstruct $w(z)$ from the other two tests on their own.

Dark energy from distance measurements

From distance measurements, we may invert Eq. (6.2) to find

$$w(z) = \frac{2(1+z)(D^2\Omega_k + 1)D'' - D' \left[\Omega_k(1+z)^2 D'^2 + 2\Omega_k D(1+z)D' - 3 - 3D^2\Omega_k \right]}{3 \left\{ [\Omega_k + \Omega_m(1+z)](1+z)^2 D'^2 - D^2\Omega_k - 1 \right\} D'}. \quad (6.11)$$

Reconstructing $w(z)$ from volume measurements (Eq. 1.21) as an analytical formula is rather tricky (as it involves the root of a quartic power). It is simpler instead to recon-

struct $w(z)$ by solving the differential equation for $f(z)$ and then differentiating to get $w(z)$.

Dark energy from volume measurements

Starting with Eq. (6.2), we solve for the derivative of the Hubble parameter and equate this with the expression for H' in terms of $w(z)$ from Eq. (6.10) and use

$$w(z) = \frac{(1+z)f'}{3f} - 1 \quad (6.12)$$

to yield a first order differential equation for f , namely

$$f'(z) = \frac{A(z) + B(z) + C(z)}{-H_0^2 V' \Omega_{\text{DE}}}, \quad (6.13)$$

where

$$A(z) = -4 \left(V' H_0 \left(c^3 \sqrt{f(z) \Omega_{\text{DE}} + X_{11}} + V' H_0^3 \Omega_k (f(z) \Omega_{\text{DE}} + X_{11}) \right) \right)^{1/2},$$

with

$$X_{ab} = (1+z)^2 (a \Omega_k + b \Omega_m (1+z)),$$

$$B(z) = 2H_0^2 V'' (f(z) \Omega_{\text{DE}} + X_{11})$$

and

$$C(z) = H_0^2 V'' \frac{X_{32}}{1+z}.$$

We solve this for $f(z)$ and then use (6.12) again to yield $w(z)$. The solution for $f(z)$ is unique since we demand $f(0) = 1$.

6.3 Reconstructing $w(z)$

If we knew Ω_m and Ω_k perfectly then our three expressions for $w(z)$ would yield the same function $w(z)$, assuming we lived in an exact FLRW universe. But what if — as is commonly assumed — we impose $\Omega_k = 0$ when *in fact* the true curvature is actually non-zero? It is usually implicitly assumed that the error on $w(z)$ will be of order Ω_k , and this is indeed true for $z \lesssim 0.9$ (see Figure 6.4). However, this intuition is strongly violated for $z \gtrsim 0.9$, even given perfect knowledge of $d_L(z)$, $H(z)$ or $V'(z)$. Furthermore, are there similar issues from an imperfect knowledge of Ω_m ?

6.3.1 Zero curvature assumption

We can easily see the implications of incorrectly assuming flatness by constructing the functions $d_L(z)$ and $H(z)$ under the assumption of the Λ CDM in a curved Universe (i.e.

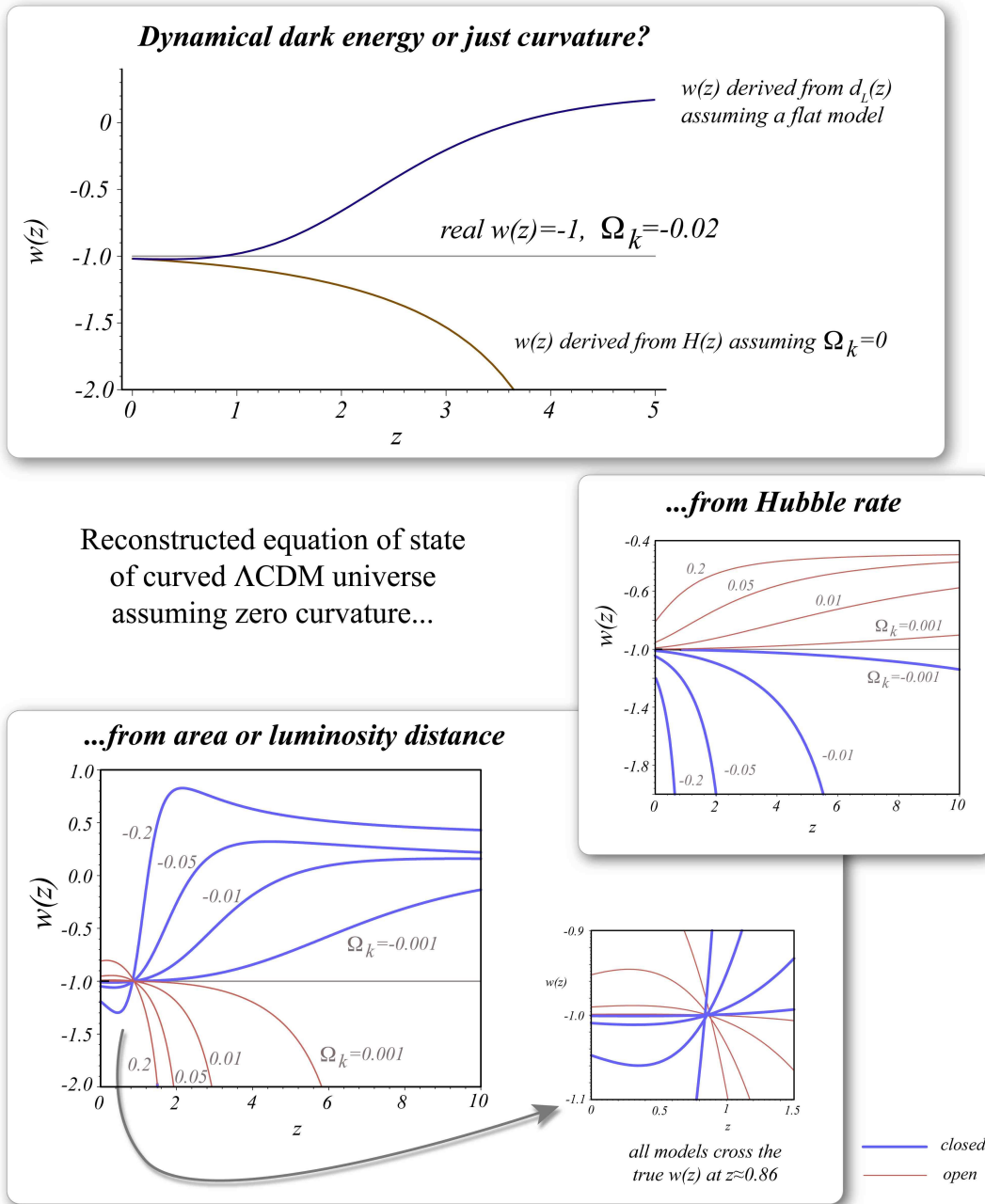


Figure 6.4: **Reconstructing the dark energy equation of state assuming zero curvature** when the true curvature is 2% in a closed Λ CDM universe. The $w(z)$ reconstructed from $H(z)$ is phantom ($w < -1$) and rapidly acquires an error of order 50% and more at redshift $z \gtrsim 2$, and diverges at finite redshift. However this doesn't necessarily constitute a problem since there are consistent models which exhibit such behaviour, e.g. a scalar field with a negative valued potential (Kunz (2008)). The reconstructed $w(z)$ from $d_L(z)$ for $\Omega_k < 0$ is phantom until $z \approx 0.86$, where it crosses the true value of -1 and then crosses 0 at high redshift, where the bending of geodesics takes over from dynamical behavior, producing errors in opposite direction to the DE reconstructed from $H(z)$. In order to make up for the missing curvature, the reconstructed dark energy is behaving like a scalar field with a tracking behavior. These effects arise even if the curvature is extremely small ($< 0.1\%$).

assuming $w = -1, \Omega_k \neq 0$) and inserting the results into Eqs (6.10) and (6.11).

If we then set $\Omega_k = 0$ in Eqs. (6.10) and (6.11) we arrive at the two corresponding $w(z)$ functions (if they exist) required to reproduce the curved forms for $H(z)$ and $d_L(z)$ in a *flat* Universe with dynamic dark energy¹. This would apply equally to $d_A(z)$ for that matter - the results are exactly the same for any distance indicator. Figure 6.4 presents this method using for simplicity the concordance value of $w = -1$ but we have checked that the qualitative results do not depend on the ‘true’ underlying dark energy model². We assume $\Omega_m = 0.3$ in all expressions though numbers quoted are weakly dependent on this. The resulting (spurious) $w(z)$ can then be thought of as the function required to yield the same $H(z)$ or $d_L(z)$ as in the actual curved Λ CDM model: e.g.,

$$d_L[\text{flat}, w(z)] = d_L[\text{curved}, w(z) = -1]. \quad (6.14)$$

For example for the Hubble rate the reconstructed $w(z)$ can be found analytically to be

$$w(z) = -\frac{1}{3} \frac{\Omega_k(1+z)^2 + 3\Omega_{\text{DE}}}{\Omega_k(1+z)^2 + \Omega_{\text{DE}}}, \quad (6.15)$$

without any dependence on a specific parameterisation.

In the figure we show what happens for Λ CDM: curvature manifests itself as evolving dark energy. In the case of the Hubble rate measurements this is fairly obvious — we are essentially solving the equation $\Omega_{\text{DE}}f(z) = \Omega_\Lambda + \Omega_k(1+z)^2$ where $f(z)$ is given by Eq. (6.4). For $\Omega_k > 0$, $w(z)$ must converge to $-1/3$ to compensate for the curvature. For $\Omega_k < 0$, the opposite occurs and a redshift is reached when $w \rightarrow -\infty$ in an attempt to compensate albeit unsuccessfully for the positive curvature. Already we can see why the assumption that the error in w is of order the error in Ω_k breaks down so drastically.

Interestingly, the curved geodesics imply that the error in w reconstructed from $d_L(z)$ and $H(z)$ have opposing signs at $z \gtrsim 0.9$, as can be seen by comparing the panels for the Hubble rate and the distance indicator in Fig. (6.4). Above the critical redshift the effect of curvature on the geodesics becomes more important than the pure dynamics, and the luminosity distance flips $w(z)$ in the opposite direction to that reconstructed from $H(z)$.

In the case of volume measurements the reconstructed $w(z)$ has a similar form to the w we obtained from the distance measurements $D(z)$. This can be seen from Eq. (1.21), where the distance information enters the equation as a square power. For example in the closed Universe case the reconstructed $w(z)$ drops to more phantom values (-2.5 compared to -1.3 for the distance measurements) in order to make up for the missing curvature.

Again the effect of curvature on the geodesics dominates the effect of dynamics for large z , and the distance contribution in the volume measurements flips the reconstructed $w(z)$ at $z = 1.6$. The critical redshift of this flip is determined by the redshift at which the curvature of the geodesics affecting distance measurements becomes more important than the expansion rate. This payoff becomes more finely balanced for volume measure-

¹We show in the Appendix an example used to obtain these expressions and produce the figures

²In fact, the results presented here are qualitatively the same for any assumed Ω_k which is different from the true value.

ments due to the fact that $H(z)$ appears both in $D(z)$ (as a square power) and on its own. Hence $w(z)$ has to work harder in reproducing curvature to counterbalance the opposing trends of expansion history and geometry, and so the balance is achieved at higher redshift. The specific redshift at which this happens is dependent on Ω_m in that lower values imply higher value of the critical redshift.

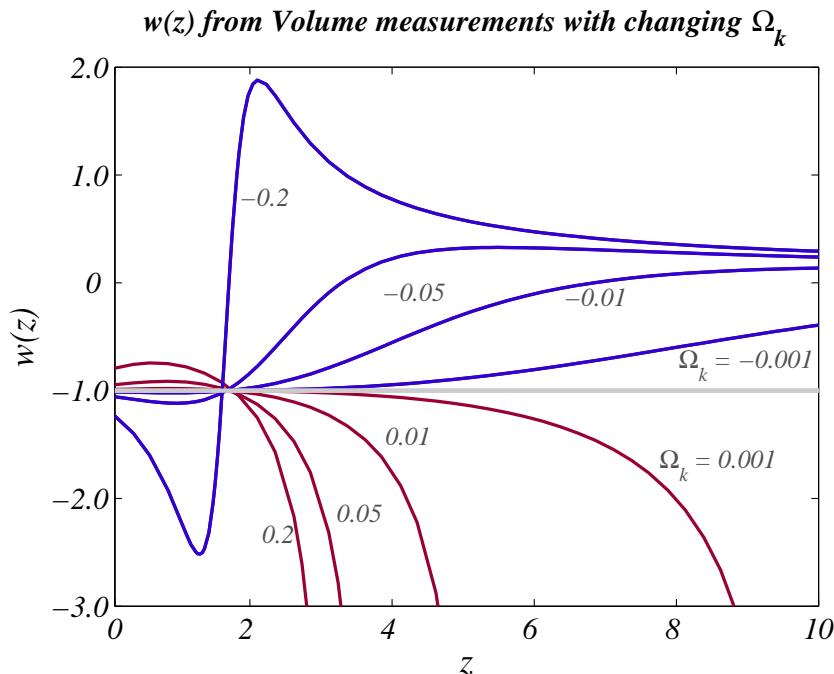


Figure 6.5: **Reconstructed dark energy from volume measurements while incorrectly assuming flatness** - Similar to the case for distance measurements in a closed Universe, the reconstructed $w(z)$ must initially be phantom in order to compensate for curvature, and crosses the true value of $w = -1$ at a redshift of $z \sim 1.6$, which is greater than the redshift of 0.86 for the distance measurements alone (Clarkson et al. (2007)). After this point, the $w(z)$ increases to overcome the curvature of the geodesics.

We have shown that incorrectly assuming flatness can result in a reconstructed $w(z)$ that mimics dynamics, yielding errors on w that are much larger than the order of errors on Ω_k . One might then ask if similar errors will result when incorrectly assuming a particular value for the matter density in the Universe, Ω_m .

6.3.2 Uncertainties in the Matter content Ω_m

We consider the similar case of reconstructing $w(z)$ in a flat Universe but here the errors occur when assuming the concordance value of $\Omega_m = 0.3$ incorrectly. For example in this case the $w(z)$ reconstructed from Hubble measurements Eq. (6.10) reduces to

$$w(z) = -\frac{1}{3} \frac{2(1+z)HH' - 3H^2}{H_0^2(1+z)^2[\Omega_m(1+z)] - H^2}. \quad (6.16)$$

Similar expressions are found for both the distance and volume measurements. The $w(z)$ curves obtained from incorrectly assuming $\Omega_m = 0.3$ are shown in Fig. 6.6. If we

assume flatness for this example we find that changing the value of Ω_m can only affect the dark energy density, and thus change the value of $H(z)$. As Ω_m is only present in all three observables through $H(z)$ or integrals of $1/H(z)$, the reconstructed $w(z)$ is the same for all three measurements. Interestingly, the reconstructed $w(z)$ curves do not go through $w = -1$ at $z = 0$, but are spread between -0.85 and -1.15 for $0.2 < \Omega_m < 0.4$. This is also shown in Fig. 6.7.

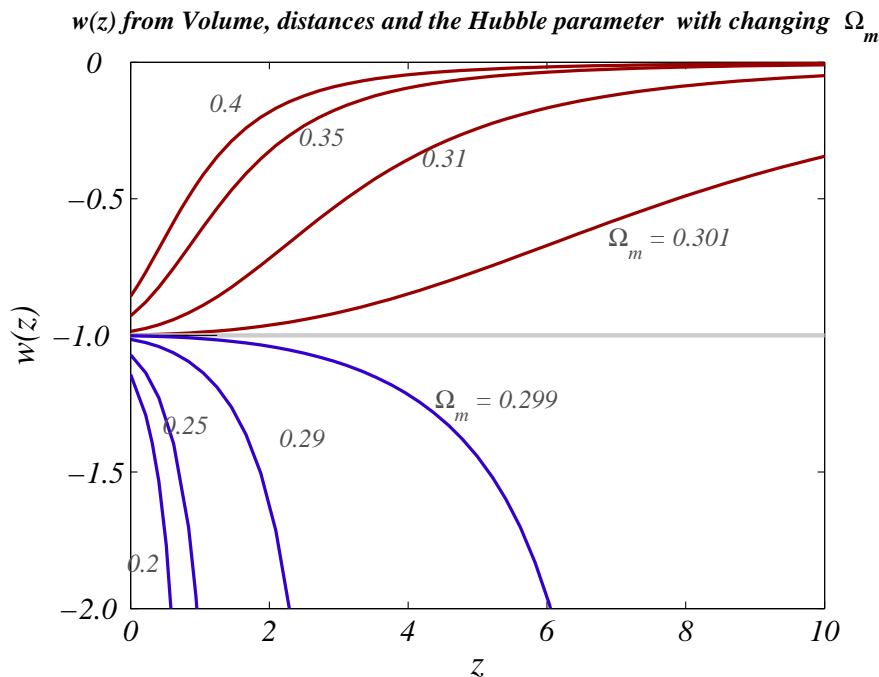


Figure 6.6: **Reconstructed dark energy from an incorrectly estimated matter density** - The reconstructed $w(z)$ for changing Ω_m from all three measurements (H , D , dV/dz). Since we assume flatness while changing Ω_m , all three observables yield the same reconstructed $w(z)$, since Ω_m only enters the functions through $H(z)$ or integrals of $1/H$. For $\Omega_m > 0.3$ the dark energy tries to compensate for the extra matter contribution and so asymptotes to $w = 0$ as $z \rightarrow \infty$. For $\Omega_m < 0.3$ the $w(z)$ is of the same form to what is reconstructed from neglecting curvature in a closed Universe (see Fig. 6.4), and the phantom w tends to $-\infty$ as it attempts to compensate for the ‘missing’ matter density.

Given any scenario of an assumed cosmology that differs from the ‘true’ Universe, we can derive the value of today, $w(z = 0)$ from both the Hubble and distance measurements as

$$\begin{aligned}
 w(0) &= \frac{3 - 4\Omega_{k*} - 3\Omega_m + \Omega_k}{6\Omega_m + 6\Omega_{k*} - 3\Omega_{m*} - 3 - 3\Omega_k} \\
 &\sim \frac{\epsilon_m}{(-1 + \Omega_{m*})} - \frac{2\Omega_k}{3(-1 + \Omega_{m*})} - 1,
 \end{aligned} \tag{6.17}$$

where $\epsilon_m = \Omega_{m*} - \Omega_m$ as defined above where the asterisk indicates assumed but incorrect values of the corresponding quantities. We vary this equation in one ‘true’ density (Ω_m or Ω_k) at a time, while keeping the other constant at the assumed value of either $\Omega_k = \Omega_{k*}$ or $\Omega_m = \Omega_{m*}$ to produce the curves in Fig. 6.7. This parameter $w(z = 0)$ al-

allows us to easily quantify the affect of assuming an incorrect cosmological model on the inferred low-redshift value of w .

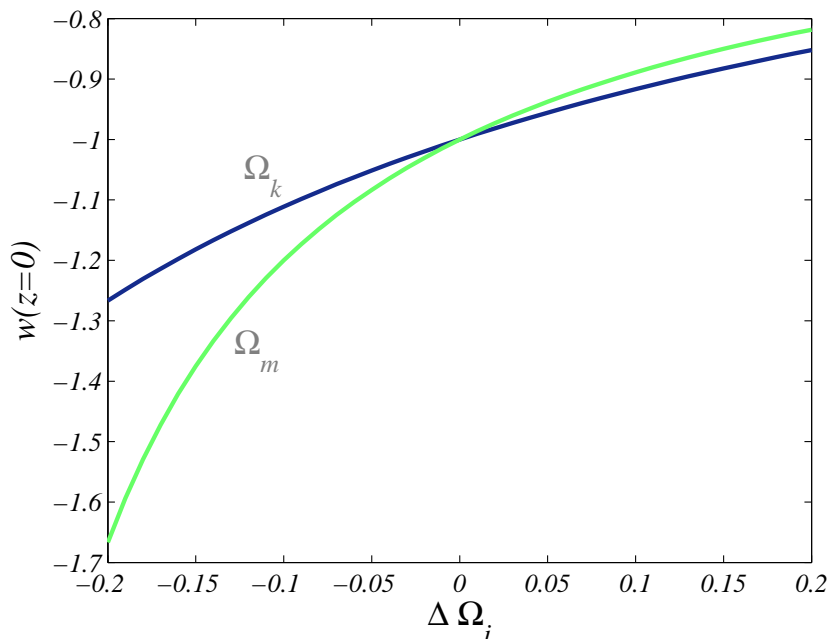


Figure 6.7: **Low redshift variation in $w(z)$ from $H(z)$ and $D(z)$** - incorrectly assuming concordance values of $\Omega_m = 0.3$ and $\Omega_k = 0$ results in a variation in the low-redshift value of $w(z)$ reconstructed from observables. The relationship between the error in the cosmological parameter and the reconstructed value for w (while keeping the other cosmological parameter fixed at the prior value) is shown for both Ω_m (the **green** curve) and Ω_k (the **blue** curve).

6.4 Parametric Degeneracies

We now want to connect the non-parametric approach we have followed above with standard approaches to degeneracies and so we expand Eqs. (6.10) and (6.11) for the Hubble rate and distance measurements to first order in $x = z/(1+z)$. This allows us to link to the parameters (w_0, w_a) used in the Chevallier-Polarski-Linder parameterisation, Eq. (2.46) which is used in the Dark Energy Task Force report. The values of (w_0, w_a) obtained using this expansion are given below.

From Hubble rate measurements

$$\begin{aligned} w_0 &= -\frac{\Omega_k + 3\Omega_{\text{DE}}}{3(1 - \Omega_m)} \\ w_a &= \frac{4}{3} \frac{\Omega_k \Omega_{\text{DE}}}{(1 - \Omega_m)^2} \end{aligned} \quad (6.18)$$

From luminosity distance measurements

$$\begin{aligned}
w_0 &= -\frac{\Omega_k + 3\Omega_{\text{DE}}}{3(1 - \Omega_{\text{m}})} \\
w_a &= -\frac{2\Omega_k(\Omega_k - \Omega_{\text{DE}})}{3(1 - \Omega_{\text{m}})^2}
\end{aligned} \tag{6.19}$$

We plot in Fig. (6.8) the non-parametric reconstructed $w(z)$ along with the reconstructed $w_{\text{CPL}}(z)$ from the coefficients given by Eqs. (6.18, 6.19) for the observables $H(z)$ and $d_L(z)$.

6.5 Conclusions and Outlook

We have explored the degeneracies between the dark energy equation of state $w(z)$ and cosmic parameters using a non-parametric approach. This means we are able to write down the precise $w(z)$ that will be reconstructed from perfect data if slightly wrong or biased values for the cosmic parameters $\Omega_k, \Omega_{\text{m}}$ are assumed. This is complementary to traditional methods which typically use an aggressive compression of the $w(z)$ function onto a couple of parameters (usually w_0, w_a) and then study the degeneracy between these and other cosmic parameters. Our approach is superior in one way however: degeneracies between $w(z)$ and some cosmic parameters such as Ω_k can appear to be quite weak in the parameterised approach. However, in the case of distance measurements this is completely artificial and due to strong assumptions about the allowed form of $w(z)$ since the degeneracy is perfect if $w(z)$ is allowed to be totally free.

We show the reconstructed $w(z)$ from measurements of Hubble rate, distance and volume measurements for both wrongly assumed Ω_k and Ω_{m} . For all 3 observables the errors in $w(z)$ that result from uncertainty in the cosmic parameters are *much* larger than the uncertainty in Ω_k or Ω_{m} , especially at large redshifts. We have shown that curvature affects measurements of $H(z)$ and $D(z)$ in complementary ways, with the error at high redshift having opposite signs for an error in Ω_k . In the case of an Ω_{m} error, Hubble, distance, and volume measurements all lead to the same erroneously reconstructed $w(z)$, a manifestation of the dark matter-dark energy degeneracy highlighted in Kunz (2007).

In this work we have assumed perfect data for Hubble rate, distance and volume at all redshifts. It would be interesting to extend our non-parametric approach to the case of imperfect data which has incomplete redshift coverage and errors on the observables. This is left to future work but will allow contact with the approaches in Shafieloo et al. (2006); Espana-Bonet and Ruiz-Lapuente (2005).

6.6 Appendix

The calculation, derivation of expressions, and plot drawing in this work were produced using MATHEMATICA and MAPLE. MATHEMATICA was used for inversion of the expressions for d_L and $H(z)$, and MAPLE was used for numerical plot production and solving of

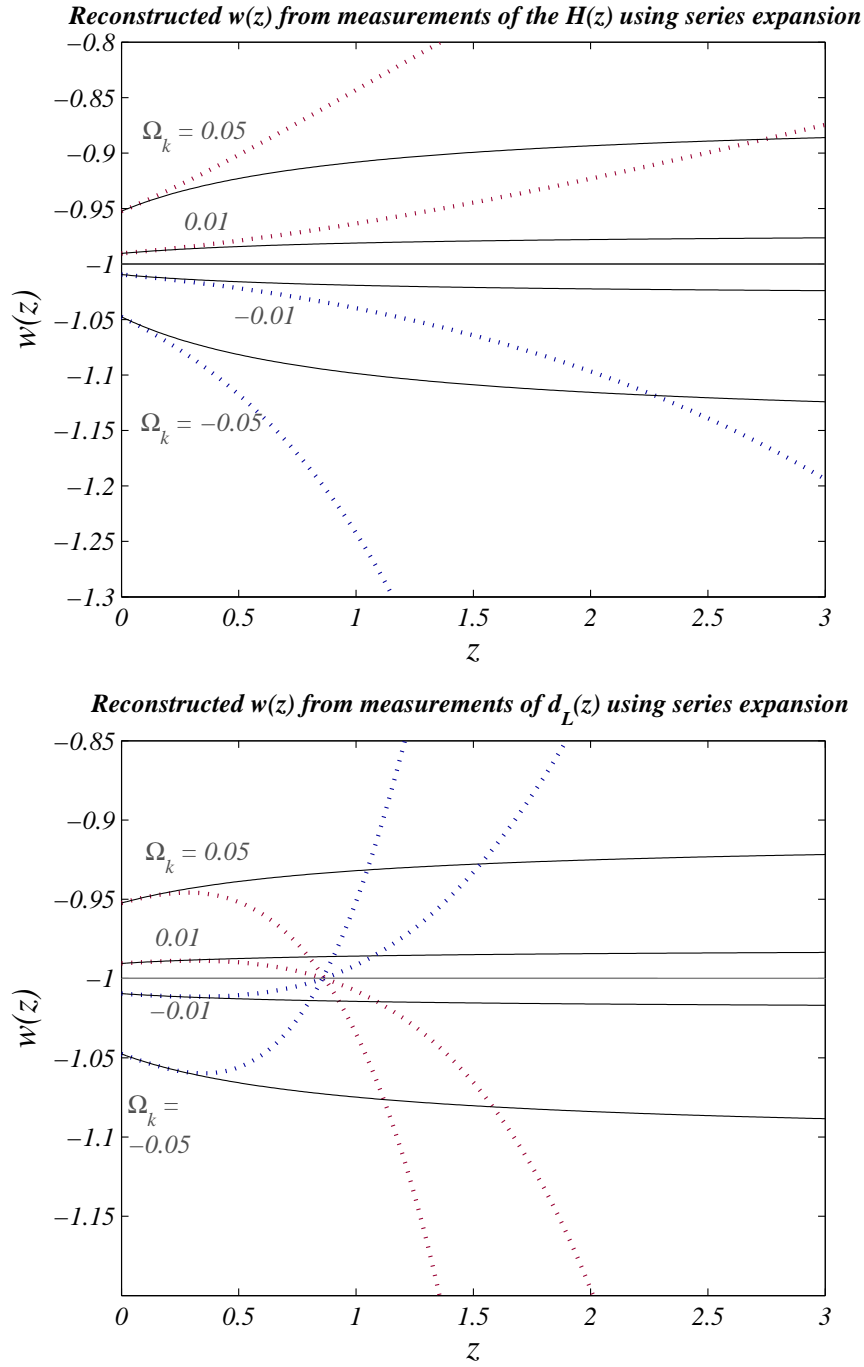


Figure 6.8: **Degeneracies in standard parameterisations** - $w(z) = w_0 + w_a \frac{z}{1+z}$ using the coefficients in Eqs. (6.19) and (6.18) (solid lines) compared with the fully non-parametric $w(z)$ inferred from Hubble and distance measurements. Using a limited parameterisation of $w(z)$ like this incorrectly makes it appear that dark energy and curvature are not completely degenerate, leading to artificially strong constraints on curvature and w_0, w_a .

the differential equation for $V'(z)$. Here we provide an example of the MAPLE code used to numerically obtain the form for d_L and the plot of the reconstructed $w(z)$ in Fig. (6.9).

Curv_dL

Define $H(z)$ and comoving distance $r_L(z)$

```
> Hubble:=z->(#subs(Omega[Lambda]=1-Omega[m]-Omega[k],H[0]*sqrt(Omega[m]
*(1+z)^3+Omega[k]*(1+z)^2+Omega[Lambda]*exp(+3*Int((1+w(z1))/(1+z1),z
1=0..z))))):
rL:=z->subs(a[0]=c/H[0]/sqrt(-Omega[k]),(a[0]*(1+z)*sin(c/a[0]*Int(1/
Hubble(z2),z2=0..z))));
```

Use r_L to define $d_L(z)$ and invert to give $w(z)$

```
> isolate(dL(z)*(c/H[0])=rL(z),Int(1/(H[0]*(Omega[m]*(1+z2)^3+Omega[k]*
(1+z2)^2+Omega[Lambda]*exp(3*Int((1+w(z1))/(1+z1),z1=0..z2)))^(1/2)),
z2 = 0 .. z));
diff(%,z);
simplify(isolate(%,Int((1+w(z1))/(1+z1),z1 = 0 .. z)));
diff(%,z):
wz:=simplify(collect(simplify(isolate(%,w(z))),diff,simplify),size);
```

Define a set of $\{\Omega_k, w(z)\}$ parameter values for the observed d_L and another to substitute in the expression yielding the recovered $w(z)$

```
> ok:='ok':
Params_real:=[Omega[m] = .3, Omega[k] = ok];
Params_prior:=[Omega[m] = .3, Omega[k] = 0];
w_real_form:=z->-1+0*(z)/(1+z);
Hubble_real:=subs(Omega[Lambda]=1-Omega[m]-Omega[k],Params_real,(simp
lify(value(eval(subs(w=w_real_form,Hubble(z2))))))assuming z2>0;
dL_real:=subs(Params_real,simplify(H[0]/c*subs(a[0]=c/H[0]/sqrt(-Ome
ga[k]),a[0]*(1+z)*sin(c/a[0]*Int(1/Hubble_real,z2=0..z))));
```

Plot a set of curves for the derived $w(z)$ and for open universes $\Omega_k = \{-0.001, -0.01, -0.05, -0.2\}$. The produced plot is shown on Fig. 6.9.

```
> plotsetup(ps,plotoutput='plot1.ps',plotoptions='portrait,width=600,he
ight=500,color=rgb,noborder');
oklist:=[-(0.001,0.01,.05,.2)];
#,0.001,0.01,.05,.2];
for i to nops(oklist) do
ok:=oklist[i]:
pp[i]:=plot([rhs(simplify(dsubs(dL(z)=dL_real,Params_prior,wz),size))
```

```

,w_real_form(z)],z=0..5,color=[red,blue],discont=false):
od:
display([seq(pp[ii],ii=1..nops(oklist))],axes=boxed,view=[default,default]);

```

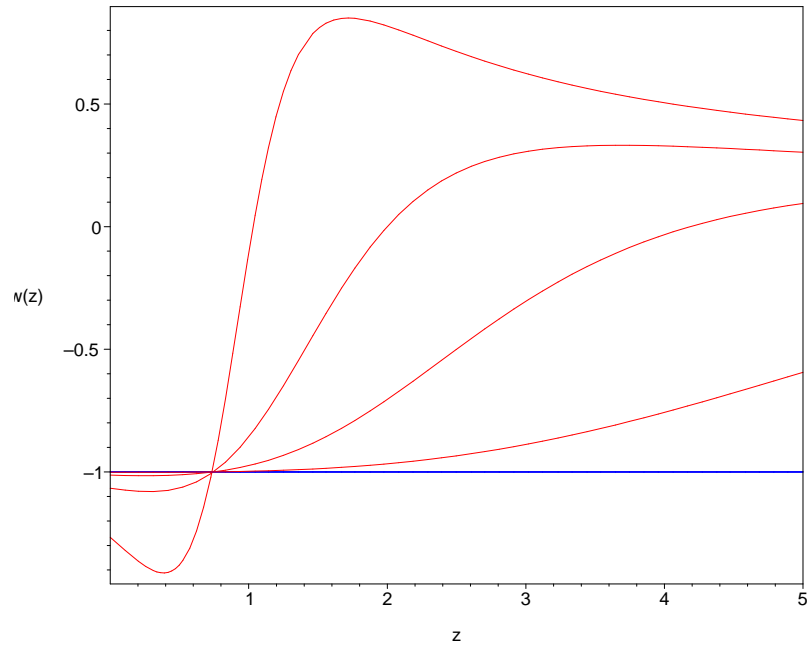


Figure 6.9: Figure produced by the sample code provided in the Appendix showing the reconstructed $w(z)$ from distance luminosity for curvature values $\Omega_k = \{-0.001, -0.01, -0.05, -0.2\}$

Chapter 7

Conclusion

The work presented in this thesis was developed from October 2005 through January 2008. During this period the WMAP satellite announced results from its first 3 years of operation, the Nobel prize for physics was awarded to John Mather and George Smoot for their work on COBE, the Riess et al team published their findings with the High- z Supernovae obtained with the Hubble Space Telescope, the ESSENCE group presented data from their supernovae project, and recently WMAP released its 5yr dataset, presenting us with the most precise temperature and polarization CMB maps to date.

The topics covered here are extensive in range but perhaps not surprisingly so. With a large wealth of precision data continuously being made available, challenging theoretical model building and improving data analyses, it is difficult not to be drawn to the appealing scope of questions being addressed. In light of this, the extent of subjects discussed in this thesis, though ranging from early to late times, outline but a small part of the exciting and urgent challenges that form cosmology today.

The consistency condition is an important ingredient of inflationary models. In chapter 3 we discussed and further examined its implications for the large class of inflationary models which is single-field slow-roll inflation. That such a relation exists has long been recognized in the literature: in inflationary models the amplitude of the two spectra is not independent and the tilt of the tensor spectrum ties together the relative amplitude of the two (Kosowsky and Turner (1995); Lidsey et al. (1997)). This is however a mere approximative result in the slow roll expansion. Here we took this relation a step further and developed a framework uncovering all the connections that can be derived between scalar and tensor spectra to any degree of approximation in the slow roll context. It is hoped this relations will one day be able to prove or exclude the inflationary paradigm, though in today's observational expectations the most optimistic forecasts for gravitational waves estimate none but the first will be put to proof in the near future (Song and Knox (2003)). However as we've shown in chapter 4 the interest of the consistency equation goes beyond the observational confirmation of inflationary theories and can be necessary to ensure the correct implementation of the predictions of inflation, guaranteeing consistency in the conclusions drawn from microwave background data.

We also showed that the hierarchy of consistency equations does exhaust the web of connections that an inflationary source for the perturbations originates. In this way other relations, claimed to derive from inflationary models in the literature – be it exact or approximate – must be deduced from this hierarchy and cannot bring new insight or information to those already exposed. We illustrated this by considering the expressions featured in Chung and Romano (2006); Lidsey and Tavakol (2003).

Chapter 4 is as we mentioned above an example of an academic application of the consistency equation beyond its observational use as a validity check. In this chapter we implemented a shift in scale in the perturbation spectra at last scattering, in the context of deriving constraints for single-field inflationary models. Because the first consistency equation is only an approximate relation if we ensure it holds at one scale it won't necessarily be valid at another. Using the second consistency equation - making a requirement on the running of the tensor spectral index - guarantees that the tensor tilt satisfies the first consistency relation at all other scales thus validating the framework we developed.

The loss of information when performing a marginalization on a subset of parameters, and its connection to the point in the dataset at which the constraints are inferred were the starting point for this work. For presentation purposes one often projects the full N -dimensional volume onto a 2D surface and we showed that for a particular class of models — where running of the spectral index is allowed — applying our method can prevent the deterioration of constraints that occurs due to the inclusion of an extra parameter. This reduction in uncertainty can be as large as 5 times, particularly when compared to that observed in the WMAP team's analysis.

The method we outlined, although here exemplified on CMB data, is of wider application and can be used to improve constraints on other data sets provided such an expansion on its parameters can be performed. It is worth mentioning that analytical expressions for the shift in scale corresponding to the pivot point may in general not be readily available. Here we applied this for decorrelating a parameter against its derivative, so the expressions for shifting variables along the expanded spectrum are linear and easily derived. As an example of a further application we suggested the normalization of the spectrum of density fluctuations σ_8 .

In chapters 5 and 6 we address the important issue of detection of dynamics in late time acceleration. The alternative being a cosmological constant scenario carrying deep foundational problems for physics, much of today's observational efforts in dark energy are focused in assessing its dynamical behaviour, $w(z)$.

In chapter 5 we examine constraints on early dark energy as provided by Big Bang Nucleosynthesis. Scaling fields are one of the best candidates for presenting us with a sizeable fraction of dark energy today, while negligible at early times, and at the same time theoretically well founded. We combine the predictions of dynamics of scaling fields with those of BBN constraints and examine implications for observables today compared to those in a Λ CDM scenario. A look at the deviations of the Hubble rate and the distance modulus tells us these measurements are below the detectivity limit forecasts for near future stage-III experiments (DETF). This means dark energy may well be dynamical even

if we don't detect any dynamics in the next decade. To notice however that allowing for phantom behaviour dilutes the constraints presented here, since $w < -1$ allows for a swifter variation in Ω_{DE} . Of particular surprise were the results associated with the common parametrization CPL, which doesn't show enough flexibility to describe a minimally coupled scaling field which satisfies the BBN bounds. Given that this parametrization is the basis for many surveys' figure-of-merit, the implication hereof is that the derivation of constraints based on its parameters may be systematically biasing away from scaling models.

Another well known problem in detecting dark energy dynamics is the well known degeneracies between cosmological parameters and dark energy's dynamical behaviour. Studies of dark energy have traditionally minimized uncertainties in the cosmological parameters, since they add an unwelcome complexity to the analysis and deteriorate already weak constraints on the $w(z)$ parametrization. In chapter 6 we examine the degeneracies between dark energy dynamics, dark matter, and curvature using a non parametric and non perturbative approach. The use of a non parametric approach allows us to write down the exact $w(z)$ that will be reconstructed if slightly wrong values for Ω_{m} , Ω_{k} are assumed, without having to assume a specific form for the EoS. The assumption of perfect data allows us to probe fundamental degeneracies that are not due to finite errors and will be true no matter what progress is made in improving future cosmic surveys. Even assuming perfect Hubble, distance and volume measurements, the bias in $w(z)$ for $z > 1$, is up to two orders of magnitude larger than the corresponding errors in Ω_{k} or Ω_{m} .

We reconstructed $w(z)$ from measurements of Hubble rate, distances, and volume, and showed that curvature has complementary effects in $H(z)$ and d_L , although the matter content is unable to distinguish between the three observables. The opposite trend observed in the Hubble rate and luminosity distance may allow to measure curvature independently of other cosmological parameters (apart from H_0) as we argued in Clarkson et al. (2007). The inability of the dark matter content to discriminate between observables illustrates the degeneracies in the whole energy-momentum tensor as discussed in Kunz (2007).

Concluding Remarks

It is hard to say where will cosmology go from here. At the moment we are optimistic about prospects for detecting gravitational waves, with the new generation of polarization experiments such as ESA's Planck Surveyor CMB satellite, which will yield anisotropy measurements up to $l \sim 3000$ improving the precision on cosmological parameters such as the Hubble constant, the geometry of the universe, and the matter content.

The search for dark matter is progressing, with experiments increasing in sensitivity so that over the next couple of decades we may have probed most of the parameter space allowed by its most compelling candidates – some form of elementary particles left over from the big bang (Spooner (2007)).

The situation with dark energy being much more complicated — we are still far from

a compelling hypothesis on what is causing acceleration — is nevertheless a reason to be optimistic. Observations have begun to probe its nature, and future experiments are focusing on distinguishing between a cosmological constant, modifications of General Relativity, or backreaction effects. The Supernova/Acceleration Probe (SNAP)¹, a proposed space-based telescope to look at Supernovae up to $z \approx 2$ will allow to significantly reduce uncertainties (both statistical and systematic) on dark-energy parameters. Planned wide-field surveys such as the Dark Energy Survey² (DES) and the Large Synoptic Survey Telescope (LSST), will probe the the effect of dark energy on the growth of structure by looking at the weak lensing signal on scales up to the arcminute. Large BAO surveys are also currently being designed, and the Atacama Cosmology Telescope³ will soon begin studying the evolution of galaxy clusters and constrain dark energy properties.

From both the observational as from the theoretical perspectives these are challenging questions to face. The answers in which we are by no means wise yet may be around the corner or miles away but they will most likely revolutionize our understanding of the universe and perhaps that of the whole of physics.

¹<http://snap.lbl.gov/>

²<http://www.darkenergysurvey.org/>

³<http://www.physics.princeton.edu/act/>

Bibliography

- Aguirre, A., Burgess, C. P., Friedland, A., and Nolte, D. (2001). Astrophysical constraints on modifying gravity at large distances. *Classical and Quantum Gravity*, 18:R223.
- Albrecht, A., Bernstein, G., Cahn, R., Freedman, W. L., Hewitt, J., Hu, W., Huth, J., Kamionkowski, M., Kolb, E. W., Knox, L., Mather, J. C., Staggs, S., and Suntzeff, N. B. (2006). Report of the dark energy task force. arXiv: astro-ph/0609591.
- Armendariz-Picon, C., Mukhanov, V., and Steinhardt, P. J. (2000). A dynamical solution to the problem of a small cosmological constant and late-time cosmic acceleration. *Physical Review Letters*, 85:4438.
- Astier, P., Guy, J., Regnault, N., Pain, R., Aubourg, E., Balam, D., Basa, S., Carlberg, R. G., Fabbro, S., Fouchez, D., Hook, I. M., Howell, D. A., Lafoux, H., Neill, J. D., Palanque-Desabrouille, N., Perrett, K., Pritchet, C. J., Rich, J., Sullivan, M., Taillet, R., Aldering, G., Antilogus, P., Arsenijevic, V., Balland, C., Baumont, S., Bronder, J., Courtois, H., Ellis, R. S., Filiol, M., Goncalves, A. C., Goobar, A., Guide, D., Hardin, D., Luset, V., Lidman, C., McMahon, R., Mouchet, M., Mourao, A., Perlmutter, S., Ripoche, P., Tao, C., and Walton, N. (2006). The supernova legacy survey: Measurement of ω_m , ω_Λ and w from the first year data set. *Astron. Astrophys.*, 447:31.
- Barreiro, T., Copeland, E. J., and Nunes, N. J. (2000). Quintessence arising from exponential potentials. *Physical Review D*, 61:127301.
- Bassett, B. A., Corasaniti, P. S., and Kunz, M. (2004). The essence of quintessence and the cost of compression. *The Astrophysical Journal*, 617:L1.
- Bassett, B. A., Nichol, R. C., and Eisenstein, D. J. (2005). Wfmos — sounding the dark cosmos. *Astronomy and Geophysics*, 46(5).
- Bean, R., Hansen, S. H., and Melchiorri, A. (2001). Early-universe constraints on a primordial scaling field. *Physical Review D*, 64:103508.
- Bernstein, G. (2006). Metric tests for curvature from weak lensing and baryon acoustic oscillations. *The Astrophysical Journal*, 637:598.
- Birkel, M. and Sarkar, S. (1997). Nucleosynthesis bounds on a time-varying cosmological 'constant'. *Astroparticle Physics*, 6:197.

- Blake, C. and Glazebrook, K. (2003). Probing dark energy using baryonic oscillations in the galaxy power spectrum as a cosmological ruler. *The Astrophysical Journal*, 594:665.
- Bonvin, C., Caprini, C., and Durrer, R. (2006). No-go theorem for k-essence dark energy. *Physical Review Letters*, 97:081303.
- Buchert, T. and Carfora, M. (2003). Cosmological parameters are dressed. *Physical Review Letters*, 90:031101.
- Charmousis, C., Gregory, R., Kaloper, N., and Padilla, A. (2006). DGP spectroscopy. *JHEP*, 0610:066.
- Chevallier, M. and Polarski, D. (2001). Accelerating universes with scaling dark matter. *International Journal of Modern Physics D*, 10:213.
- Chung, D. J. H. and Romano, A. E. (2006). Approximate consistency condition from running spectral index in slow-roll inflationary models. *Physical Review D*, 73:103510.
- Chung, D. J. H., Shiu, G., and Trodden, M. (2003). Running of the scalar spectral index from inflationary models. *Physical Review D*, 68:063501.
- Clarkson, C., Bassett, B. A., and Lu, T. H.-C. (2008). A general test of the copernican principle. *Physical Review Letters*, 101(1).
- Clarkson, C., Cortês, M., and Bassett, B. A. (2007). Dynamical dark energy or simply cosmic curvature? *Journal of Cosmology and Astro-Particle Physics*, 8.
- Coley, A. A. and Pelavas, N. (2007). Averaging in spherically symmetric cosmology. *Physical Review D*, 75:043506.
- Copeland, E., Kolb, E. W., Liddle, A. R., and Lidsey, J. E. (1994). Reconstructing the inflaton potential—perturbative reconstruction to second order. *Physical Review D*, 49:1840.
- Copeland, E. J., Grivell, I. J., and Liddle, A. R. (1998a). Cosmological parameter estimation and the spectral index from inflation. *Monthly Notices of the Royal Astronomical Society*, 298:1233.
- Copeland, E. J., Kolb, E. W., Liddle, A. R., and Lidsey, J. E. (1993). Observing the inflaton potential. *Physical Review Letters*, 71:219.
- Copeland, E. J., Liddle, A. R., and Wands, D. (1998b). Exponential potentials and cosmological scaling solutions. *Physical Review D*, 57:4686.
- Copeland, E. J., Sami, M., and Tsujikawa, S. (2006). Dynamics of dark energy. *International Journal of Modern Physics D*, 15:1753.
- Copi, C. J., Schramm, D. N., and Turner, M. S. (1995). Assessing big-bang nucleosynthesis. *Physical Review Letters*, 75:3981.

- Corasaniti, P. S., Kunz, M., Parkinson, D., Copeland, E. J., and A. Bassett, B. (2004). The foundations of observing dark energy dynamics with the wilkinson microwave anisotropy probe. *Physical Review D*, 70:083006.
- Deffayet, C., Gabadadze, G., and Iglesias, A. (2006). Perturbations of self-accelerated universe. *JCAP*, 0608:012.
- Dickinson, C., Battye, R. A., Cleary, K., Davies, R. D., Davis, R. J., Genova-Santos, R., Grainge, K., Gutierrez, C. M., Hafez, Y. A., Hobson, M. P., Jones, M. E., Kneissl, R., Lancaster, K., Lasenby, A., Leahy, J. P., Maisinger, K., Odman, C., Pooley, G., Rajguru, N., Rebolo, R., Rubino-Martin, J. A., Saunders, R. D. E., Savage, R. S., Scaife, A., Scott, P. F., Slosar, A., Molina, P. S., Taylor, A. C., Titterton, D., Waldram, E., Watson, R. A., and Wilkinson, A. (2004). High sensitivity measurements of the cmb power spectrum with the extended very small array. *Monthly Notices of the Royal Astronomical Society*, 353:732.
- Dodelson, S. (2003). *Modern Cosmology*. Academic Press.
- Doran, M., Karwan, K., and Wetterich, C. (2005). Observational constraints on the dark energy density evolution. *JCAP*, 0511:007.
- Doran, M. and Robbers, G. (2006). Early dark energy cosmologies. *JCAP*, 0606:026.
- Dvali, G., Gabadadze, G., and Porrati, M. (2000). Metastable gravitons and infinite volume extra dimensions. *Physics Letters B*, 484:112.
- Espana-Bonet, C. and Ruiz-Lapiente, P. (2005). Dark energy as an inverse problem. arXiv: hep-ph/0503210.
- Faulkner, T., Tegmark, M., Bunn, E. F., and Mao, Y. (2007). Constraining $f(r)$ gravity as a scalar tensor theory. *Phys. Rev. D*, 76(6).
- Ferreira, P. G. and Joyce, M. (1998). Cosmology with a primordial scaling field. *Physical Review D*, 58:023503.
- Finelli, F., Rianna, M., and Mandolesi, N. (2006). Constraints on the inflationary expansion from three year WMAP, small scale cmb anisotropies and large scale structure data sets. *JCAP*, 0612:006.
- Freivogel, B., Kleban, M., Martinez, M. R., and Susskind, L. (2006). Observational consequences of a landscape. *JHEP*, 0603:039.
- Giannantonio, T., Crittenden, R. G., Nichol, R. C., Scranton, R., Richards, G. T., Myers, A. D., Brunner, R. J., Gray, A. G., Connolly, A. J., and Schneider, D. P. (2006). A high redshift detection of the integrated sachs-wolfe effect. *Physical Review D*, 74:063520.
- Glazebrook, K., Blake, C., Couch, W., Forbes, D., Drinkwater, M., Jurek, R., Pimblet, K., Madore, B., Martin, C., Small, T., Forster, K., Colless, M., Sharp, R., Croom, S., Woods, D., Pracy, M., Gilbank, D., Yee, H., and Gladders, M. (2007). The WiggleZ project:

- AAOmega and dark energy. In Metcalfe, N. and Shanks, T., editors, *Cosmic Frontiers*, volume 379 of *Astronomical Society of the Pacific Conference Series*.
- Gong, Y., Wu, Q., and Wang, A. (2008). Dark energy and cosmic curvature: Monte-carlo markov chain approach. *The Astrophysical Journal*, 681:27.
- Grivell, I. J. and Liddle, A. R. (2000). Inflaton potential reconstruction without slow-roll. *Physical Review D*, 61:081301.
- Guth, A. H. and Kaiser, D. I. (2005). Inflationary cosmology: Exploring the universe from the smallest to the largest scales. *Science*, 307:884.
- Ho, S., Hirata, C. M., Padmanabhan, N., Seljak, U., and Bahcall, N. (2008). Correlation of CMB with large-scale structure: I. ISW tomography and cosmological implications. *Phys Rev. D.*, 78(4).
- Hoffman, M. B. and Turner, M. S. (2001). Kinematic constraints to the key inflationary observables. *Physical Review D*, 64:023506.
- Huang, Z.-Y., Wang, B., and Su, R.-K. (2007). Uncertainty on determining the dark energy equation of state due to the spatial curvature. *International Journal of Modern Physics A*, 22:1819–1834.
- Huterer, D. and Turner, M. S. (2001). Probing the dark energy: methods and strategies. *Physical Review D*, 64:123527.
- Ichikawa, K., Kawasaki, M., Sekiguchi, T., and Takahashi, T. (2006). Implication of dark energy parametrizations on the determination of the curvature of the universe. *JCAP*, 0612:005.
- Ichikawa, K. and Takahashi, T. (2007). Dark energy parametrizations and the curvature of the universe. *JCAP*, 0702:001.
- Johri, V. B. (2004). Parametrization of dark energy equation of state. arXiv: astro-ph/0409161.
- Johri, V. B. and Rath, P. K. (2007). Parametrization of dark energy equation of state revisited. *Int. J. Mod. Phys.*, D16:1581–1591.
- Jones, W. C., Ade, P., Bock, J., Bond, J., Borrill, J., Boscaleri, A., Cabella, P., Contaldi, C., Crill, B., de Bernardis, P., De Gasperis, G., de Oliveira-Costa, A., De Troia, G., di Stefano, G., Hivon, E., Jaffe, A., Kisner, T., Lange, A., MacTavish, C., Masi, S., Mauskopf, P., Melchiorri, A., Montroy, T., Natoli, P., Netterfield, B., Pascale, E., Piacentini, F., Pogosyan, D., Polenta, G., Prunet, S., Ricciardi, S., Romeo, G., Ruhl, J., Santini, P., Tegmark, M., Veneziani, M., and Vittorio, N. (2006). A measurement of the angular power spectrum of the cmb temperature anisotropy from the 2003 flight of boomerang. *The Astrophysical Journal*, 647:823.

- Kernan, P. J. and Sarkar, S. (1996). No crisis for big bang nucleosynthesis. *Physical Review D*, 54:3681.
- Kinney, W. H. (2002). Inflation: flow, fixed points and observables to arbitrary order in slow roll. *Physical Review D*, 66:083508.
- Kinney, W. H., Kolb, E. W., Melchiorri, A., and Riotto, A. (2006). Inflation model constraints from the wilkinson microwave anisotropy probe three-year data. *Physical Review D*, 74:023502.
- Knox, L., Song, Y.-S., and Zhan, H. (2006). Weighing the universe with photometric redshift surveys and the impact on dark energy forecasts. *The Astrophysical Journal*, 652:857.
- Kolb, E. and Turner, M. (1990). *The Early Universe*. Addison-Wesley.
- Kosowsky, A. and Turner, M. S. (1995). CBR anisotropy and the running of the scalar spectral index. *Physical Review D*, 52:1739.
- Kunz, M. (2007). The dark degeneracy: On the number and nature of dark components. arXiv: astro-ph/0702615.
- Kunz, M. (2008). Private communication.
- Kunz, M., Trotta, R., and Parkinson, D. (2006). Measuring the effective complexity of cosmological models. *Physical Review D*, 74:023503.
- Kuo, C. L., Ade, P. A. R., Bock, J. J., Cantalupo, C., Daub, M. D., Goldstein, J., Holzappel, W. L., Lange, A. E., Lueker, M., Newcomb, M., Peterson, J. B., Ruhl, J., Runyan, M. C., and Torbet, E. (2004). High resolution observations of the cmb power spectrum with acbar. *The Astrophysical Journal*, 600:32.
- Kurki-Suonio, H., Muhonen, V., and Valiviita, J. (2005). Correlated primordial perturbations in light of CMB and LSS data. *Physical Review D*, 71:063005.
- Langlois, D. (2004). Inflation, quantum fluctuations and cosmological perturbations. hep-th/ 0405053.
- Leach, S. M., Liddle, A. R., Martin, J., and Schwarz, D. J. (2002). Cosmological parameter estimation and the inflationary cosmology. *Physical Review D*, 66:023515.
- Lewis, A. and Bridle, S. (2002). Cosmological parameters from cmb and other data: a monte-carlo approach. *Physical Review D*, 66:103511.
- Li, N. and Schwarz, D. J. (2007). On the onset of cosmological backreaction. *Phys. Rev. D.*, 76(8).
- Liddle, A. and Lyth, D. (2000). *Cosmological Inflation And Large-Scale Structure*. Cambridge University Press.

- Liddle, A. R. (2007). Information criteria for astrophysical model selection. *Monthly Notices of the Royal Astronomy Society*, 377:L74–L78.
- Liddle, A. R., Parkinson, D., Leach, S. M., and Mukherjee, P. (2006). The WMAP normalization of inflationary cosmologies. *Physical Review D*, 74:083512.
- Liddle, A. R., Parsons, P., and Barrow, J. D. (1994). Formalising the slow-roll approximation in inflation. *Physical Review D*, 50:7222.
- Lidsey, J. E., Liddle, A. R., Kolb, E. W., Copeland, E. J., Barreiro, T., and Abney, M. (1997). Reconstructing the inflaton potential — an overview. *Reviews of Modern Physics*, 69:373.
- Lidsey, J. E. and Tavakol, R. (2003). Running of the scalar spectral index and observational signatures of inflation. *Physics Letters B*, 575:157.
- Linde, A. (2008). Inflationary cosmology. In *Lecture Notes in Physics, Berlin Springer Verlag*, volume 738 of *Lecture Notes in Physics, Berlin Springer Verlag*.
- Linder, E. V. (2003). Exploring the expansion history of the universe. *Physical Review Letters*, 90:091301.
- Linder, E. V. (2005). Curved space or curved vacuum? *Astroparticle Physics*, 24:391.
- Linder, E. V. (2008a). The dynamics of quintessence, the quintessence of dynamics. *General Relativity and Gravitation*, 40:329.
- Linder, E. V. (2008b). Mapping the cosmological expansion. *Reports on Progress in Physics*, 71:056901.
- Lyth, D. H. and Liddle, A. R. (1992). Cobe, gravitational waves, inflation and extended inflation. *Physics Letters B*, 291:391.
- Mackay, D. (2003). *Information Theory, Inference, and Learning Algorithms*. Cambridge University Press, Cambridge, UK.
- Martin, J. and Ringeval, C. (2006). Inflation after WMAP3: Confronting the slow-roll and exact power spectra with cmb data. *JCAP*, 0608:009.
- Mersini-Houghton, L., Wang, Y., Mukherjee, P., and Kafexhiu, E. (2008). Nontrivial geometries: Bounds on the curvature of the universe. *Astroparticle Physics*, 29:167–173.
- Neupane, I. P. (2004a). Accelerating cosmologies from exponential potentials. *Classical and Quantum Gravity*, 21:4383.
- Neupane, I. P. (2004b). Cosmic acceleration and M theory cosmology. *Mod. Phys. Lett. A*, 19:1093.
- Pagel, B. (1997). *Nucleosynthesis and Chemical Evolution of Galaxies*. Cambridge University Press, Cambridge, UK.
- Parkinson, D. (2008). Lecture notes on bayesian techniques (unpublished).

- Parkinson, D., Blake, C., Kunz, M., Bassett, B. A., Nichol, R. C., and Glazebrook, K. (2007). Optimising baryon acoustic oscillation surveys - I: Testing the concordance Λ CDM cosmology. *Monthly Notices of the Royal Astronomical Society*, 377:185.
- Pearson, T. J., Mason, B. S., Readhead, A. C. S., Shepherd, M. C., Sievers, J. L., Udomprasert, P. S., Cartwright, J. K., Farmer, A. J., Padin, S., Myers, S. T., Bond, J. R., Contaldi, C. R., Pen, U. L., Prunet, S., Pogosyan, D., Carlstrom, J. E., Kovac, J., Leitch, E. M., Pryke, C., Halverson, N. W., Holzzapfel, W. L., Altamirano, P., Bronfman, L., Casasus, S., May, J., and Joy, M. (2003). The anisotropy of the microwave background to $l = 3500$: Mosaic observations with the cosmic background imager. *The Astrophysical Journal*, 591:556.
- Peiris, H. and Easter, R. (2006a). Recovering the inflationary potential and primordial power spectrum with a slow roll prior: Methodology and application to WMAP 3 year data. *JCAP*, 0607:002.
- Peiris, H. and Easter, R. (2006b). Slow roll reconstruction: Constraints on inflation from the 3 year WMAP dataset. *JCAP*, 0610:017.
- Percival, W. J., Baugh, C. M., Bland-Hawthorn, J., Bridges, T., Cannon, R., Cole, S., Colless, M., Collins, C., Couch, W., Dalton, G., De Propriis, R., Driver, S. P., Efstathiou, G., Ellis, R. S., Frenk, C. S., Glazebrook, K., Jackson, C., Lahav, O., Lewis, I., Lumsden, S., Maddox, S., Moody, S., Norberg, P., Peacock, J. A., Peterson, B. A., Sutherland, W., and Taylor, K. (2001). The 2df galaxy redshift survey: The power spectrum and the matter content of the universe. *Monthly Notices of the Royal Astronomical Society*, 327:1297.
- Percival, W. J., Nichol, R. C., Eisenstein, D. J., Frieman, J. A., Fukugita, M., Loveday, J., Pope, A. C., Schneider, D. P., Szalay, A. S., Tegmark, M., Vogeley, M. S., Weinberg, D. H., Zehavi, I., Bahcall, N. A., Brinkmann, J., Connolly, A. J., and Meiksin, A. (2007). The shape of the SDSS DR5 galaxy power spectrum. *The Astrophysical Journal*, 657:645.
- Perlmutter, S., Gabi, S., Goldhaber, G., Groom, D. E., Hook, I. M., Kim, A. G., Kim, M. Y., Lee, J. C., Pennypacker, C. R., Small, I. A., Goobar, A., Pain, R., Ellis, R. S., McMahon, R. G., Boyle, B. J., Bunclark, P. S., Carter, D., Irwin, M. J., Glazebrook, K., Newberg, H. J. M., Filippenko, A. V., Matheson, T., Dopita, M., and Couch, W. J. (1997). Measurements of the cosmological parameters ω and λ from the first 7 supernovae at $z \geq 0.35$. *The Astrophysical Journal*, 483:565.
- Rasanen, S. (2006). Constraints on backreaction in dust universes. *Classical and Quantum Gravity*, 23:1823.
- Ratra, B. and Peebles, P. J. E. (1988). Cosmological consequences of a rolling homogeneous scalar field. *Phys. Rev. D*, 37(12):3406–3427.
- Riess, A. G., Filippenko, A. V., Challis, P., Clocchiattia, A., Diercks, A., Garnavich, P. M., Gilliland, R. L., Hogan, C. J., Jha, S., Kirshner, R. P., Leibundgut, B., Phillips, M. M., Reiss, D., Schmidt, B. P., Schommer, R. A., Smith, R. C., Spyromilio, J., Stubbs, C.,

- Suntzeff, N. B., and Tonry, J. (1998). Observational evidence from supernovae for an accelerating universe and a cosmological constant. *Astronomical Journal*, 116:1009.
- Riess, A. G., Strolger, L.-G., Casertano, S., Ferguson, H. C., Mobasher, B., Gold, B., Challis, P. J., Filippenko, A. V., Jha, S., Li, W., Tonry, J., Foley, R., Kirshner, R. P., Dickinson, M., MacDonald, E., Eisenstein, D., Livio, M., Younger, J., Xu, C., Dahlen, T., and Stern, D. (2007). New Hubble space telescope discoveries of type Ia supernovae at $z > 1$: Narrowing constraints on the early behavior of dark energy. *Ast. Phys. Journal*, 659:98–121.
- Sandvik, H., Tegmark, M., Zaldarriaga, M., and Waga, I. (2004). The end of unified dark matter? *Physical Review D*, 69:123524.
- Schramm, D. N. and Turner, M. S. (1998). Big-bang nucleosynthesis enters the precision era. *Reviews of Modern Physics*, 70:303.
- Sen, A. A. and Sethi, S. (2002). Quintessence model with double exponential potential. *Physics Letters B*, 532:159.
- Seo, H.-J. and Eisenstein, D. J. (2003). Probing dark energy with baryonic acoustic oscillations from future large galaxy redshift surveys. *The Astrophysical Journal*, 598:720.
- Shafieloo, A., Alam, U., Sahni, V., and Starobinsky, A. A. (2006). Smoothing supernova data to reconstruct the expansion history of the universe and its age. *Monthly Notices of the Royal Astronomical Society*, 366:1081.
- Song, Y.-S. and Knox, L. (2003). The detectability of departures from the inflationary consistency equation. *Physical Review D*, 68:043518.
- Song, Y.-S., Peiris, H., and Hu, W. (2007). Cosmological constraints on $f(r)$ acceleration models. *Physical Review D*, 76:063517.
- Spergel, D. N., Bean, R., Dore, O., Nolta, M. R., Bennett, C. L., Dunkley, J., Hinshaw, G., Jarosik, N., Komatsu, E., Page, L., Peiris, H. V., Verde, L., Halpern, M., Hill, R. S., Kogut, A., Limon, M., Meyer, S. S., Odegard, N., Tucker, G. S., Weiland, J. L., Wollack, E., and Wright, E. L. (2007). Wilkinson microwave anisotropy probe (WMAP) three year results: Implications for cosmology. *APJS*, 170:377.
- Spooner, N. J. (2007). Direct dark matter searches. *Journal of the Physical Society of Japan*, 76(11).
- Stewart, E. D. (1997). Flattening the inflaton's potential with quantum corrections. *Physics Letters B*, 391:34.
- Stewart, E. D. and Lyth, D. H. (1993). A more accurate analytic calculation of the spectrum of cosmological perturbations produced during inflation. *Physics Letters B*, 302:171.
- Tegmark, M., Blanton, M., Strauss, M., Hoyle, F., Schlegel, D., Scoccimarro, R., Vogeley, M., Weinberg, D., Zehavi, I., Berlind, A., Budavari, T., Connolly, A., Eisenstein, D.,

- Finkbeiner, D., Frieman, J., Gunn, J., Hamilton, A., Hui, L., Jain, B., Johnston, D., Kent, S., Lin, H., Nakajima, R., Nichol, R., Ostriker, J., Pope, A., Scranton, R., Seljak, U., Sheth, R., Stebbins, A., Szalay, A., Szapudi, I., Verde, L., Xu, Y., others, ., and for the SDSS Collaboration (2004). The 3D power spectrum of galaxies from the SDSS. *The Astrophysical Journal*, 606:702.
- Tegmark, M., Eisenstein, D., Strauss, M., Weinberg, D., Blanton, M., Frieman, J., Fukugita, M., Gunn, J., Hamilton, A., Knapp, G., Nichol, R., Ostriker, J., Padmanabhan, N., Percival, W., Schlegel, D., Schneider, D., Scoccimarro, R., Seljak, U., Seo, H., Swanson, M., Szalay, A., Vogeley, M., Yoo, J., Zehavi, I., Abazajian, K., Anderson, S., Annis, J., Bahcall, N., Bassett, B., Berlind, A., Brinkmann, J., Budavari, T., Castander, F., Connolly, A., Csabai, I., Doi, M., Finkbeiner, D., Gillespie, B., Glazebrook, K., Hennessy, G., Hogg, D., Ivezić, Z., Jain, B., Johnston, D., Kent, S., Lamb, D., Lee, B., Lin, H., Loveday, J., Lupton, R., Munn, J., Pan, K., Park, C., Peoples, J., Pier, J., Pope, A., Richmond, M., Rockosi, C., Scranton, R., Sheth, R., Stebbins, A., Stoughton, C., Szapudi, I., Tucker, D., Berk, D. V., Yanny, B., and York, D. (2006). Cosmological constraints from the SDSS luminous red galaxies. *Physical Review D*, 74:123507.
- Trotta, R. (2007). Applications of bayesian model selection to cosmological parameters. *Monthly Notices of the Royal Astronomical Society*, 378:72.
- Virey, J. M. and Ealet, A. (2007). Sensitivity and figures of merit for dark energy supernovae surveys. *Astronomy and Astrophysics*, 464:837–843.
- Wang, Y. and Mukherjee, P. (2007). Observational constraints on dark energy and cosmic curvature. *Physical Review D*, 76:103533.
- Weinberg, S. (1970). Direct determination of the metric from observed redshifts and distances. *Astrophysical Journal Letters*, 161:L233.
- Weller, J. and Albrecht, A. (2002). Future supernovae observations as a probe of dark energy. *Physical Review D*, 65:103512.
- Wetterich, C. (1988). Cosmologies with variable Newton's constant. *Nucl. Phys. B*, (302):668.
- Wood-Vasey, W. M., Miknaitis, G., Stubbs, C. W., Jha, S., Riess, A. G., Garnavich, P. M., Kirshner, R. P., Aguilera, C., Becker, A. C., Blackman, J. W., Blondin, S., Challis, P., Clocchiatti, A., Conley, A., Covarrubias, R., Davis, T. M., Filippenko, A. V., Foley, R. J., Garg, A., Hicken, M., Krisciunas, K., Leibundgut, B., Li, W., Matheson, T., Miceli, A., Narayan, G., Pignata, G., Prieto, J. L., Rest, A., Salvo, M. E., Schmidt, B. P., Smith, R. C., Sollerman, J., Spyromilio, J., Tonry, J. L., Suntzeff, N. B., and Zenteno, A. (2007). Observational constraints on the nature of the dark energy: First cosmological results from the ESSENCE supernova survey. *Astrophysics Journal*, 666:694–715.
- Wright, E. L. (2007). Constraints on dark energy from supernovae, gamma ray bursts, acoustic oscillations, nucleosynthesis and large scale structure and the hubble constant. *Astrophysical Journal*, 664:633–639.

- Yamamoto, K., Parkinson, D., Hamana, T., Nichol, R. C., and Suto, Y. (2007). Optimizing future imaging survey of galaxies to confront dark energy and modified gravity models. *Physical Review D*, 76:023504.
- Zhao, G.-B., Xia, J.-Q., Li, H., Tao, C., Virey, J.-M., Zhu, Z.-H., and Zhang, X. (2007). Probing for dynamics of dark energy and curvature of universe with latest cosmological observations.